Universidade do Minho
Escola de Engenharia

Carla Susana Correia Pereira

Diabetic retinopathy diagnosis through multi-agent approaches

outubro de 2013

Diabetic retinopathy diagnosis through multi-agent approaches

Carla Susana Correia Pereira

UMinho | 2013

Universidade do Minho
Escola de Engenharia

Carla Susana Correia Pereira

Diabetic retinopathy diagnosis through multi-agent approaches

Programa Doutoral em Engenharia Biomédica

Trabalho efetuado sob a orientação de:
Professor Doutor João Luís Pereira Monteiro
Doutor Manuel João Oliveira Ferreira
Doutor Luís Manuel Rodrigo Gonçalves

outubro de 2013

À memória de Gonçalo

*(*4-12-1996 †30-1-2010)*

Aos meus pais

Acknowledgments

Aos meus orientadores pela orientação, incentivo, apoio e sugestões dados ao longo de todo este trabalho e que foram fundamentais para o seu término.

Aos elementos do laboratório SIC - CReSTIC em Reims, por tão bem me terem acolhido e me terem feito sentir em casa durante os 3 meses que estive lá. Em particular à Zahia e ao Jason pela disponibilidade, discussões e conselhos que foram essenciais à realização deste trabalho.

Aos meus colegas, amigos e professores presentes em diferentes fases deste trabalho, em particular, à Prof. Graça, aos elementos que foram passando pelo laboratório de Gualtar, ao Filipe no CCG, à Lara e à Karima no Crestic, por proporcionarem um bom e inspirador ambiente de trabalho. Ao Nelson e à Diana, que mais recentemente começaram a seguir de perto o meu trabalho e deram comentários e sugestões valiosas.

Aos meus amigos de mais longa data, em particular aqueles que caminharam ao meu lado nesta fase da vida, compartilhando as alegrias e desilusões típicas de um doutoramento. A vocês deixo ainda aqui desejos de que o fim do vosso doutoramento corra muito bem e que tenham um futuro muito risonho. E espero que os nossos caminhos continuem muito próximos.

A ti Nuno, que foste o alicerce de todo este trabalho, pois a força e a motivação vieram em grande parte de ti.

Aos meus pais, irmãos, irmãs, cunhados e sobrinhos que, de uma ou outra forma, contribuíram para que eu conseguisse chegar ao fim de mais uma etapa.

A todos o meu muito OBRIGADO!!!

THANK YOU!!!

MERCI BEAUCOUP!!!

Funds

Work supported by FEDER funds through the "Programa Operacional Factores de Competitividade – COMPETE" and by national funds by FCT- Fundação para a Ciência e a Tecnologia. C. Pereira thanks the FCT for the SFRH / BD / 61829 / 2009 grant.

Diabetic retinopathy diagnosis through multi-agent approaches

Abstract

Diabetic retinopathy has been revealed as a serious public health problem in occidental world, since it is the most common cause of vision impairment among people of working age. The early diagnosis and an adequate treatment can prevent loss of vision. Thus, a regular screening program to detect diabetic retinopathy in the early stages could be efficient for the prevention of blindness. Due to its characteristics, digital color fundus photographs have been the preferred eye examination method adopted in these programs. Nevertheless, due to the growing incidence of diabetes in population, ophthalmologists have to observe a huge number of images. Therefore, the development of computational tools that can assist the diagnosis is of major importance. Several works have been published in the recent past years for this purpose; but an automatic system for clinical practice has yet to come. In general, these algorithms are used to normalize, segment and extract information from images to be utilized by classifiers which aim to classify the regions of the fundus image. These methods are mostly based on global approaches that cannot be locally adapted to the image properties and therefore, none of them perform as needed because of fundus images complexity.

This thesis focuses on the development of new tools based on multi-agent approaches, to assist the diabetic retinopathy early diagnosis. The fundus image automatic segmentation concerning the diabetic retinopathy diagnosis should comprise both pathological (dark and bright lesions) and anatomical features (optic disc, blood vessels and fovea). In that way, systems for the optic disc detection, bright lesions segmentation, blood vessels segmentation and dark lesions segmentation were implemented and, when possible, compared to those approaches already described in literature. Two kinds of agent based systems were investigated and applied to digital color fundus photographs: ant colony system and multi-agent system composed of reactive agents with interaction mechanisms between them. The ant colony system was used to the optic disc detection and for bright lesion segmentation. Multi-agent system models were developed for the blood vessel segmentation and for small dark lesion segmentation. The multi-agent system models created in this study are not image processing techniques on their own, but they are used as tools to improve the traditional algorithms results at the micro level. The results of all the proposed

approaches are very promising and reveal that the systems created perform better than other recent methods described in the literature.

Therefore, the main scientific contribution of this thesis is to prove that multi-agent systems based approaches can be efficient in segmenting structures in retinal images. Such an approach overcomes the classic image processing algorithms that are limited to macro results and do not consider the local characteristics of images. Hence, multi-agent systems based approaches could be a fundamental tool, responsible for a very efficient system development to be used in screening programs concerning diabetic retinopathy early diagnosis.

Diagnóstico de retinopatia diabética através de abordagens multi-agente

Resumo

A retinopatia diabética tem-se revelado como um problema sério de saúde pública no mundo ocidental, uma vez que é a principal causa de cegueira entre as pessoas em idade ativa. Contudo, a perda de visão pode ser prevenida através da deteção precoce da doença e de um tratamento adequado. Por isso, um programa regular de rastreio e monitorização da retinopatia diabética pode ser eficiente na prevenção da deterioração da visão. Devido às suas características, a fotografia digital colorida do fundo do olho tem sido o exame adotado neste tipo de programas. No entanto, devido ao aumento da incidência da diabetes na população, o número de imagens a serem analisadas pelos oftalmologistas é elevado. Assim sendo, é muito importante o desenvolvimento de ferramentas computacionais para auxiliar no diagnóstico desta patologia. Nos últimos anos, têm sido vários os trabalhos publicados com este propósito; porém, não existe ainda um sistema automático (ou recomendável) para ser usado nas práticas clínicas. No geral, estes algoritmos são usados para normalizar, segmentar e extrair informação das imagens que vai ser utilizada por classificadores, cujo objetivo é identificar as regiões da imagem que se procuram. Estes métodos são maioritariamente baseados em abordagens globais que não podem ser localmente adaptadas às propriedades das imagens e, portanto, nenhum apresenta a performance necessária devido à complexidade das imagens do fundo do olho.

Esta tese foca-se no desenvolvimento de novas ferramentas computacionais baseadas em sistemas multi-agente, para auxiliar na deteção precoce da retinopatia diabética. A segmentação automática das imagens do fundo do olho com o objetivo de diagnosticar a retinopatia diabética, deve englobar características patológicas (lesões claras e escuras) e anatómicas (disco ótico, vasos sanguíneos e fóvea). Deste modo, foram criados sistemas para a deteção do disco ótico e para a segmentação das lesões claras, dos vasos sanguíneos e das lesões escuras e, quando possível, estes foram comparados com abordagens já descritas na literatura. Dois tipos de sistemas baseados em agentes foram investigados e aplicados nas imagens digitais coloridas do fundo do olho: sistema de colónia de formigas e sistema multi-agente constituído por agentes reativos e com mecanismos de interação entre eles. O sistema de colónia de formigas foi usado para a deteção do disco ótico e para a segmentação das lesões claras.

Modelos de sistemas multi-agente foram desenvolvidos para a segmentação dos vasos sanguíneos e das lesões escuras. Os modelos multi-agentes criados ao longo deste estudo não são por si só técnicas de processamento de imagem, mas são sim usados como ferramentas para melhorar os resultados dos algoritmos tradicionais no baixo nível. Os resultados de todas as abordagens propostas são muito promissores e revelam que os sistemas criados apresentam melhor performance que outras abordagens recentes descritas na literatura.

Posto isto, a maior contribuição científica desta tese é provar que abordagens baseadas em sistemas multi-agente podem ser eficientes na segmentação de estruturas em imagens da retina. Uma abordagem deste tipo ultrapassa os algoritmos clássicos de processamento de imagem, que se limitam aos resultados de alto nível e não têm em consideração as propriedades locais das imagens. Portanto, as abordagens baseadas em sistemas multi-agente podem ser uma ferramenta fundamental, responsável pelo desenvolvimento de um sistema eficiente para ser usado nos programas de rastreio e monitorização da retinopatia diabética.

Contents

List of Figures

List of Tables

Nomenclature

2D Two dimensional

ACO Ant colony optimization

ACS Ant colony system

AMD Age-related macular degeneration

AS Ant system

ASM Active shape model

AUC Area under roc curve

CCD Charge-coupled device

CIE Luv International Commission on Illumination, Luv

DiaRetDB1 Diabetic retinopathy database, calibration level 1

DRIVE Digital retinal images for vessel extraction

DRS Diabetic retinopathy study

ETDRS Early treatment diabetic retinopathy study

FN False negative

FOV Field of view

FP False positive

FROC Free-response receiver operating characteristic

HCAA Hospitalar Center of Alto Ave

HEI-MED Hamilton eye institute macular edema dataset

HLS Hue, lightness and saturation

ICM Iterative conditional modes

IRMA Intraretinal microvascular abnormalities

IVUS Intravacular ultrasound

kNN k-nearest neighbors

LaTIM Laboratoire de Traitement de l'Information Médicale

MA Microaneurysm

MAS Multi-agent system

MRF Markov random fields

MRI Magnetic resonance imaging

NN Neural networks

OD Optic disc

PCA Principal component analysis

RGB Red, green and blue

ROC Receiver operating characteristic

ROC Retinopathy online challenge

STARE Structured analysis of the retina

SVM Support vector machines

TAN Topological active net

TN True negative

TP True positive

1. Introduction

In this chapter, a brief description of the problem under consideration, as well as the motivation for this study realization are made. Then, the goals of this work are succinctly indicated. Finally, the thesis structure is presented.

1.1. Problem definition

Diabetic retinopathy (DR) is a specific microvascular complication of diabetes and it has been revealed as a serious public health problem in occidental world, since it is the most common cause of vision impairment among people of working age. The early diagnosis and an adequate treatment can prevent loss of vision. But this is not an easy task because patients with DR have no symptoms until visual loss develops, when the macular area is affected. Therefore a regular screening program to detect retinopathy in the early stages could be efficient for the prevention of blindness. Digital color fundus photographs have been the preferred eye examination method adopted in these programs, because they permit a high quality record for detecting early signs of DR and monitoring its progression. Furthermore, their acquisition is cheap and noninvasive [1, 2].

Due to the growing incidence of diabetes in population, caused by the population growth, aging, physical inactivity and an increasing prevalence of obesity, the number of people affected by DR has grown to alarming numbers. Consequently, ophthalmologists have to observe a huge number of images that is a time consuming and exhausting process, being worsened by the lack of ophthalmologists in less developed areas. In that way, an effective prevention of diabetic retinopathy in an ophthalmologist based screening has been compromised. Thus, the development of computational tools that can assist the early diagnosis is of major importance.

The digital nature of fundus photographs allows automatic analysis to reduce the workload of ophthalmologists and the health costs of the screening program of the disease. In recent years, a series of approaches based on image processing, pattern recognition and machine learning algorithms, have been proposed for the early DR diagnosis in color fundus images. In general, these algorithms are used to normalize, segment and extract information from images to be utilized by classifiers which aim to classify the regions of the fundus images. The fundus image automatic segmentation should comprise both anatomical and pathological features. The fundus anatomic structures are optic disc, blood vessels and fovea. The DR characteristic

pathological features include dark lesions (microaneurysm, hemorrhages, neovessels) and bright lesions (hard exudates and cotton wool spots). Several works have been reported in literature concerning the segmentation of each of these structures [3, 4]. Despite all these studies, automatic fundus analysis remains a difficult task and an automatic system for clinical practice has yet to come [3, 4]. The main difficulties of these systems come from the fact that anatomical and pathological retinal objects mutually affect each other segmentation, producing false positives. For example, the blood vessels extraction may be influenced by the bright lesions and dark lesions presence; the optic disc may influence the bright lesions segmentation, and its detection may be affected by bright lesions and blood vessels. Moreover, the digital color fundus photographs frequently present poor contrast, noise, and great inter- and intra-image variability, affecting the performance of many algorithms.

Using typical image processing operators, such as convolution kernels, leads to rigid systems that are not able to adapt and generalize to unknown situations. In fact, these algorithms cannot take into account the image local information, since they process the entire image in the same way, forcing the designer to refer heuristics or more advanced algorithms. Therefore, there is a need to increase the adaptability of segmentation algorithms.

The methods reported in literature for the fundus image analysis are mostly based on global approaches that cannot be locally adapted to the image properties and therefore, none of them perform as needed because of this kind of image complexity. In recent years, researchers have been working in multi-agent systems applied to digital image processing. The main goal of multi-agent systems research is to find methods that allow the building of complex systems composed of relatively independent modules (called agents) that, while operating on local knowledge and possessing only limited abilities, are nonetheless capable of enacting the desired global behaviors. The novelty of this thesis lies on the use of this type of approach - multi-agent systems - for the analysis of fundus images.

1.2. Aim and objectives

The aim of this thesis is the development of tools based on multi-agent systems, for the early diabetic retinopathy diagnosis through fundus image analysis. The objectives consist in the development of algorithms for the optic disc detection, blood vessels segmentation, bright lesions segmentation and dark lesions segmentation. Moreover, the potentialities of these tools will be evaluated through the comparison with other state of the art techniques.

Since the multi-agent systems based approaches have never been applied in the digital color fundus images, this thesis pretends to explore the use of such systems for the objectives defined. In this kind of approach, each agent can locally process and interpret the image information, avoiding the development of rigid systems.

Moreover, the multi-agent systems provide a general way to give some independence to each of the image processing methods, allowing an increased software engineering capacity for the designer. In that way, the multi-agent systems may add competences to the conventional image processing algorithms, that will be studied in this thesis for the diabetic retinopathy early diagnosis through color fundus photographs.

1.3. Outline of this thesis

The rest of this thesis is divided into seven chapters plus the thesis conclusion chapter.

Chapter 2 describes some theoretical and physiological concepts related to the eye and the diabetic retinopathy. Furthermore, some retinal imaging techniques, image acquisition protocols and the importance of digital color fundus image for screening programs are explained. It also refers the importance of automatic system development for the diabetic retinopathy diagnosis.

Chapters 3 and 4 present the fundamental theoretical concepts needed to understand the developed algorithms described in the next sections. Chapter 3 introduces multi-agent systems theory including definitions and properties of agent, multi-agent system, environment and interactions. It also contains the explanation about two important phenomena related to the behavior of this kind of systems - emergence and self-organization. Chapter 4 describes a particular case of a simple multi-agent system, the ant colony optimization. In this chapter, the characteristics of the biological and artificial ant systems, as well as the mathematical formulation of the artificial ant system, are mentioned. Moreover, Chapters 3 and 4 present literature reviews related to the use of multi-agent systems and ant colony optimization algorithms, respectively, in medical images.

Chapters 5, 6, 7 and 8 correspond to the practical sections of this study and describe algorithms for the optic disc detection, bright lesions segmentation, blood vessels segmentation and dark lesions segmentation, respectively. These chapters are organized in a similar way, beginning with an introduction section followed by a literature review about the detection of the respective retinal feature. Then, the used methodology is described and results, discussion and conclusion are presented next.

In Chapter 9, the principal conclusions taken along this study are indicated and some points of further work to overcome the problems still existent in the fundus images analysis are proposed.

2. Background

In this chapter, some theoretical concepts about the eye, its anatomy and imaging techniques are described, in order to understand the importance of the digital color fundus images used in this study. It also refers the diabetic retinopathy problematic, as well as the relevance of the screening programs to prevent vision impairment and the image acquisition protocols most suitable for these programs. Finally, the importance of the development of computer based systems for the automatic diabetic retinopathy early diagnosis is discussed.

2.1. Eye structure

The eye is a slightly asymmetrical globe with about 24.5 mm in diameter. It is essentially compounded by three concentric layers with several structures. These structures are responsible for controlling the light into the eye, operating on the same basic principle as a camera. Figure 2.1 illustrates an eye cross section where main structures are indicated. The light goes into the eye through the pupil and it is focused on the retina. The lens is responsible for focusing images from different distances on the retina and the iris controls the amount of light entering the eye.

The outer layer of the eye is called sclera and it is an opaque, fibrous and protective membrane which is responsible for the eye shape. The intermediate layer is the choroid, a vascular layer which supplies oxygen and nourishment to the eye structures. The inner layer is the retina that with its components, represents the most important structure for this thesis.

The retina contains light sensitive cells that convert light stimuli into electric impulses. According to its shape, these photoreceptor cells can be divided in two groups: cones and rods, responsible for the daytime and night vision, respectively. Cone cells are concentrated in the fovea and become gradually sparser towards the border of the retina. The rods are situated at the outer edges of the retina and are also used for the peripheral vision. Due to the high amount of cone cells, the fovea is responsible for the accurate vision. This structure is located near the macula center. The macula is an oval spot with a diameter of about 4 to 5 mm and situated near the center of the retina.

The nerve fibers containing the electrical impulses, converge and leave the eye towards the brain by means of the optic nerve. The head of the optic nerve is called

optic disc or papilla, and it is also known by "blind spot" of the eye since it does not contain any light sensitive cells. The optic disc is situated 3 to 4 mm to the nasal side of the fovea and measures about 2 mm in diameter. The optic disc also serves as the point of convergence and entrance of the retinal blood vessels.

The fundus eye corresponding to the central issue in this research study is compounded by the three membranes described above: sclera, choroid and retina.

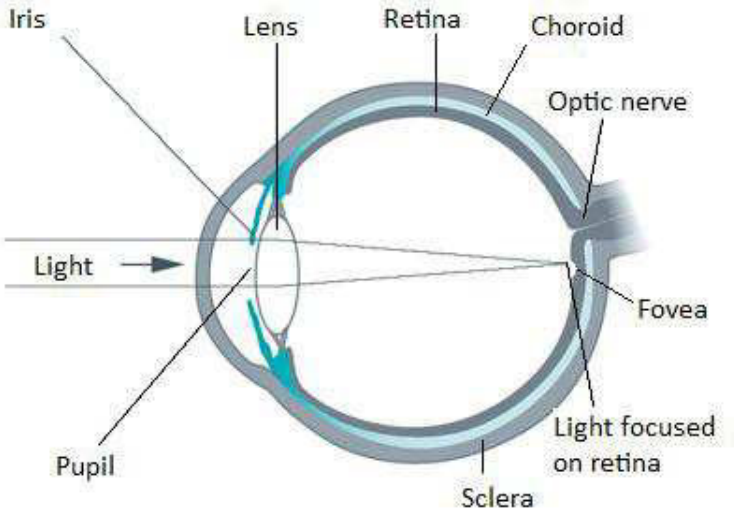

Figure 2.1.: Eye cross section

2.2. Fundus eye´s imaging techniques

For ophthalmologists, the human retina promises to be a window into the health of a patient. The direct ophtalmoscope, still used today, was the first instrument used by ophthalmologists for the direct examination of the retina. It was made known by Helmholtz at the end of the XIX century, and since then it has not changed much. The modern ophtalmoscope is a handheld instrument that contains a small battery-powered lamp to direct a beam of light into the eye by way of a mirrored prism. Despite being widespread in the clinical practice, the use of this instrument yields poor sensitivity and results are highly dependent on the observer experience.

An alternative or complement to ophtalmoscope is the fundus photograph, which first instrument appeared in the middle of the XX century. This was a photographic 35mm back connected to an optical system that focuses on the fundus oculi, illuminated by a coaxial flash. Around 1990, the first digital fundus camera appeared, where the optical system is connected to a charge-coupled device (CCD) and the image is sent to a computer for visualization and storage [5]. The use of digital photography brought advantages over the film in DR research studies and clinical

practice. Actually, digital fundus cameras allow the in vivo viewing of the retina for disease diagnosis and patient consultation and, more convenient, for image storage, indexing, retrieval, and transmission [6].

With a color fundus camera it is possible to acquire an image of the fundus eye. The visible part of it is constituted by the retina with its vascular network and the optic nerve head. The choroid is usually obscured by the retinal deepest layer, the pigmented epithelium that gives to retina its reddish color in color images. Therefore, choroidal vessels are not normally visible in an image taken with a fundus camera, unless the pigmented epithelium is very lightly pigmented or in case of pathological depigmentation, where retina becomes almost transparent and the choroid becomes visible.

From the existent examination modes with fundus camera, only two types will be referred in this study. They are the fluorescein angiography (Figure 2.2 - left) and the color fundus photography (Figure 2.2 - right) .

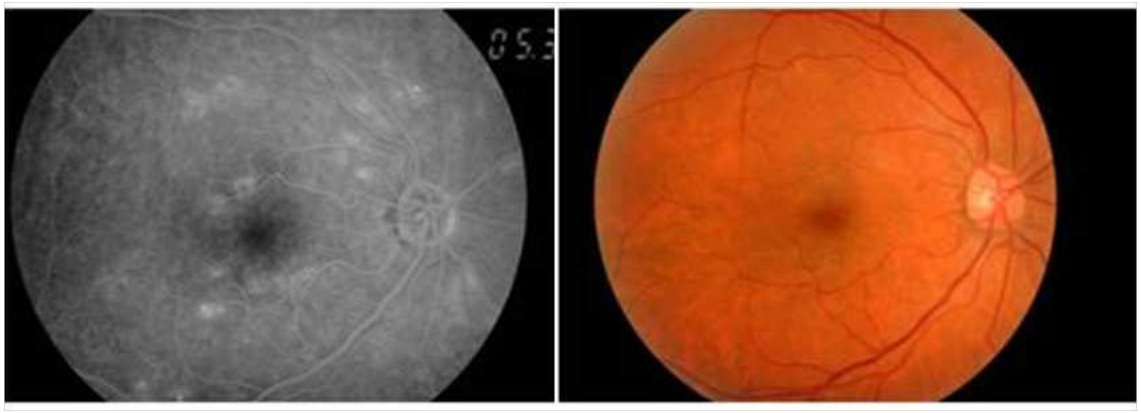

Figure 2.2.: Fundus photographs. The left one is a fluorescein angiography and the right one is the color fundus photography of the same eye

2.2.1. Fluorescein angiography

The eye angiogram uses a fluorescein dye that is injected into a cubital vein of the patient. Once injected, the dye takes about 10 to 15 seconds to circulate through the body. When the dye enters the eye blood vessels, a series of photos are taken to map the dye's progress in the retina. More pictures are taken after most of the dye has passed through the eyes to see if any of it has leaked out of the blood vessels. Any dye that leaks out of the blood vessels will color the tissues and fluid in the eye. In that way, it is possible to observe the diabetic retinopathy vascular abnormalities due to the dye hyperfluorescence on the retina and the dye hypofluorescence in areas where perfusion is inadequate. In fact, the diabetic retinopathy vascular abnormalities (see section 2.3) include microaneurysms and dot or blot hemorrhages that can be

distinguished with these kind of images, since the former appear as small bright dots while the latter are dark [7].

Currently, the correct assessment of these images requires a specialist, which presents difficulties in remote or less developed areas. Moreover, angiography is a relatively invasive and dangerous procedure, since a dye is injected into the body with a very slow excretion procedure.

2.2.2. Digital color fundus photography

The digital color images represent a good complementary exam for the fluorescein angiography, since it is a non-invasive and easy to use procedure, and it is more desirable for use in less developed areas, because the images can be obtained by trained health professionals. Though the diabetic retinopathy lesions are also visible, these images are more difficult to interpret and it is not possible to distinguish microaneurysm from dot and blot hemorrhages.

In this kind of images, a normal fundus eye is composed by the retina and its anatomical structures: optic disc, blood vessels and macula (Figure 2.3).

The normal optic disc is characterized as a bright yellow disc with a well defined contour, especially at the temporal side. It contains a central depression that is the physiological cup from which the blood vessels emerge.

The blood vessels divide dichotomously, first into superior and inferior branches and then into temporal and nasal branches. The retinal arteries are narrower (arteriovenous ratio of 2:3) and lighter than retinal veins.

The macula is the area centered within the temporal arcades, placed 1.5 disc diameters away from the optic disc temporal margin. It is darker in color than the fundus background and it incorporates a central depression to form fovea, the retina most sensitive part [8].

2.3. Retinal abnormalities in diabetic retinopathy

Diabetic retinopathy is one of the diabetes *mellitus* vascular complications. Diabetes *mellitus* is a chronic pathology affecting a huge number of persons especially in developed countries. According to [9], 11.7% of the population in Portugal with age between 20 and 79 years is diabetic. Moreover, the same study refers that 34.8% of the population have or are at risk of having diabetes, and almost an half of the diabetic people do not know about the disease. That is, in Portugal there are approximately 905 thousand people with diabetes and more or less 1 million and 780 thousand people with diabetes not diagnosed.

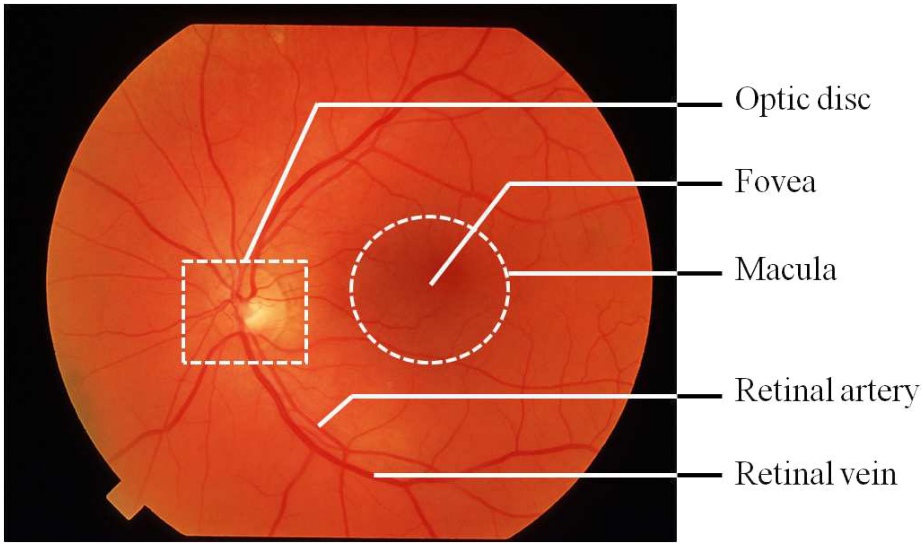

Figure 2.3.: Normal color fundus image with the retinal structures marked

Diabetes is characterized by disordered metabolism and abnormally high blood sugar (hyperglycemia) that affects blood vessels, nervous system and other internal structures. Diabetic retinopathy arises from microvascular retinal changes that occur in the presence of hyperglycemia during long periods of time. The diabetic retinopathy appearing and development depends on several factors: diabetes type, hormonal and metabolic issues, patient age, sex and ethnicity.

2.3.1. Lesions

The diabetes has as consequence some structural changes in the retinal tiny vessels resulting in the diabetic retinopathy characteristic lesions. The most common are microaneurysms, oedema, hemorrhages, hard exudates, cotton wool spots and neovessels. A brief description of these lesions taken from [7] and relevant for this study will be present next.

2.3.1.1. Microaneurysms

Microaneurysms appear as small red dots (10-100 µm in diameter) in the color fundus images (Figure 2.4 a) left and below) and as bright spots in the fluorescein angiography. The larger microaneurysms are surrounded by a circle of oedema, with hard exudates delimiting the boundary. Most microaneurysms are seen at the posterior pole around the optic disc and macular area, where they can represent the DR first sign. The microaneurysms are frequently indistinguishable from the small hemorrhages and a fluorescein angiography is needed to distinguish them. Counting the amount of microaneurysms can be used as a clinical evidence of the DR progression.

2.3.1.2. Oedema

The oedema is the result of the serum leaking into retina after capillaries being damaged. As closer the oedema is to the fovea more affected is the vision. If the oedema occurs at the fovea center may cause the permanent loss of vision. This kind of lesion is difficult to see in the direct ophthalmoscopy, but is usually associated with the presence of microaneurysms and exudates.

2.3.1.3. Hard exudates

Hard exudates are also an indicator of the capillaries damaged since they are a result of the extravasated plasma proteins, mainly lipoproteins. In fundus images they appear as yellow-white dots, shiny and with sharp borders (Figure 2.4 a) left and above). It is important to distinguish the exudates from other kind of lesion that is not related to diabetes: the drusen. The latter frequently represent age-related macular degeneration manifestations and are not sight-threatening in themselves. Their appearance is similar with hard exudates in terms of shape and size, but the color and contour are a little different. Furthermore, drusen are not associated with other diabetic retinopathy lesions, like the exudates that most of the times are seen together with microaneurysms. This is also useful to distinguish these lesions. In addition, since drusen are generally related to age-related macular changes (for instance, hypopigmentation), they frequently manifest in a symmetrical way between the two eyes.

2.3.1.4. Cotton wool spots

Cotton wool spots result from small artery occlusion. Their name comes from their similarity to the cotton wool appearance since they are gray-white opaque patches with poorly defined edges (Figure 2.4 a) right and above). Their location is peri-papillary and close to blood vessels.

2.3.1.5. Hemorrhages

Hemorrhages are caused by the blood leaking into the retina through the damaged capillary wall. Their appearance depends on its location in the retina. If they are superficial, their flame-shape (Figure 2.4 a) right and below) is due to the blood alignment with the superficial axons in the nerve fiber layer. Hemorrhages located in the deepest layer are of dot and blot shape. The dot hemorrhages are tiny red spots being indistinguishable from microaneurysms. The blot hemorrhages are larger and with irregular borders.

2.3.1.6. Intraretinal microvascular abnormalities

Intraretinal microvascular abnormalities (IRMA) represent new tiny blood vessels that grow within retinal tissue. The origin of these vessels is generally from the venous side of the retinal circulation and they grow toward an area of capillary obstruction. Despite of being new vessels, they do not bleed or cause pre-retinal or vitreous hemorrhages. On fluorescein angiography, in contrast with proliferative new vessels, they do not leak. Moreover, it is possible to distinguish IRMA from normal retinal vessels by their haphazard branching, with unusually large angles between branches and an irregular caliber that varies from fine thread-like vessels to dilated capillaries in the same IRMA.

2.3.1.7. Neovessels

The neovessels are new abnormal vessels that appear in the retina and grow towards the eye center (the vitreous). Since they represent very fragile vessels, they frequently bleed causing vitreous and pre-retinal hemorrhages, which lead to vision impairment. These proliferative new vessels arise either from vessels on the optic disc (Figure 2.4 b)) or from more peripheral large vessels.

(a) **(b)**

Figure 2.4.: Diabetic retinopathy characteristic lesions observed in color fundus images. a) From left to right and from above to below: hard exudates, cotton wool spot, microaneurysm and flame shape hemorrhage. b) Neovessels over the optic disc

2.3.2. Classification of diabetic retinopathy

The diabetic retinopathy classification needs to represent a continuous scale of risk depending on clinical features, and to be meaningful to all specialists involved in diabetes care [10]. The Early Treatment Diabetic Retinopathy Study (ETDRS) photography has been recognized as the gold standard for clinical trials in grading DR. Grading protocols were derived from the Airlie House Symposium's classification of DR [11], modified for the Diabetic Retinopathy Study (DRS) [12], and extended for the ETDRS [13]. The latter has been widely applied in research settings, publications and it has shown satisfactory reproducibility and validity. However, its use in everyday clinical practice has not proven easy or practical for several reasons. First the photographic grading system contains 90 levels, much more than what is necessary for clinical care. Moreover, such number of levels, together with the detailed specific definitions and the requirements of comparison with standard photographs, become the ETDRS grading procedure difficult to memorize and use in clinical setting [5, 10]. Therefore, a simpler adaptation of the ETDRS classification proposed in [14] is now widely used. This classification system proposes scales to grade diabetic retinopathy (Table 2.1) and macular oedema (Table 2.2).

Table 2.1.: Diabetic retinopathy classification according to [14]

Classification	**Features**
Apparently no DR	Without alterations
Mild non-proliferative DR	Only microaneurysms
Moderate non-proliferative DR	More than only microaneurysms but less than severe non-proliferative DR
Severe non-proliferative DR (If instead of considering "or" use "and" the DR is considered very severe non-proliferative)	Any of the following: more than 20 intraretinal hemorrhages in each of four quadrants; venous beading in at least two quadrants; intraretinal microvascular abnormalities (IRMA) in at least one quadrant and no signs of proliferative DR
Proliferative DR	One or more of the following: neovascularization; vitreous or pre-retinal hemorrhage

2.3.3. Treatment

During the initial stages of diabetic retinopathy, no treatment is needed, unless macular oedema is present. Controlling levels of blood sugar, blood pressure and blood cholesterol is important in slowing the progression of any type of retinopathy or maculopathy and it prevents the need for future treatments [10].

Table 2.2.: Diabetic macular oedema classification according to [14]

Classification	Features
Diabetic macular oedema apparently absent	No apparent retinal thickness or hard exudates in posterior pole
Mild diabetic macular oedema	Some retinal thickening and presence of hard exudates in the posterior pole but distant from the macular center
Moderate diabetic macular oedema	Some retinal thickening and presence of hard exudates approaching the macular center but not involving it
Severe diabetic macular oedema	Some retinal thickening and presence of hard exudates involving the macular center

Proliferative diabetic retinopathy is the most serious treatable stage of the pathology. At this stage the treatment depends on the specific problems of the retina and includes focal and scatter laser treatments and vitrectomy. Laser treatments can stop or slow the leakage of blood and fluid in the eye, because leaks from abnormal blood vessels are reduced with laser burns. With laser treatments, the main goal is to prevent further vision loss. However, if patients have vision problems before surgery, they may not recover completely normal vision after the procedure. The vitrectomy is applied when there is a severe bleeding in the middle of the eye (vitreous). This procedure has to be done in a surgery center or hospital using local or general anesthesia. During a vitrectomy, blood is removed from the vitreous and replaced with a salt solution that helps in maintaining the eye's normal shape.

These surgery procedures often slow or stops the diabetic retinopathy progression, but it is not a cure. Since diabetes is a lifelong condition, future retinal damage and vision loss are possible. Therefore, control and prevention by doing some regular exams is very important to stop the progress of the disease and avoid repetition of treatments [7, 10].

2.4. Diabetic retinopathy screening

Diabetic retinopathy is one of the most prevalent but preventable blinding diseases. Some studies [12, 13] have demonstrated that the blinding complications from diabetes can be largely prevented medically, by glycemic and blood pressure control, as well as by early detection and timely treatment of diabetic retinopathy with adequate techniques. Actually, the treatment is most effective before the eye disease becomes symptomatic, that is, before the macular area is affected and thus, also the vision [15]. In Portugal, diabetes affects the vision of at least 25 000 patients and 13 000 are totally blind due to DR. Every year, more than 3000 patients have

irreversible vision loss, and 90% of these cases can be preventable by an adequate metabolic control and treatment [16].

Over the last few years, in several developed countries, there has been an effort to implement screening for diabetic retinopathy with the aim of detecting it early and, thus, prevent visual impairment and blindness in those with diabetes. Screening guidelines have been developed by professional organizations such as the Sociedade Portuguesa de Oftalmologia [16] and the American Diabetes Association [17]. In Europe, the St Vincent Declaration Working group suggests that the aims of screening are mainly [7]: diagnosis of sight-threatening retinopathy requiring treatment; detection of mild diabetic retinopathy needing follow-up but no treatment; diagnosis of concomitant eye disease such as cataract or glaucoma. In USA, the American Diabetes Association [17] establishes screening guidelines related to the examination frequency as summarized in Table 2.3.

Table 2.3.: Recommended eye examination schedule for patients with diabetes (adapted from [17])

Type of diabetes	**First retinal examination**	**Follow-Up**
Type 1	3-5 years after diagnosis	At least yearly
Type 2	At time of diagnosis	At least yearly
Before pregnancy	Before conception and early in the first trimester of pregnancy	Less than severe NPDR, every 3-12 months; otherwise, every 1-3 months

Clinical trials have demonstrated the retinopathy screening benefits. Actually, vision impairment and blindness can be preventable using existent technology and the associated costs are much smaller than the costs achieved with the blind patients [16]. However, current care frequently falls far below screening recommendations due to the insufficient number of eye care specialists. The development of digital imaging and, more recently, digital retinal photography could be a way to overcome the barriers to access for diabetic retinopathy screening.

Screening methods include direct and indirect ophthalmoscopy, stereoscopic color film fundus photography, mydriatic or nonmydriatic digital color, and monochromatic photography. With the increasing rate of diabetic patients, the favorite examination for the diabetic retinopathy screening have been the digital color photograph as it is a non-invasive, fast and easy to use procedure. In fact, the images can be obtained by a trained health professional and posteriorly observed by an ophthalmologist or forwarded to a reading center for interpretation and grading [15].

Although retinal imaging programs are important in improving access to care and identifying patients who need further evaluation, they do not replace comprehensive eye exams by ophthalmologists. A full evaluation is required when a screening

retinal photograph is unreadable and for follow-up the abnormalities detected by the screening system.

2.5. Image Acquisition Protocols

Since the development of fundus camera, its daily use in clinical practice has become a reality, leading to some issues about which acquisition protocols may assure the highest sensitivity and specificity for the early identification of sight-threatening pathologies.

The gold standard for the diabetic retinopathy detection and classification is 30-degree stereoscopic color fundus photographs in 7 standard fields, as defined by the ETDRS group [13]. The seven fields are illustrated in Figure 2.5 and Figure 2.6 and described in Table 2.4. For the diabetic retinopathy detection, this technique has superior sensitivity and specificity than direct and indirect ophthalmoscopy [15]. However, its practical usefulness is reduced by the complexity of acquisition procedure, by the evaluation complexity of images for the ophthalmologist, and by the discomfort for the patient involved in the procedure. Therefore, seven-field stereoscopic fundus photography is a good gold standard but is not suitable for widespread implementation [5].

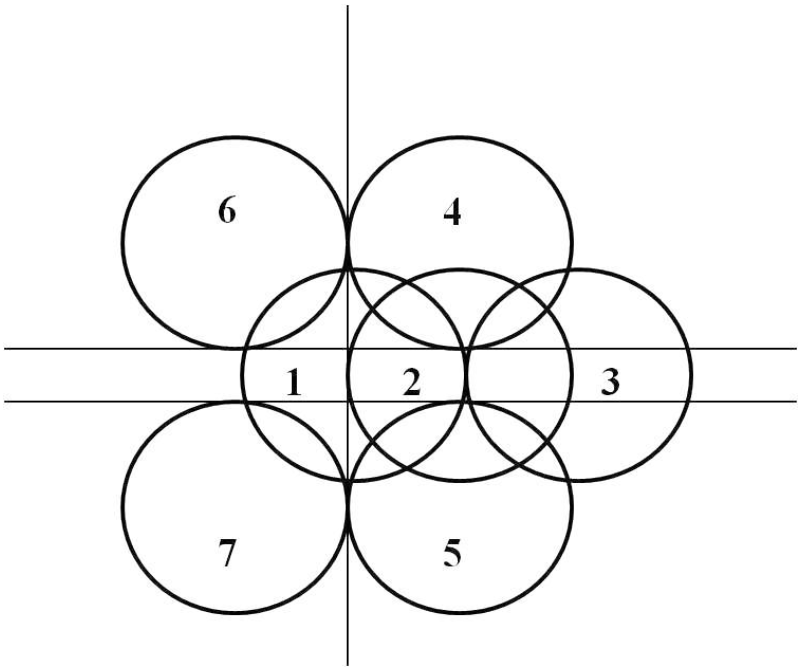

Figure 2.5.: Standard ETDRS 7-fields schematic for left eye (adapted from [18])

With the development of digital retinal photography and the increasing in fundus camera quality, a number of protocols simpler than ETRDS protocol have been proposed and validated against that gold standard.

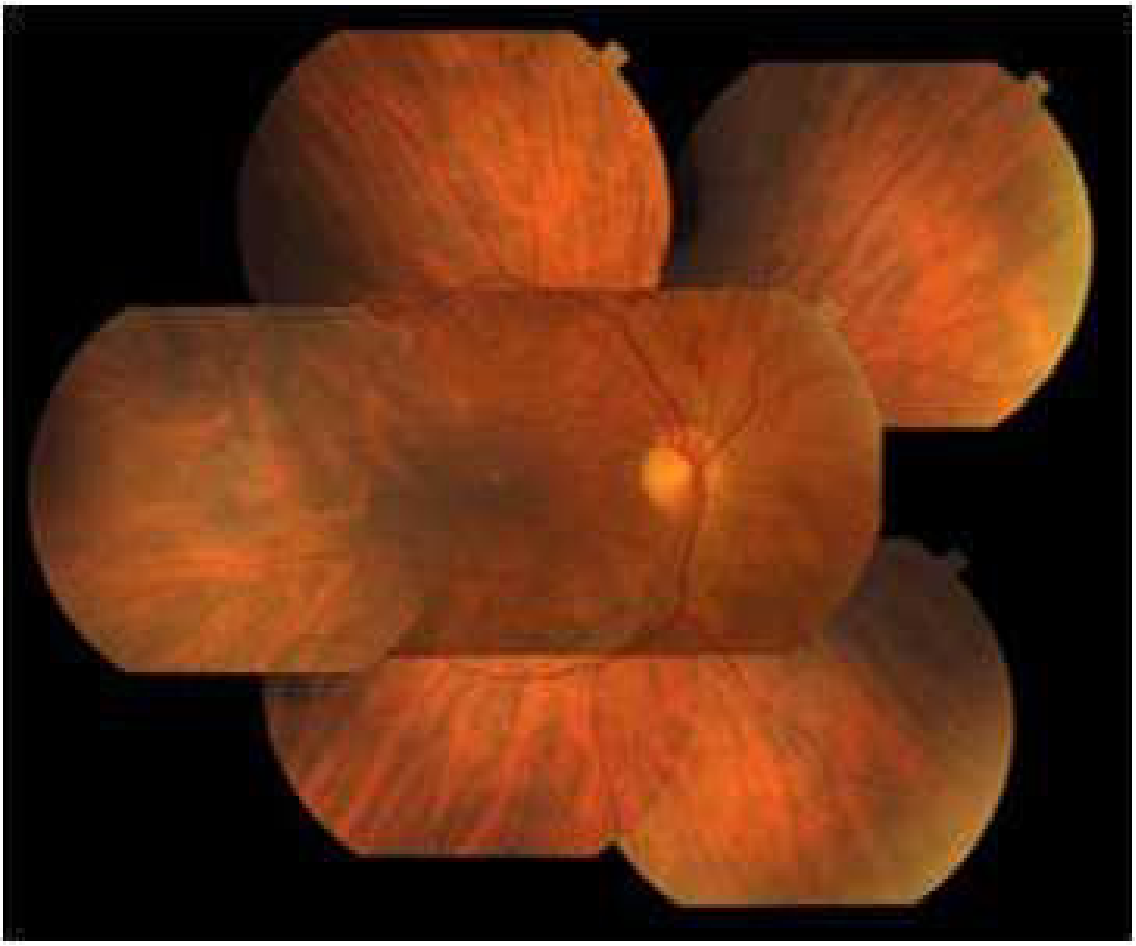

Figure 2.6.: 7 mydriatic ETDRS 30-degree color fundus fields of right eye (adapted from [19])

For instance, from the EURODIAB IDDM Complications Study [20] a wide angle retinal photography was developed. In EURODIAB protocol two 45-degree color photographs of each eye are taken. One is macula centered, positioned such that the exact center of the optic disc lay at the nasal end of the horizontal meridian of the field of view. The other is the disc/nasal field and is acquired such that the optic disc is positioned one disc-diameter from the temporal edge of the field, on the horizontal meridian.

The Joslin Diabetes Eye Health Care Model also developed the Joslin Clinic protocol [18] with the aim of reducing patient discomfort and providing an easy picture taking by non-certified photographers. The Joslin Clinic protocol consists of three field nonmydriatic 45-degree photographs, represented in Figure 2.7 superimposed to the ETDRS protocol.

Several other imaging procedures have been developed and validated in the Fundus Photograph Reading Center from University of Wisconsin [21].

Table 2.4.: Early Treatment Diabetic Retinopathy Study Seven Standard Field Descriptions

ETDRS field	Field description
Field 1	Optic Disc: 30° field focused centrally on the optic disc
Field 2	Macula: 30° field focused on the macula center
Field 3	Temporal to Macula: 30° field focused so the nasal edge of the field crosses the macula center
Field 4	Superior temporal: 30º field focuses so the field lower edge is tangent to a horizontal line passing through the optic disc upper edge and the field nasal edge is tangent to a vertical line passing through the optic disc center
Field 5	Inferior temporal: 30° field focused so the field upper edge is tangent to a horizontal line passing through the optic disc lower edge and the field nasal edge is tangent to a vertical line passing through the optic disc center
Field 6	Superior nasal: 30° field focused so the field lower edge is tangent to a horizontal line passing through the upper edge of the optic disc, and the field temporal edge is tangent to a vertical line passing through the optic disc center
Field 7	Inferior nasal: 30° field focused so the field upper edge is tangent to a horizontal line passing through the lower edge of the optic disc, and the field temporal edge is tangent to a vertical line passing through the optic disc center

According to Portuguese guidelines [16], two 45-degree color photographs taken from ETDRS protocol fields 1 and 2 (Figure 2.8) should be used in the systematic screening for DR.

2.6. Automatic systems related to diabetic retinopathy studies

The combination between the large number of diabetic patients, the growing diabetes incidence in the population and the facility of acquiring digital retinal images, has made the development of novel image analysis methods an expanding research area. From the clinical perspectives, image processing and analysis algorithms can be conceived for the diabetic retinopathy diagnosis improvement in three domains [22]:

- Image enhancement: retinal images taken at standard examinations usually present noise, poor contrast and variability inter-image and intra-image. The

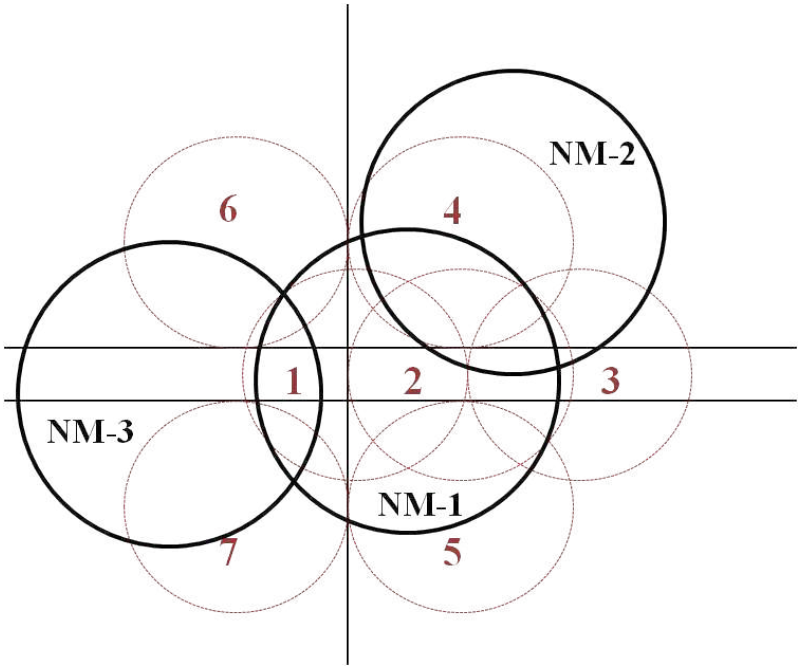

Figure 2.7.: Joslin Clinic nonmydriatic fields (black circles) superimposed to the 7 standard ETDRS protocol (dotted red) (adapted from [18])

Figure 2.8.: Color fundus photographs from right eye (left) and left eye (right) taken according to the Portuguese guidelines for DR screening

use of different fundus cameras, illumination, acquisition angle and retinal pigmentation is responsible for the inter-image variation. The intra-image variation is a consequence of the light diffusion, the presence of abnormalities, variation in fundus reflectivity and fundus thickness [23]. Therefore, techniques for improving contrast and sharpness, reducing noise and normalizing color are required.

- Mass screening: retinal image acquisition for systematic screening of DR has been becoming a common practice. A huge number of images results from these screening programs and frequently the number of specialists is insufficient for analyzing all these images. Moreover, in a screening setting, the number of images without any DR sign is typically over 90% [2]. Therefore, an automated system that can exclude images with no signs of DR can improve efficiency in

preventing DR.

- Monitoring the pathology: Comparing images taken at different examinations allows the evaluation of a treatment or the disease progression. Though, this is a time-consuming task and open to human error. Therefore, computer tools including automatic registration and evaluation of changes between images could provide a more effective disease monitoring [24].

The development of digital retinal photography makes possible the creation of computer-based systems to be used in screening programs and save the workload of ophthalmologists, letting hospitals and eye care specialists use their resources in other important tasks. In fact, an automatic screening system would embrace more people and more often, since it would be more inexpensive than screening by humans. Another advantage of an automatic screening system is its immunity to human weaknesses such as fatigue, sickness and dispersion in ophthalmologists diagnose making, decreasing the DR diagnosis error.

As referred above, the main goal in developing a computer-based screening system is to exclude the normal images, since they represent the most part of the screening images. Then, only images deemed suspect by the system would be delivered to a human expert for further classification. Therefore, if the screening first phase is performed automatically by a computer, it must have as high sensitivity as possible so that no pathological fundus images are missed by the computer. The British Diabetic Association recommends that any procedure for screening DR should have at least 80% sensitivity and 95% specificity [25]. Sensitivity means the percentage of abnormal fundus images classified as abnormal by the procedure. Specificity means the percentage of normal fundus images classified as normal by the procedure.

During this study, it will be possible to notice that several approaches for developing a computer based system to be applied in retinopathy screening have been proposed in the literature. These algorithms consist of image processing and analysis techniques used to normalize, segment and extract information from retinal images. Frequently, they also have classifiers aiming to classify the fundus image regions, which are the diabetic retinopathy characteristic lesions and the eye fundus anatomical structures. However, an automatic system ready to be applied in clinical practices is not available yet.

This study was based on such findings and recommendations and, hence, the development of novel algorithms for being applied in fundus images concerning the DR early diagnosis is the focus of this thesis.

3. Multi-Agent Systems

In recent years, multi-agent systems (MAS) have attracted much researchers´ attention in many fields of the computer science and engineering applications. Theories, programming languages and tools have been developed for explaining, modeling, and developing MAS to be applied in many different applications such as workflow and business process management, information retrieval and management, electronic commerce, human-computer interfaces, virtual environments, social simulation [26].

The MAS are composed of multiple interacting intelligent elements, called agents. These kinds of systems can be used to solve complex problems that are difficult or impossible for an individual agent to solve. Therefore, the main goal of multi-agent systems's research is to find methods that allow the building of complex systems composed of autonomous agents who, while operating on local knowledge and possessing only limited abilities, are nonetheless capable of enacting the desired global behaviors [27].

In this chapter the constituents of a multi-agent system as well as their properties, fundamental for understanding the developed algorithms described in the next chapters, are referred. At the end of the chapter, a literature review related to the use of MAS in medical images is presented.

3.1. MAS elements

A multi-agent system is generally composed by a set of agents situated in a virtual or real environment. The agents interact with each other to coordinate their behavior in a particular organization that can be dynamic and/or self-adaptive. The self-adaptation results from the agents' interaction to adapt themselves to the environment and its constraints. The differentiation of the agents and their complex interaction allow the emergence of a global result. This global result influences the agents of the system, making them converging towards a common and often unexpected solution that is not comprehended at the individual level. The dynamic of the system results from an emergent phenomenon giving additional functionality that each agent cannot provide individually. For instance, the organization of an ant colony provides the shortest path between their nest and a food point.When the ants walk to and from the food source, leave some amount of pheromone on the ground and this pheromone trail is used by ants to communicate with each other. Ants probabilistically prefer to follow a direction regarding the quantity of pheromone on

it. Therefore, this process could be considered as a positive feedback loop, as the more ants follow a trail, the more attractive this trail becomes to the other ants. This phenomenon would be impossible to get through the work of a single ant. It is the whole (environment + agents + interactions) that allows an organization to emerge [28].

According to Ferber [29]:

> *"The term 'multi-agent system' (or MAS) is applied to a system comprising the following elements:*
>
> *(1) An environment, **E**, that is, a space which generally has a volume.*
>
> *(2) A set of objects, **O**. These objects are situated, that is to say, it is possible at a given moment to associate any object with a position in **E**. These objects are passive, that is, they can be perceived, created, destroyed and modified by the agents.*
>
> *(3) An assembly of agents, **A**, which are specific objects ($\boldsymbol{A} \subseteq \boldsymbol{O}$) representing the active entities of the system.*
>
> *(4) An assembly of relations, **R**, which link objects (and thus agents) to each other.*
>
> *(5) An assembly of operations, **Op**, making it possible for the agents of **A** to perceive, produce, consume, transform and manipulate objects from **O**.*
>
> *(6) Operators with the task of representing the application of these operations and the reaction of the world to this attempt at modification, which we shall call the laws of the universe."*

Figure 3.1 illustrates a schematic with the typical structure of a MAS. The latter contains several agents, each one with different perceptions and actions over the environment, represented by its own sphere of influence. In some cases, these spheres of influence may overlap giving rise to dependency relationships between the agents [26]. The MAS can contain more than one organization of agents and so, it should be described on organizational concepts such as roles (function/position), groups (communities), tasks (activities) and interaction protocols (dialogue structure). There are several generic multi-agent structures which have been studied, considering the interaction between the agents and the interaction between the agents and their environment. The Agent/Group/Role model [31] formalizes the organization of groups of agents. The IRM4MLS [32] model is proposed to generalize the interaction of agents which are not in the same groups/levels.

3.1.1. Definition of Agent

Definition of agent has been vague. Some definitions found in literature are:

> *"An agent is a computer system that is situated in some environment, and that is capable of autonomous action in this environment in order to meet its design objectives." [26]*

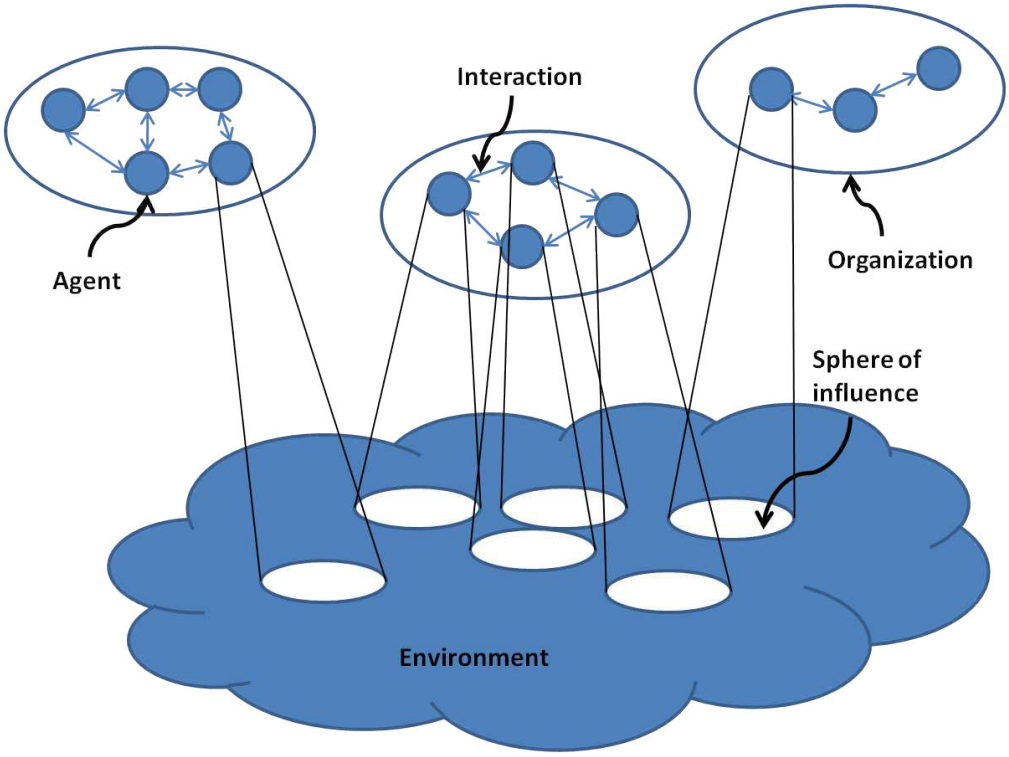

Figure 3.1.: Typical structure of a multi-agent system (adapted from [30])

> *"An agent is a physical or virtual entity*
> *(a) which is capable of acting in an environment,*
> *(b) which can communicate directly with other agents,*
> *(c) which is driven by a set of tendencies (in the form of individual objectives or of a satisfaction/survival function which it tries to optimize),*
> *(d) which possesses resources of its own,*
> *(e) which is capable of perceiving its environment (but to a limited extent),*
> *(f) which has only a partial representation of this environment (and perhaps none at all),*
> *(g) which possesses skills and can offer services,*
> *(h) which may be able to reproduce itself,*
> *(i) whose behavior trends towards satisfying its objectives, taking account of the resources and skills available to it and depending on its perception, its representations and the communications it receives." [29]*

Despite of not being consensual the definition of agent, there are two essential capabilities that these computer systems have – autonomy and interaction between each other (there are no agents without MAS) [26]. The first characteristic enables them to perform some autonomous action in which they decide for themselves what they need to do in order to satisfy their design objectives. The second characteristic consists not simply in exchanging data between them, but also in engaging in analogues

of the kind of social activity that we all are involved in every day of our lives: co-operation, coordination, and negotiation [26] . Moreover, the definitions above refer that an agent is situated in an environment, in which the agents should have the ability to extract the information they need and act on it in an autonomously way. Therefore, each agent must have the appropriate sensors and actuators to perform the tasks for which it was designed (Figure 3.2).

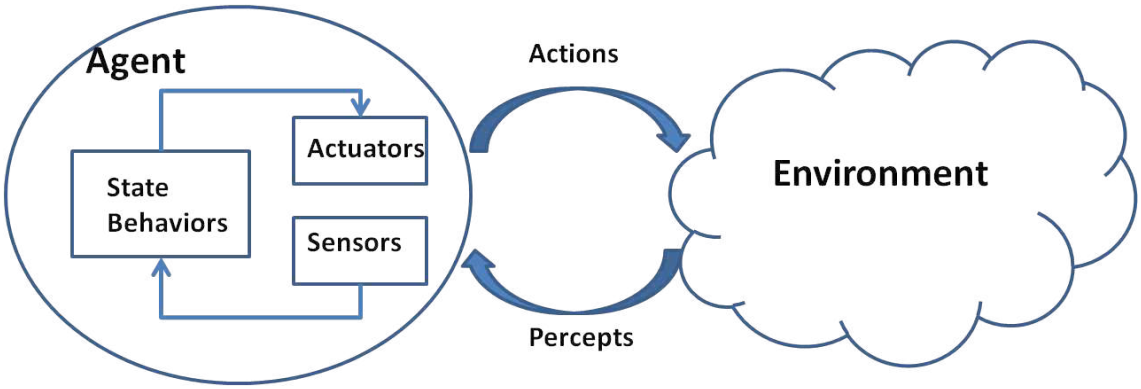

Figure 3.2.: An agent and its environment. The agent percepts sensory input from the environment and produces as output actions that affect it.

Wooldridge [26] defines an agent as a computer system based on software with the following properties:

- Autonomy. The agents work without direct human or other agents intervention and possess some control over their actions and internal state;
- Reactivity. The agents percept their environment and rapidly respond to changes that occur in it.
- Proactiveness. The agents can take initiative and exhibit goal-directed behavior.
- Social ability. The agents interact with other agents and possibly with humans.

As it is possible to see in the next sections of this chapter, the agents are frequently created without considering all these properties, in particular the proactiveness.

3.1.2. Types of agents

Based on the agent properties described by Wooldridge, it is possible to classify the agents in two types: reactive and cognitive. The frontier between these two categories is arbitrary. The cognitive agents have a symbolic representation of their environment. They have thus a high level of understanding of their environment and they know the purpose for which they cooperate. This understanding can be

determined, for example, by the Believe/Desire/Intention architecture [33] inspired from psychology researches [34]. On the other hand, a reactive agent has only a limited vision about its environment. It lacks the capacity to interpret and is limited to its perceptions. Therefore, it reacts to stimuli and can influence its environment by producing non-interpreted information. The reactive agents do not know the system global function. This is also often the case of cognitive agents. A schematic with these two types of agents is illustrated in Figure 3.3.

Approaches using cognitive agents can usually put together different and complex behaviors and thus produces high-level results. The problem of using such agents is that the collaborative behavior between them should be established by approximate heuristics, and are often difficult to implement. For instance, in image processing this would consist of putting together several algorithms of different natures. Since these approaches are of different basis, it is difficult to combine them by means other than using heuristics. Ultimately, for a generalized segmentation goal, the high level processes are difficult to relate without using heuristic or questionable parameters [28].

Approaches constituted by reactive agents permit a better identification of the agents' role and their cooperation, since agents operate at the lowest level. Actually, for image processing purposes, approaches consist of agents with low granularity influence on the environment and among themselves, are fundamentally more interesting, but are not devoid of difficulties. Agents can then be based on common fundamental properties of the image processing and their interactions seem more natural. However, these types of approaches are far from being simply procedural to reach a goal. The problem of the emergent approaches is the degree of unpredictability of the results, resulting from the agent interaction that is simple yet complex. Even the mathematics cannot always help in the prediction of the multi-agent system convergence, in so far as a single agent or a single critical event during the system evolution can switch its future where mathematicians saw the system moving towards equilibrium. Considering a system consisting of several layers of agents, even after having developed each of these layers as emergent, it is difficult to imagine a global emergent layer by making them interacting together. Therefore, it is common to develop side approaches based on meta reasoning, and formalizing how the system is organized and self-organizing, encapsulating the emergent / creative / pro-innovative property of the system for defined and specific tasks, and through observed natural emergent processes [28]. Then, emergent phenomena from agent interactions are framed into a defined space of possible solutions, by structuring the environment/system in which they evolve [35].

Classifying the agents as cognitive and reactive, though essential and sufficient for the scope of this study, it is a very limited classification for understanding the multi-agent system potentialities. In fact, more detailed and embracing classifications can be found in literature, such as Nwana et al.[36] study which proposes a typology of agents that identifies seven distinct dimensions for classification. Thus, agents can be static or mobile, deliberative (cognitive) or reactive. They can possess autonomy,

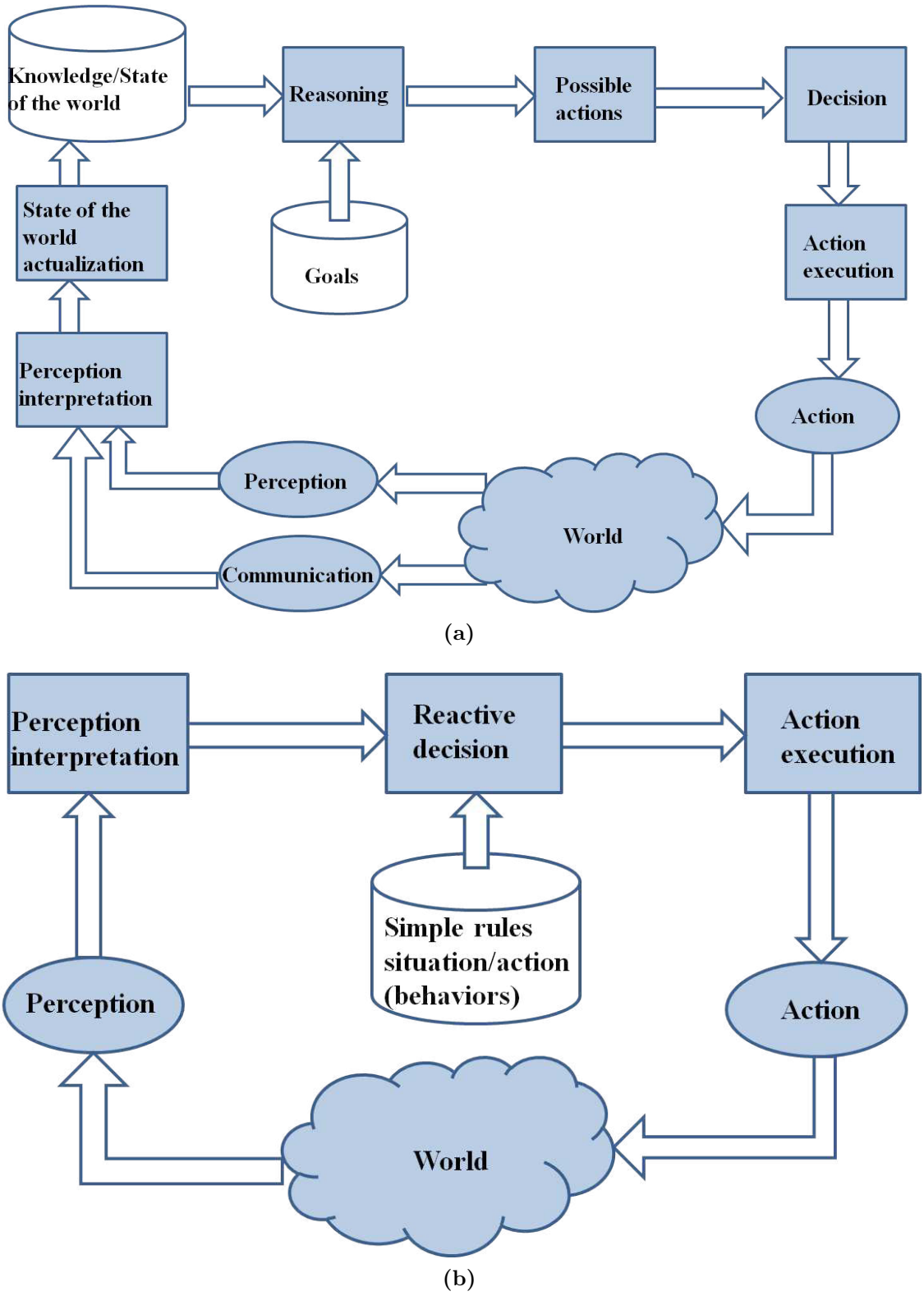

Figure 3.3.: General schematic of typical agent architecture. a) Cognitive architecture; b) Reactive architecture (adapted from [30])

cooperation mechanisms and learning capacities. Moreover, they are also classified according to their function and can be hybrid, that is, combine two or more agent philosophies in a single agent.

From the combination of the autonomy, cooperation and learning characteristics, Nwana et al. [36] identifies four types of agents as illustrated in Figure 3.4.

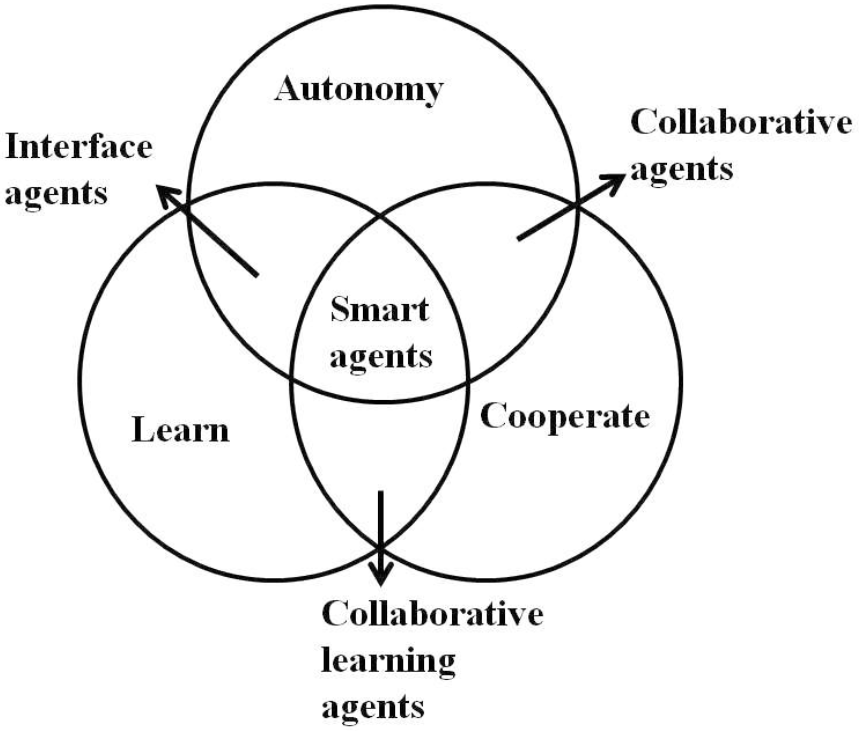

Figure 3.4.: Category of agents defined by Nwana [36]

It is important to emphasize that these distinctions are not definitive. Several types of agent can be used for the same application. However, for this study the reactive agents are the most important and the predominant in the practical chapters.

3.1.3. Environments

The agents are situated in a particular environment, percept its information and perform actions on it. The environment characteristics are important to define the agent architecture and its method of operation. Before designing an agent, a careful consideration of possible perceptions and actions and the complexity of the agent tasks is required [30].

According to Russel and Norvig [37], the environment can be classified based on the following properties:

- Accessible versus inaccessible. In an accessible environment the agent can acquire, through its sensors, up-to-date, complete and accurate environment information.
- Static versus dynamic. A static environment remains unchanged except by the influences of the agents' actions. On the other hand, a dynamic environment has other processes operating on it, and hence there are changes occurring beyond the agent's control.
- Deterministic versus non-deterministic. In a deterministic environment every action results in a single guaranteed effect and there is no uncertainty about the state that will result from performing an action.
- Discrete versus continuous. The environment is discrete if there is a finite number of possible perceptions and actions in it.

At this thesis scope, the environment will be mainly constituted by images, that represent an accessible, static, deterministic and discrete environment, considering the above properties.

Environmental properties have a role in determining the complexity of the agent design process, but they are by no means the only factors that play a part. The second important property that plays a part is the nature of the interaction between agent and environment.

3.1.4. Interaction

According to Ferber [29] *"an interaction occurs when two or more agents are brought into a dynamic relationship through a set of reciprocal actions. (...) The agents interact through a series of events, during which they are in contact with each other in some way, whether this contact is direct or takes place through another agent or through the environment."* Therefore, when talking about interaction, any kind of mechanisms allowing some individuals to orchestrate and influence each other's actions can be referred. These interactions mechanisms are crucial elements in a social organization. They are represented by sophisticated patterns of agent behaviors such as coordination, negotiation and communication.

Coordination means the act of working together with the aim of achieving a common goal (task, agreement). The coordination between agents can occur in cooperative or competitive environments. At the cooperative environment, agents act to increase the overall utility function of the system and not their personal utility. Moreover, they are more committed to increase the global performance instead of the individual performance. On the contrary, at the competitive environments, agents possess its own schedule and motivation and they are only interested in their personal satisfaction. The competitive environment is mostly used in scenarios involving acquisition of products and services and, thus, is not relevant to the present work.

During the coordinating actions of the goal-driven agents some conflicting goals typically appear. That is, sometimes, not all agents may be able to satisfy their respective goals simultaneously. This can happen, for example, with regard to contested resources or with multiple demands on an agent's time and attention. Therefore, conflict resolutions are required and this can be done by negotiation mechanisms between agents. Negotiation is thus the process by which two or more entities communicate in a certain way, to reach a joint decision. There are several negotiation mechanisms, from which the most common are auctions, argumentation, game theory and heuristic approximations.

Hereupon, for interacting and cooperating with each other, agents should have some communicative abilities. The communication is essential for an agent organization, since it is because agents communicate that they can cooperate, coordinate their actions, carry out tasks jointly and so, became truly social beings [29]. There are essentially two ways of communication: direct and indirect. Examples of direct communication include shared blackboards and message-passing. In order to message-passing, each agent must be able to: deliver and receive messages which can be represented by strings or objects; parse the messages to correctly decode the message to its parts (syntactic level); and understand the information contained in the messages, that is, the ontology describing the symbols must be shared or explicitly expressed among the agents (semantic level). Indirect communication involves the implicit transfer of information from agent to agent through modification of the environment. An example of indirect communication has taken inspiration from social insects' use of pheromones to mark trails or to recruit other agents for tasks (see chapter 4) [38].

3.2. System behavior

In order to infer the potentiality of the MAS as an organization of individual entities, it is important to understand the meaning of two concepts already referred above: emergence and self-organization. Emergence and self-organization refer to processes and phenomena that can be observed in nature. Examples are brain-cells producing "intelligence" while networking, food foraging of ants, honey bees organizing their comb, magnetic fields, thermodynamics systems. Despite these two concepts often appear as synonyms in the literature, some authors agree that they correspond to different characteristics of a system's behavior [39, 40].

3.2.1. Emergence

The emergent phenomena have been studied since the Greek antiquity and can be found in some ancient writings with the notion of "the whole before the parts" or "the whole is more than all the parts". This phenomenon exists in a large number of scientific fields, e.g. psychology, biology, physics and many more [39, 41].

Wolf and Holvoet described in their paper [40]: *"a system exhibits emergence when there are coherent emergents at the macro-level that dynamically arise from the interactions between the parts at the micro-level. Such emergents are novel with respect to the individual parts of the system."* In fact, from local interactions of small, "simple" pieces, or agents at the micro-level, a global behavior "emerges" at the macro-level. And this global behavior is not evident in the parts alone. The macro-level referred here corresponds to the system as a whole, and the micro-level considers the system from the point of view of its individual parts. The emergent phenomenon requires at least these two levels, and needs to be observable at least at the macro level. In general, there are some interdependencies between the levels, because the macro level constrains the micro level and the micro level causes the macro level.

Some properties that the emergent systems must show are [40, 41]:

- Novelty, since something new is produced at the macro-level that did not exist previously, i.e, the individuals at the micro-level have no explicit representation of the global behavior;
- Coherence, in the sense that the global system behavior has its own identity but it is strongly linked to parts that produce it.
- Decentralized control, because it uses only local mechanisms to influence the global behavior. There is no central control, i.e. no single part of the system directs the macro-level behavior. The actions of the parts are controllable but the whole is not directly controllable
- Robustness and flexibility, because emergents are relatively insensitive to perturbations or errors. Increasing damage will decrease performance, but degradation will be "graceful": the quality of the output will decrease gradually, without sudden loss of function. The failure or replacement of a single entity will not cause a complete failure of the emergent. This flexibility makes that the individual entities can be replaced, yet the emergent system can remain.

3.2.2. Self-organization

The concept of self-organization is more widely used than the one of emergence, but it can be also interpreted in different ways. Generally, "self-organization" serves as a concept for a variety of natural self-organizing systems. Moreover, it is used to classify distributed computer systems and algorithms that seemingly "exhibit" self-organizing properties. Presently there are two possibilities to engineer self-organizing systems: take inspiration from nature or trial and error [39].

In fact, several examples of self-organizing systems can be found in nature, both in the non-living system (galaxies, stars) and in the living world (cells, organisms, ecosystems). Natural self-organizing systems are composed by a large number of individuals who interact and coordinate to achieve tasks that overcome by far their

capabilities as single individuals. The social behavior of humans is also self-organized and allows the emergence of complex global behaviors. Human beings typically work with local information and through local direct or indirect interactions producing complex societies.

Among artificial multi-agent based self-organizing systems, a lot of the self-organized phenomena found in nature provide a useful inspiration to solve computer science problems. Nevertheless it is also possible to observe applications coming from the establishment of new mechanisms and whole infrastructures supporting self-organization of artificial systems [41].

Wolf and Holvoet [40] described that, "*self-organization is a dynamical and adaptive process where systems acquire and maintain structure themselves, without external control.*" In other words, in a self-organizing system, the organization is intrinsic and results from internal constraints or mechanisms, due to local interactions between its components. For the self-organizing systems the main characteristics are [40]:

- Increase in order – Organization can be seen as the arrangement of selected parts so as to promote a specific function. This restricts the behavior of the system in such a way as to confine it to a smaller volume of its state space. This smaller region of state space is called an attractor. In essence, an organization can be looked at as an increase in the order of the system behavior which enables the system to acquire a spatial, temporal, or functional structure. A system with no order cannot exhibit useful behavior. But also a system with too much order can have this problem. It is possible that processes organize themselves into conditions so complex that no usable functionality can result from it.
- Autonomy referring the absence of external control, as the system needs to organize itself without interference from outside.
- Adaptability or robustness with respect to changes – in self-organizing systems, robustness is used in terms of adaptability in presence of perturbations and change. A self-organizing system is expected to cope with that change and to maintain its organization autonomously. In other words, a self-generated, adaptive behavior is needed, and taking into account past experiences can be helpful.
- Dynamical, i.e. far-from-equilibrium - An essential property of self-organization is that it is a process. Over time, there is an increase in order, i.e. a dynamic towards more order.

3.2.3. Stigmergy

A combination of emergence and self-organizing phenomena often occurs in dynamical systems. In the case of dynamic self-organizing systems with decentralized control and local interactions, the notion of emergent properties is closely linked

with self-organization (Figure 3.5). Examples of such a system can be observed in social insects as ants, bees, wasps and termites. In these societies, the emergent collective behavior is the outcome of a process of self-organization, in which insects are engaged through their repeated actions and interactions with their surrounding environment. The interaction with the environment involves the mechanism of stigmergy, in which the environment is used as a medium of inscription of past behaviors effects to influence the future ones. That is, the individuals of the system use the environment to communicate and interact indirectly with each other. This mechanism also represents a self-catalytic process, since the more a process occurs, the more it has chance to occur in the future. More generally, this mechanism shows how simple systems can produce a wide range of more complex coordinated behaviors, simply by exploiting the influence of the environment [42].

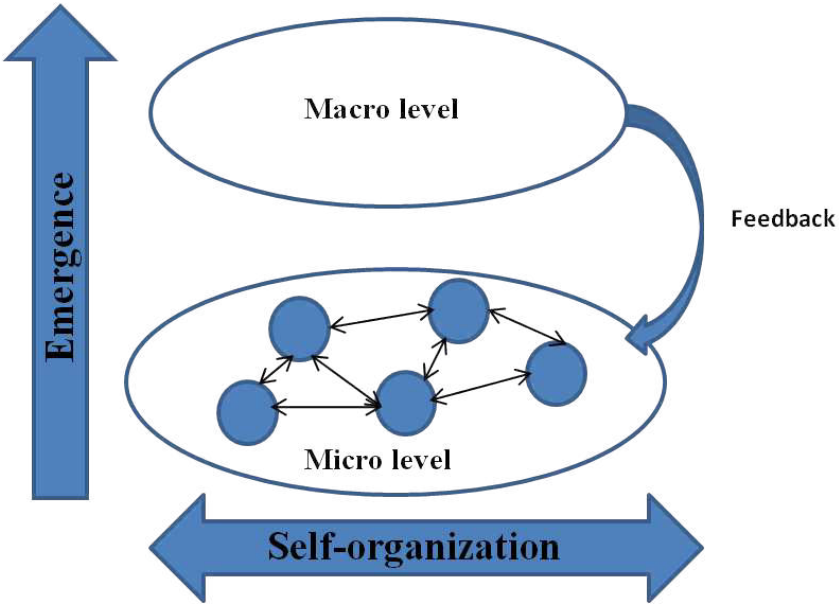

Figure 3.5.: Self-organization and emergence

3.3. MAS applied in image processing – a literature review

Within the image processing domain, MAS can be used essentially in two ways [43]: 1) they can be used to exploit different macro levels results provided by image processing algorithms, using negotiation among agents [44, 45, 46], or 2) they can be used as artificial social systems, composed of entities, usually reactive and autonomous, which exploit micro level image processing results [43, 47, 48], adapted to the intrinsic image processing issue.

For this application, the environment often plays several roles. The micro-level corresponds to a medium of interaction where the agents communicate and interact indirectly via changing the environment. At the macro-level, it can represent a collective memory. By saving the set of modifications made by interacting entities, the environment memorizes the reproduced dynamics which will influence future interactions. Also at the macro-level, it can control the micro-level because, as a feedback, the environment may be modified by an observer for influencing the dynamics of the micro-level and its global trajectory.

There are some works described in the literature that associate MAS with image processing. In this domain, almost all the MAS models include mechanisms for cooperation. The global task of the system is decomposed into sub-tasks assigned to the agents. Each agent can communicate with other agents to ask for a service, to give relevant and necessary information to the stability of the system, to send new constraints to meet or to give orders. The cooperation between all the agents allows the emergence of a global behavior, that is, in this case, the segmentation of an image or the object recognition.

In Haroun et al. [44] approach, the fuzzy C-mean algorithm is initially used to segment the image in an imprecision way. Then, a region growing algorithm designed in a massive multi-agent environment is proposed. The agents are of two types: one image agent and several region agents. The image agent controls the region agents by creating and destroying them or by activating and deactivating their behaviors. The region agents are initially positioned over a seed pixel and their behaviors can be three: growing, negotiation and fusion. A schematic of this approach is represented in Figure 3.6. The use of agents and their cooperation allows a better quality of segmentation. The segmentation by region growing is done in parallel since all regions grow simultaneously in the image. This prevents that some pixels are added to the first developed region.

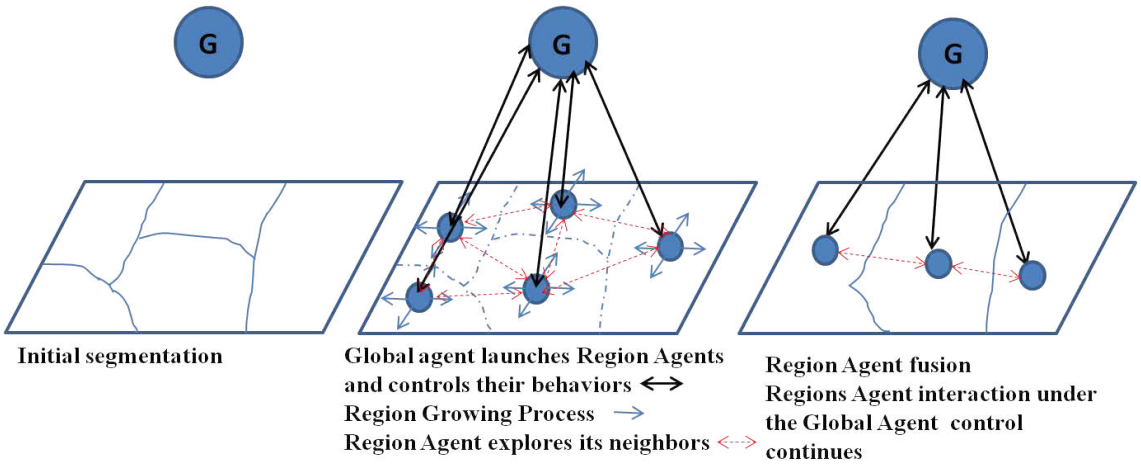

Figure 3.6.: Schematic representation of a MAS approach [44] with centralized control

A MAS model including several region agents controlled by a global agent was also described by Benamrane and Nassane [46]. In this approach the global agent is responsible for the initial segmentation by a region growing approach. Then, on each region it creates and launches the region agents which will cooperate in a synchronous and parallel manner to do the required fusions according to some criteria. The fusion steps are done iteratively and under the coordination of the global agent. The proposed approach presented good results in Magnetic Resonance Imaging (MRI), particularly in the tumor regions segmentation. However, the authors referred its execution time to be high.

Duchesnay et al. [48] presented an approach based on an agents'society organized as an irregular pyramid where agents are situated in the image and perform local cooperation and local adaptation. The initial environment is constituted by two images: a region segmentation image obtained by the quadtree method, and an edge image resulted from a succession of edge procedures. Each level of the pyramid is an agent organization in which the region agents stand in an area of the image and the edge agents represent an edge primitive. The agents run a sequence of behaviors at each level: territory marking and feature extraction; exploration to determine the neighbors; merging planning based on similarity features; and finally, cooperation and negotiation mechanisms with each other to decide on the fusion, and destruction /reproduction to create new region agents in higher levels of the pyramid. Therefore, the proposed method does not require substantial tuning effort and it is completely autonomous. Furthermore, there is no need of prior information to segment images, and the method can be applied in different kinds of images. Figure 3.7 shows a simple representation of this approach.

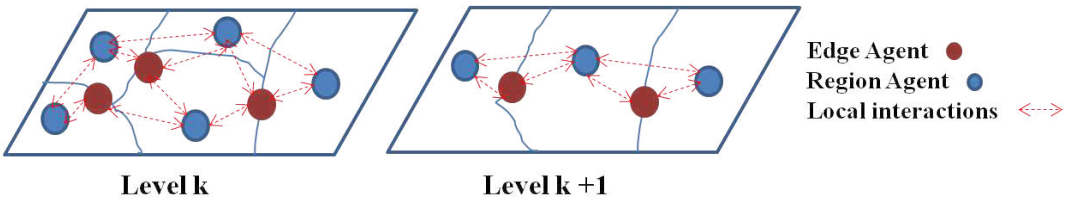

Figure 3.7.: Schematic representation of a MAS approach [48] with decentralized control

Idir et al. [49] also proposed a pyramid scheme for the segmentation of the mammography images. The pyramid base consists of the initial segmentation of the image by means of a region growing process (regions primitives). The edge primitives are obtained by a Canny edge detector. The behaviors are similar to the Duchesnay approach [48]. Though, they also include agents to control the good functioning of the multi-agent system: user interfaces-agents, monitor-agent, sequencer-agent and agent known as a dual-agent which influence and control the fusion process.

The last two approaches have in common the integration of region and edge primitives resulting in an improvement of the initial pre-segmentation. In fact, this

cooperation reduces the false contours resulting from noise presence, and closes uninterrupted contours due to the duality of the two approaches.

Liu and Tang [47] described an approach in which the emerging phenomenon of the system is edge detection. In the proposed agent-based approach, agents operate directly on the individual pixels of a digital image by continually sensing their neighboring regions and checking the homogeneity criteria of relative contrast, region mean, and regional standard deviation. Agents that are able to detect a homogeneous region replicate themselves on their neighbors to explore the entire region.The offspring agents have the same properties as their parent and siblings. The authors affirmed that their system is more robust than conventional methods of splitting and merging of regions. However, the agents have no mechanisms of cooperation, neither between them or with the environment. Their actions are based solely on their perception and their replication mechanism.

Mahdjoub et al. [43] proposed an approach in which the MAS model interprets information given by traditional image processing filters, to reconstruct and reorganize it. The system initializes with exploration agents looking for edges according to the gradient vector flow. This gradient attracts the exploration agents towards existing edges. After finding an edge, they create the edge following agents to follow the detected edges. The role of these agents is to rebuild the edges by approximating them with segments. A segment is represented by two agents collocated on its extremities, called node agents. If the node agent is not linked with another node agent is called end agent. The role of the end agents is to negotiate with each other the closing of the edge they are representing. These negotiations are part of the reinterpretation by the system of the information provided by the image processing algorithms. The result of the local behavior of all these agents is the emergence of a representation of the image edges.

Mazouzi et al. [50] presented a multi-agent approach for range image segmentation. They use reactive agents moving over the image and acting on the visited pixels, according to both its state and the state of the pixel on which it is situated. The agent first searches for a planar region using the region seed formed by the last visited pixels. Then, while moving inside the planar region, the agent adapts to it, memorizes its properties (plane equation) and smooths the visited pixels. At the boundaries between the planar regions, the agents are in competition to align the pixels of the frontiers to their respective regions. This interaction between agents allows the preservation of the region edges against smoothing. Around the aligned pixels, an artificial electrostatic-like potential field is created and updated, in order to allow agents to be gathered around pixels of region edges and make them concentrate their actions at these pixels. Also a relaxation mechanism of potential field is introduced to allow the releasing of the agents gathered around pixels of interest and thus to explore other regions of the image. In that way, with this approach, the image edges, for which no explicit detection is coded in any agent, result from the collective action of all agents.

Bovenkamp et al. [51] proposed a multi-agent system for the segmentation of the intravascular ultrasound (IVUS) images. The main characteristic of this approach is the elaboration of a high-level knowledge-based control over the low-level image processing algorithms. In this system, each agent is responsible for the detection of exactly one type of image object. The agents interact with each other through communication, act on the environment by performing image processing operations and perceive that same environment by accessing image processing results. So, the agents cooperate and dynamically adapt the segmentation algorithms, according to the contextual knowledge, the local information, and their personal beliefs. In this work, the problem of the control over the segmentation algorithms seems to be well resolved. However, no agent or even behavior has been proposed to deal with the problem of uncertain and noisy data.

Richard et al. [45] proposed a hierarchical architecture of situated and cooperative agents for the management of the various processing steps required for the localization of cerebral tissue in MRI images. Several types of agents are defined: global control agent, local control agent, and tissue-dedicated agent. The image is divided by the global agent in several 3D zones, each containing one local control agent and tissue-dedicated agents. The local control agents create the tissue-dedicated agent, estimate model parameters and confront tissue models for final labeling decisions. The tissue-dedicated agents collaborate with their neighbors situated in the adjacent partitions in order to serve their respective local agent and to progress ultimately toward the global goal.

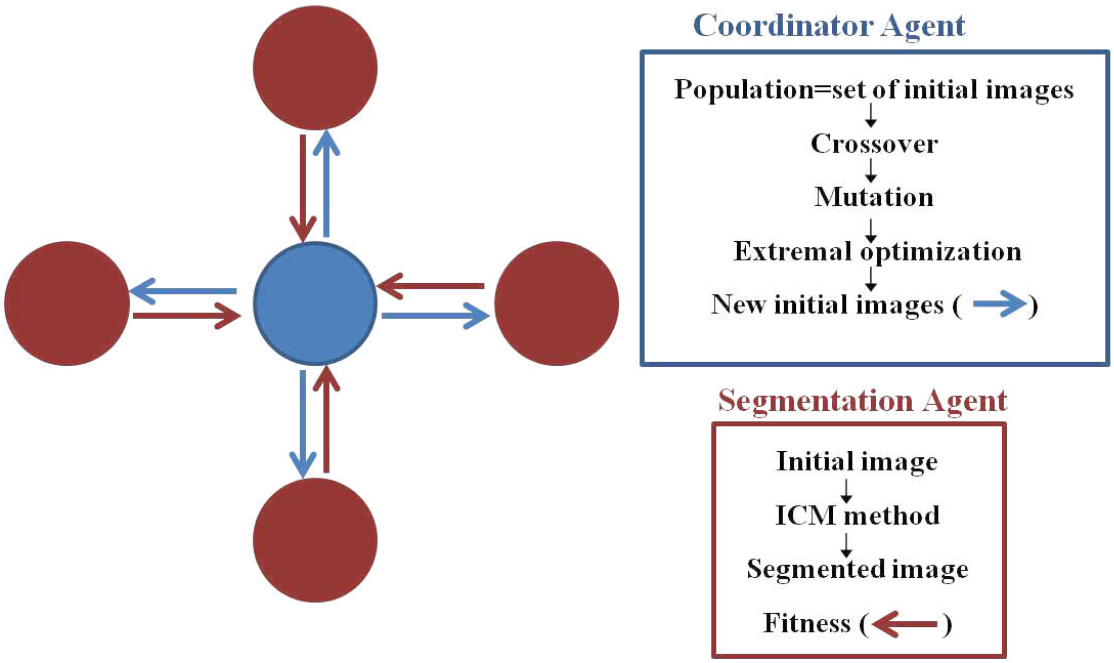

Figure 3.8.: Schematic representation of Melkemi et al. [52] approach

The algorithm proposed by Melkemi et al. [52] and illustrated in Figure 3.8 is

structured as a multi-agent system composed of a set of segmentation agents interconnected around a coordinator agent. Segmentation agents use the Markov random fields (MRF) based iterated conditional modes (ICM) method to accomplish their segmentation tasks. The coordinator agent combines the crossover and mutation genetic operators with the extremal optimization local search to provide new initial images for the segmentation agents.

Table 3.1 refers the image modality of each of the above approaches when tested in medical images. Moreover, it also briefly mentions the multi-agent systems architecture of each approach. The centralized approaches here refer to local agent behaviors controlled by a global agent. It can be noticed that, except the approach of Liu and Tang, all other approaches presents some kind of interaction mechanisms, mainly cooperative actions by means of direct and indirect communication. Furthermore, for the reasons referred in subsection 3.1.2, reactive agents have been the preferred architecture for medical image applications. Bovenkamp et al. and Richard et al. approaches also possesses reactive agents, but which are specialized and use some knowledge for interpretation of objects present in the image.

Table 3.1.: Medical image modality used to test the multi-agent system approaches and respective architecture

Researcher	**Image modality**	**Observations**
Liu and Tang [47]	Brain scan image	Reactive agents in a decentralized approach without cooperation mechanisms
Duchesnay et al. [48]	Computed tomography breast image	Reactive agents organized as an irregular pyramid
Bovenkamp et al. [51]	Intravascular ultrasound images	Decentralized approach developed with the cognitive architecture Soar
Richard et al. [45]	Brain magnetic resonance images	Situated cooperative agents organized in a centralized approach
Haroun et al. [44]	Brain magnetic resonance images	Reactive agents in a centralized approach and developed with Madkit platform
Idir et al. [49]	Mammography images	Reactive agents organized as an irregular pyramid
Mahdjoub et al. [43]	Lung computed tomography images	Reactive agents in a decentralized approach
Benamrane and Nassane [46]	Brain magnetic resonance images	Centralized approach of reactive agents working in JADE platform

4. Ant Colony Optimization

Ant colony optimization (ACO) is inspired by the behavior of real ants in the wild, mainly by their foraging behavior. Within the artificial intelligence community, ant based algorithms belongs to the swarm intelligence category. Swarm intelligence is an approach to problem solving that encompasses the implementation of multi-agent systems that are based on the collective behavior of nature, decentralized and self-organized systems like real world insect swarms.

The first ant system (AS) algorithm was a stochastic local search method proposed in the early nineties. Since then, the AS has attracted an increasing number of researchers, and in the meantime it has reached a significant level of maturity. In fact, many successful applications are now available for a wide variety of computationally hard problems [53].

In this chapter the transition from the biological to artificial ant colony is exposed. Furthermore, the AS metaheuristic proposed by Dorigo et al. [53] is explained, because it is essential to understand the ACO used in practical chapters of this thesis. At the end of this chapter, a literature review related to the use of artificial ant colony in images is described.

4.1. Biological Ant Colony

In many real ant species, ants make their own tasks independently from each other. Nevertheless, when act as a community, they are capable to solve their daily complex problems, which require sophisticated planning, without any kind of supervising or controlling. For instance, when searching for food in the environment (foraging behavior), ants leave their nest and wander randomly until they reach a source of food. While moving, ants lay a pheromone trail on the ground. After carrying a piece of food, they return back to the nest and deposit an amount of pheromone along its route, that depends on the quantity and quality of the food. Pheromones are chemical compounds whose presence and concentration can be sensed by fellow insects, and like many other media for indirect communication, pheromones can last a long time in the environment, though they may diffuse or evaporate. Therefore, when an ant encounter a trail of pheromone while exploring the environment, it is attracted to follow this trail until the food, and on its way it enforces the initial trail by laying additional amounts of pheromone. The more a trail is followed, the more it is enforced and has a chance of being followed by other ants in the future. At the

end of the process, the ants through collaboration find the shortest path to the food source [42, 53]. Figure 4.1 represents an illustration of the ants foraging behavior.

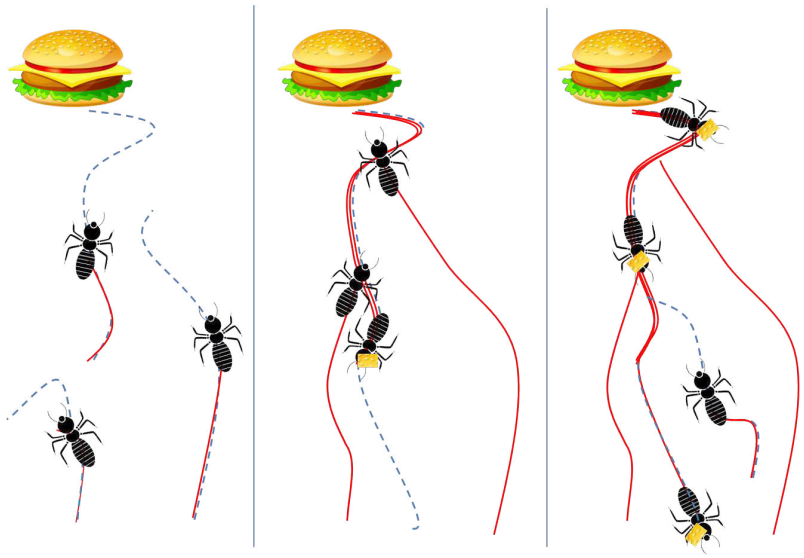

Figure 4.1.: Representation of the ants foraging behavior

4.2. Artificial Ant System - from biological to computational entities

Using simple reactive agents allows the transition from the natural to artificial ant colony. These agents cooperate by exchange information through environment modifications. That is, artificial ants communicate indirectly via artificial pheromone trails.

For mathematically modeling an artificial ant system behavior, some assumptions have been made [54]:

- Ants move through a discrete environment defined by nodes or states S;
- Each ant possesses an internal memory used to store the path followed by the ant;
- Starting from an initial state, each ant iteratively moves in its search space (environment) trying to build a feasible solution to the given problem;
- Ants move from one state to another according to a transition rule, which may include problem specific constraints and may utilize the ants internal memory;
- The amount of pheromone deposited by each ant is determined by a problem specific pheromone rule;

Therefore, the exploration space can be referred as a graph where artificial ants move from one node to another searching for a solution. After constructing a solution, the ant evaluates it and deposits pheromone proportional to its quality. The ants transition from one node to another depends on two main factors: heuristic information and artificial pheromone trail.

Heuristic information When constructing a solution, the ant has to decide to which neighboring node to move. This decision is made according to a probabilistically rule taking into account the pheromone values and some heuristic information. The heuristic information is meaningfully to find a good solution in the beginning of the algorithm since all pheromone values are equal. Actually, the heuristic information is application based and is known a priori to the algorithm run, without suffering modifications during the process.

Pheromone matrix The pheromones associated with the edges of the construction graph are represented as a matrix (below) and measure the pheromone deposition from ants previous transitions between the same states.

$$\tau = \left\{ \begin{array}{cccc} \tau_{1,1} & \tau_{1,2} & \tau_{1,3} & \tau_{1,4} \\ \tau_{2,1} & \tau_{2,2} & \tau_{2,3} & \tau_{2,4} \\ \tau_{3,1} & \tau_{3,2} & \tau_{3,3} & \tau_{3,4} \\ \tau_{4,1} & \tau_{4,2} & \tau_{4,3} & \tau_{4,4} \end{array} \right\}$$

All values of the matrix are initialized to some appropriate value and then suffers modifications along the algorithm run. If the initialization value is too high it spends some iterations until the pheromones updates influences the behavior of the ants. On the other hand, if this value is too low, the search is early trended to a suboptimal part of the solution space.

Algorithm 4.1 Ant Colony Optimization Metaheuristic

```
Set parameters, initialize pheromone trails
while termination condition not met do
    ConstructAntSolutions
     ApplyLocalSearch
     UpdatePheromonesTrails
endwhile
```

Algorithm 4.1 describes the AS metaheuristic proposed by Dorigo et al. [53]. After initialization, the algorithm iterates over three components: construction of a number of solutions by the ants; an optional improvement of these solutions by local search; updated of the pheromone values.

During the construction step, a set of artificial ants constructs solutions from elements of a finite set of solution components. A solution construction contains a

certain number of construction steps made by each ant. The construction process starts with an empty partial solution, which is extended at each construction step by adding a feasible solution component. The solution component is chosen from the set of components that can be added to the current partial solution without violating any constraint, that is, the solution component usually corresponds to a node neighboring of the current position in the graph. This choice is taken according to a decision rule which varies across different artificial ant colony variants. The most common is given in Equation 4.1 that corresponds to the one used in the original AS.

$$p_{i,j}^{(n)} = \frac{\left(\tau_{i,j}^{(n-1)}\right)^{\alpha} (\eta_{i,j})^{\beta}}{\sum_{j \in \Omega_i} \left(\tau_{i,j}^{(n-1)}\right)^{\alpha} (\eta_{i,j})^{\beta}} \; if \; j \in \Omega_i \tag{4.1}$$

Equation 4.1 refers the transition probability that on n^{th} construction step the ant k^{th} moves from node i to node j, where $\tau_{i,j}^{(n-1)}$ and $\eta_{i,j}$ are the quantity of pheromone and the heuristic information on the edge from node i to node j, respectively; Ω_i is the neighborhood nodes for the ant, given that it is at node i; α and β are constants that control the influence of the pheromone and heuristic information, respectively. The values of $p_{i,j}^{(n)}$ are limited to $[0, 1]$ due to the normalization factor represented by the denominator of Equation 4.1.

After constructing solutions, it might be a need to include additional actions to improve the solutions obtained by the ants through local search. This phase is highly problem specific and optional.

The last component of the AS algorithm consists of updating the pheromone values. The goal of this phase is to increase the pheromone values associated with good or promising solutions and to decrease those associated with bad ones. Normally, this is obtained by decreasing all the pheromone values through pheromone evaporation, and by increasing the pheromone values related to a chosen set of good solutions. The intended purpose of pheromone evaporation is that the algorithm "forgets" older solutions after some time, preventing premature convergence to sub-optimal solutions and promotes the exploration of new areas of the search space. The AS pheromone update follows the Equation 4.2, where $\rho \in (0, 1]$ is the pheromone evaporation rate, K is the number of ants, $\Delta\tau_{i,j}^{k}$ is the quantity of pheromone deposited on path *(i,j)* by the k^{th} ant.

$$\tau_{i,j}^{(n)} = (1 - \rho)\tau_{i,j}^{(n-1)} + \sum_{k=1}^{K} \Delta_{i,j}^{(k)} \tag{4.2}$$

4.3. Ant Colony System

An ant colony system (ACS) differs from the AS in way solutions are constructed and pheromone trails are updated [53]. Actually, the most important difference is the introduction of a local pheromone update in addition to the pheromone update at the end of each construction process (offline pheromone update).

The local pheromone update is performed by each ant immediately after moving from one node to another, that is, after each construction step. The ant updates pheromone in the last path traversed according to Equation 4.3, where $\varphi \in (0, 1]$ is the pheromone decay coefficient and τ_0 is the initial value of the pheromone.

$$\tau_{i,j} = (1 - \varphi).\tau_{i,j} + \varphi.\tau_0 \tag{4.3}$$

Using local pheromone update allows a diversification of the search performed by subsequent ants during an iteration. In fact, by decreasing the pheromone quantity on the path traversed, ants stimulate subsequent ants to opt for other paths, and therefore, to construct different solutions. In that way, it is less likely that during one iteration there are several ants producing the same solution.

The offline pheromone update is performed at the end of each iteration by only one ant, which can either be the iteration-best or the best-so-far ant. The update is making according to Equation 4.4 where $\Delta_{i,j}^{(k)} = 1/L_{best}$ and L_{best} can either be the iteration-best or the best-so-far.

$$\tau_{i,j}^{(n)} = \begin{cases} (1-\rho)\tau_{i,j}^{(n-1)} + \rho\Delta_{i,j}^{(k)}, & if\ (i,j)\ belongs\ to \\ & best\ tour \\ \tau_{i,j}^{(n-1)}, & otherwise \end{cases} \tag{4.4}$$

Another relevant variation between ACS and AS is the fact that ants use a different decision rule during the construction process, known as pseudorandom proportional rule. This rule states that the probability of an ant k to move from node i to node j depends on a random variable q uniformly distributed over [0,1] and a parameter $q_0 \in [0, 1]$, according to Equation 4.5.

$$\begin{aligned} if\ q \leq q_0: \quad p_{i,j} &= \begin{cases} 1, & if\ j = argmax_{j \in N_k(i)} \tau_{i,j}.(\eta_{i,j})^{\beta} \\ 0, & otherwise \end{cases} \\ else\ (q > q_0) & \qquad Eq.4.1\ is\ used \end{aligned} \tag{4.5}$$

4.4. Ant colony optimization in image processing - a literature review

Several methods find in the literature utilize artificial ant colony systems, implemented as agent-based algorithms which simulates the behavior of real ants with some differences. The created artificial ants behave like intelligent agents with memory and ability to see. They share their experiences in order to search optimal paths iteration by iteration.

Using ant algorithms to perform image analysis and processing tasks is a relatively new technique. Ant techniques have been used essential for low level image segmentation through edge detection methods and clustering approaches [54].

For the edge detection algorithms, the use of pheromones aspect of ant algorithms is done in a novel way. The digital image corresponds to the environment/search space where ants occupy pixels and move around the image on a pixel-wise fashion. The main goal of the AS algorithm is to locate and map out the image edges for which heuristic information is needed. The heuristic information weighs higher the probability of an ant moving from its current position to the allowed neighboring pixel that has the greatest edge characteristics (for example, the greatest change in image gradient). When moving between pixels each ant lays an amount of pheromone, which may also be a function of the change in image gradient. The pheromone evaporation takes place at a fixed rate per iteration. As the original AS, the transition rule usually is a function of the heuristic information and the pheromone map. Normally, these algorithms initialize with a number of ants located in random positions within the image. Then a convergence toward the edge areas within image occurs, and the resulting pheromone trails map the boundaries between image segments.

The main differences between this kind of algorithms and the "traditional" AS are that individual ants never construct complete solutions of their own, and the pheromone values are not only used to guide the ants' movements but also represent the final solution in its entirety [54].

Examples of such algorithms are described in studies of Nezamabadi-pour et al. [55], Tian et al. [56], Jevtic et al. [57] Ma et al. [58] and Zhang et al. [59]. A schematic of a typical ACO for edge detection is represented in Figure 4.2.

In the clustering methods, the pheromone is not used as a visual solution, but instead applies a more standard ant algorithm for optimizing the mapping of pixels to clusters within the image. For example, Han and Shi [60] used the ACO algorithm to perform fuzzy clustering in image segmentation. Three features were used for the clustering and searching process, including gray level, gradient and neighborhood of the pixels. They improved the heuristic function and the initialization of the clustering centers to accelerate the clustering process and to improve the efficiency of the proposed approach. Also as an optimization technique, the ACO was used in work of Tao et al. [61] to look for the optimal combination of the fuzzy parameters,

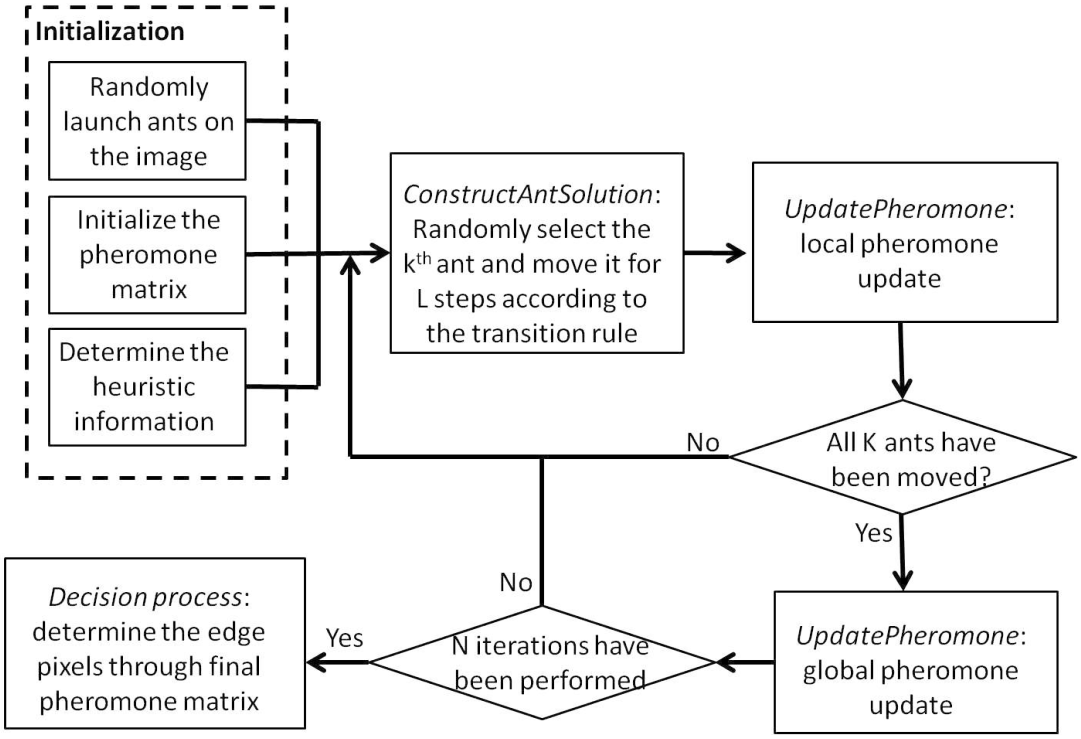

Figure 4.2.: Schematic of a typical ACO algorithm found in literature used for edge detection in images (adapted from [56])

as they used the fuzzy entropy for the segmentation of infrared objects. In Lu et al. [62] study, the authors used the ACO algorithm to improve the traditional edge detection approaches. The ants used the local information of the original image to search for paths among break edges and to explore compensable edges.

In medical image processing, the ant colony optimization algorithm has been already used in brain MRI images [63] and in retinal images for the optic disc [64], macula [65] and vessels segmentation [66, 67]. Therefore, the application of ACO algorithms to medical images is rather recent and rudimentary and still need improvements.

5. Detection of the optic disc location

This chapter describes a method for the optic disc detection in fundus images, based on an ant colony optimization approach preceded by anisotropic diffusion. Experimental results demonstrate the good performance of the proposed approach, because the optic disc is detected in most of all the images tested, even in the images with great variability.

5.1. Introduction

The localization of the optic disc (OD) is of great importance in the retinal image analysis because it is used as a landmark for the other features in fundus images. For instance, the location of OD is usually used to locate the macular area, and some blood vessels tracking methods start from the OD. Moreover, the accurate localization of OD is indispensable in the detection of some lesions such as exudates, because the OD has similar attributes in terms of brightness and contrast [68]. In fact, OD is characterized as a bright yellow disc from which the blood vessels emerge. While the accurate segmentation of the OD is sometimes very useful, such as for the glaucoma diagnosis in which the OD diameter increases, for this work the location of this retinal structure is sufficient to distinguish it from the bright lesions characteristic of the diabetic retinopathy. As it will be shown in section 5.2, there are many works reported in the literature with the purpose of detecting and segmenting the OD, based on its shape, brightness, size and as the point of convergence of the retinal vessels.

In this study, a new approach based on an ant colony system is proposed for locating the OD. Ant colony optimization is a branch of a larger field referred to as Swarm Intelligence and is inspired by the observation of the collective foraging behavior of real ant colonies (see chapter 4 for more information). Recently, an ACO approach [64] was also used in fundus images to detect edges, and therefore, to segment the OD and other retinal structures. The cited authors analyzed the results in terms of visual quality, computation time and preservation of useful edges. The work described in this thesis for the OD detection starts with an anisotropic diffusion process, which aims to smooth the retinal blood vessels. Then, an ACO algorithm based on the approach developed by Tian et al. [56] to edge detection was applied to the resultant image to detect OD edges.

5.2. Related work

Locating and segmenting the OD have been attempted by several recent researches. Ying et al. [68] presented an algorithm to localize and segment the optic disc based on local fractal analysis. Since the OD area is the converging point of all major vessels, it presents the highest fractal dimension compared to other bright regions, such as hard exudates and artifacts. The algorithm proposed in [69] was based on the algorithm of Hoover and Goldbaum [70], where they locate the optic disc by searching for regions of high intensity, diversity of gradient directions and convergence of vessels. Papers [71, 72] were also based on the geometrical directional pattern of the retinal vasculature and aimed to locate the optic disc as the point of convergence of all vessels. The work developed by Fleming et al. [73] aimed to locate the optic disc and the fovea. The approach began with the detection of the main vessels known as the temporal arcades, and which form approximately semi-elliptical paths enclosing the fovea. The optic disc was located using a circular form of the Hough transform and the fovea was detected by template matching. The model of the fovea was derived from a set of training images of high quality. Hough transform was also employed in [74, 75], where the OD boundary was estimated using edge detectors or morphological operators.

Some morphological operators were used in [22, 76, 77]. Reza et al. [76] used the green plane image and a morphological opening for detecting the connected components. The extended maxima operator was then applied to identify groups of pixels that have significantly higher values compared to their immediate surroundings. The last steps consisted of a minima imposition procedure and the watershed transform. The Lee et al. [77] algorithm began with the segmentation of the vasculature using morphological operations. After the blood vessel structures were removed by anisotropic diffusion smoothing, the next step was to estimate coarsely the optic disc contour. In that way, a collection of contour points was determined by analyzing its intensity profiles. Walter et al. [22] applied morphological filtering techniques and an area threshold on the lightness channel of the HLS color space. The contours were detected using the watershed transform on the red channel of the RGB color space.

Li and Chutatape [78] presented an approach to locate the optic disc in the intensity plane based on the principal component analysis (PCA). They detected its shape by applying a modified active shape model (ASM).

The papers [79, 80, 81] present methods to segment the optic disc based on snake models. Snake is an active contour that deforms to locate minimal energy points. Therefore, the OD boundary is delineated by iteratively fitting the snake active contour. A variant of deformable models is the active net model. In [82] an extension of this model, called topological active net (TAN) was used to locate the OD at the same time that performs its segmentation. Moreover, the TAN model was optimized by means of a genetic algorithm.

A supervised method was used in the paper [83]. Some vessel characteristics and the pixel intensities were used as the parameters for a regression model of the optic disc position. The authors used the k-nearest neighbors (kNN) regression to determine the relationship between the dependent variable d, representing the distance to the optic disc center, and a feature vector measured around a circular template.

The results of some of the above approaches are summarized in Table 5.1. In general, these methods have difficulties in dealing with pathological images as many of them showed worse results in the presence of pathological images in the database. In fact, the algorithms proposed by Novo et al. [82] and Abràmoff et al. [83] that demonstrate the best results used few pathological images and with only mild early diabetic retinopathy. In addition, the retinal images frequently present poor contrast, noise, and great inter- and intra-image variability which affect the performance of many algorithms.

Table 5.1.: Results from works reported in literature related to the segmentation of optic disc

Researcher	**Database**	**Success rate (%)**
Hoover and Goldbaum [70]	81 (STARE)	89
Zhu et al. [75]	40 (DRIVE)	90
Lee et al. [77]	23	92
Xu et al. [81]	100	94
Walter et al. [22]	30	96.7 (localization) 90 (boundary)
Ying et al. [68]	40 (DRIVE)	97.5
Foracchia et al. [71]	81 (STARE)	98
Fleming et al. [73]	1056	98.4
Li and Chutatape [78]	35	99 (localization) 94 (boundary)
Youssif et al. [72]	81 (STARE) 40 (DRIVE)	98.8 100
Abrámoff et al. [83]	1000	99.9
Novo et al. [82]	233 (VARIA) 40 (DRIVE)	100 100

5.3. Materials and methods

The proposed approach is constituted by two main steps. First an anisotropic diffusion process is applied to smooth the retinal images, particularly, the dark structures, such as blood vessels. Then, the ACO algorithm is used to detect the other retinal structures edges, mainly the OD edges.

5.3.1. Anisotropic Diffusion

Anisotropic diffusion is similar to the process that generates a scale-space, where an image is embedded into a parameterized family of successively more and more blurred images based on a diffusion process. In fact, anisotropic diffusion is normally implemented by means of an approximation of the generalized diffusion equation and each new image in the family is determined by applying this equation to the previous image. Thus, the anisotropic diffusion is an iterative process continued until a sufficient degree of smoothing is obtained [84]. Qualitatively, the effect of anisotropic diffusion is to smooth the original image while preserving brightness discontinuities [85].

The first elegant formulation of anisotropic diffusion was introduced by Perona and Malik [86] (Equation 5.1).

$$\frac{\partial I}{\partial t} = div\left(c\left(x,y,t\right)\nabla I\right) = \nabla c.\nabla I + c\left(x,y,t\right)\triangle I \tag{5.1}$$

They used the original image $I(x,y,0)$ as the initial condition. In Equation 5.1, t is an artificial time parameter, *div* represents the divergence operator, $\triangle$ and ∇ indicate the Laplacian and the gradient operators, respectively, with respect to the space variables, and *c(x,y,t)* is the diffusion coefficient. This coefficient controls the rate of diffusion and can be one of the two functions described in Equations 5.2 and 5.3 [86].

$$g_1\left(\|\nabla I\|\right) = e^{-\left(\|\nabla I\|/K^2\right)} \tag{5.2}$$

$$g_2\left(\|\nabla I\|\right) = \frac{1}{1+\left(\frac{\|\nabla I\|}{K}\right)^2} \tag{5.3}$$

The constant K in the above equations controls the sensitivity to edges and is usually chosen experimentally or as a function of the image noise.

The right choice of the diffusion coefficient, also called edge-stopping function, can significantly influence the extent to which discontinuities are preserved. In fact, the scale spaces obtained by these two functions are different: the first privileges high contrast edges over low contrast edges, and the second privileges wide regions over smaller ones and so preserves edges better than g_1. However, in both cases the diffusion process converges to an image with constant gray level when $t \to \infty$ [86] .

Perona and Malik discretized their anisotropic diffusion equation [85] and this is represented in Equation 5.4, where *I(s,t)* is a discretely sampled image, s denotes

the pixel position in a discrete two dimensional (2D) grid, $t \geq 0$ now denotes discrete time steps (iterations), the constant λ determines the rate of diffusion, η_s indicates the spatial neighborhood of pixel s and $|\eta_s|$ is the number of neighbors. For 2D images, usually 4 neighborhoods are used: north, south, west and east, except at the image boundaries. Perona and Malik linearly approximated the image gradient magnitude in a particular direction, at iteration t according to Equation 5.5.

$$I\left(s, t+1\right) = I\left(s, t\right) + \frac{\lambda}{\mid \eta_s \mid} \sum_{p \in \eta_s} g\left(\mid \nabla I_{s,p}(t) \mid\right) \nabla I_{s,p}(t) \tag{5.4}$$

$$\nabla I_{s,p}(t) = I(p,t) - I(s,t),\ p \in \eta_s \tag{5.5}$$

5.3.2. Ant Colony Optimization

Ant Colony Optimization algorithm is a stochastic local search method that has been inspired by the foraging behavior of some ant species. For instance, locating the shortest path between the colony and a food source is done by an exchange of information about the route that should be followed. When the ants walk to and from the food source, leave some amount of pheromone on the ground; this pheromone trail is used by ants to communicate with each other. Ants probabilistically prefer to follow a direction proportional to the quantity of pheromone on it [53].

The proposed approach utilizes a specific number of ants moving on the image driven by the local variation of the image intensity values. This variation establishes a pheromone matrix with the same size of the image, which represents the edge information at each pixel location of the image [61].

ACO is an iterative algorithm. At each iteration, a specific number of artificial ants are considered. Each of them builds a solution over the solution space through their movements and by constructing the pheromone information. The process starts with an initialization stage, and then runs for N iterations to construct the pheromone matrix by iteratively performing both the construction and the update processes. At the end, a decision process is performed to determine the edges.

Suppose that K ants are used to find the optimal solution (image edges) in a space X, i.e., in an image I with size $M_1 \times M_2$, and where each pixel can be viewed as a node; the ACO algorithm implemented could be summarized as in Algorithm 5.1.

Similar to the artificial ant based systems described in chapter 4, the above algorithm contains two crucial issues that have to be defined: the establishment of the probabilistic transition matrix and the pheromone matrix update. For the former the

Algorithm 5.1 Summary of the implemented Ant Colony Optimization algorithm

1. Initialize randomly the positions of the K ants and the pheromone matrix $\tau^{(0)}$
2. For the construction step index n=1:N
   i. For the ant index k=1:K
      1. Consecutively move the k$^{\text{th}}$ ant for L steps, according to a probabilistic transition matrix p$^{(n)}$ (with a size of $M_1M_2 \times M_1M_2$), and locally update the pheromone matrix $\tau^{(n)}$
   ii. Global update of the pheromone matrix $\tau^{(n)}$
3. Make the solution decision according to the final pheromone matrix $\tau^{(N)}$

probabilistic action rule determined by Dorigo et al. [53] was used (Equation 5.6).

$$p^n_{(l,m),(i,j)} = \frac{\left(\tau^{(n-1)}_{i,j}\right)^{\alpha} (\eta_{i,j})^{\beta}}{\sum_{(i,j)\in\Omega_{(l,m)}} \left(\tau^{(n-1)}_{i,j}\right)^{\alpha} (\eta_{i,j})^{\beta}} \; if \; (i,j) \in \Omega_{(l,m)} \tag{5.6}$$

This equation indicates the probability that at n$^{\text{th}}$ construction step of ACO, the k$^{\text{th}}$ ant moves from node (l,m) to node (i,j). $\tau^{(n-1)}_{i,j}$ is the pheromone information value of the arc linking the two nodes under consideration; $\Omega_{(l,m)}$ is the set of feasible components, that is, edges $(l,m),(i,j))$ where (i,j) is a node not yet visited by ant k; α and β are constants that represent the influence of pheromone and heuristic information, respectively; $\eta_{i,j}$ represents the heuristic information for going from node (l,m) to node (i,j), fixed to be the same for each construction step. In paper [56] this parameter was determined by local statistics at the pixel position (i,j) as referred in Equation 5.7, where $Z = \sum_{i=1:M_1} \sum_{j=1:M_2} V_c(I_{i,j})$ is a normalization factor,$I_{i,j}$ is the pixel intensity value at position (i,j) of image I, and the function $V_c(I_{i,j})$ is a function of a local group of pixels. The value of this function depends on the image intensity values variation on this group of pixels with the shape showed in Figure 5.1. Consequently, for pixel $I_{i,j}$, the function $V_c(I_{i,j})$ is described as the Equation 5.8.

$$\eta_{i,j} = \frac{1}{Z} V_c\left(I_{i,j}\right) \tag{5.7}$$

$$\begin{aligned} V_c(I_{i,j}) = f(&|I_{i-2,j-1} - I_{i+2,j+1}| + |I_{i-2,j+1} - I_{i+2,j-1}| \\ &+ |I_{i-1,j-2} - I_{i+1,j+2}| + |I_{i-1,j-1} - I_{i+1,j+1}| \\ &+ |I_{i-1,j} - I_{i+1,j}| + |I_{i-1,j+1} - I_{i+1,j-1}| \\ &+ |I_{i-1,j+2} - I_{i+1,j-2}| + |I_{i,j-1} - I_{i,j+1}|) \end{aligned} \tag{5.8}$$

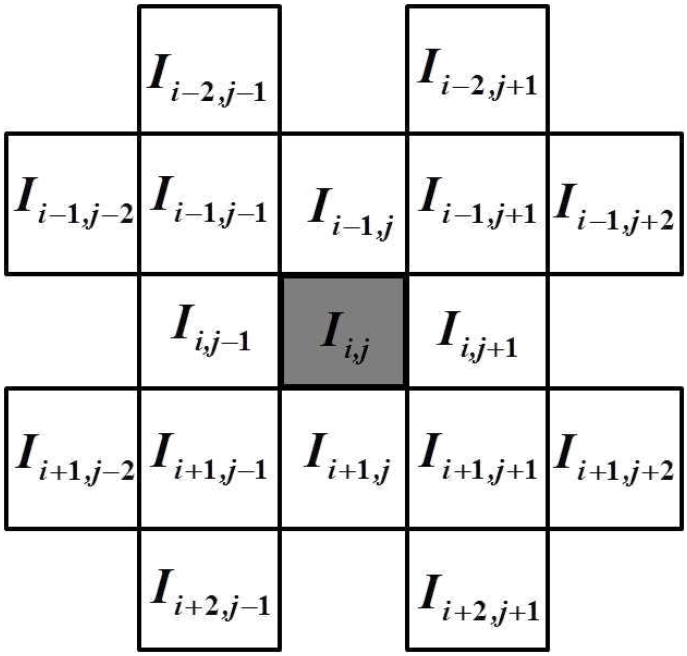

Figure 5.1.: Local configuration at the pixel $I_{i,j}$ for determining the variation V_c

In order to establish the function $f(.)$ in Equation 5.8, four different functions were considered by Tian et al. [56]. They are mathematically expressed in Equation 5.9-5.12. The parameter λ, present in each of these equations, adjusts the function's shape.

$$f(x) = \lambda x \; for \; x \geq 0 \tag{5.9}$$

$$f(x) = \lambda x^2 \; for \; x \geq 0 \tag{5.10}$$

$$f(x) = \begin{cases} sin\left(\frac{\pi x}{2\lambda}\right), & for \, 0 \leq x \leq \lambda \\ \tau_{i,j}^{(n-1)}, & otherwise \end{cases} \tag{5.11}$$

$$f(x) = \begin{cases} \frac{\pi x sin\left(\frac{\pi x}{\lambda}\right)}{\lambda}, & for \, 0 \leq x \leq \lambda \\ 0, & otherwise \end{cases} \tag{5.12}$$

As far as the pheromone matrix is considered it needs to be updated twice during the ACO process. The first update occurs after the movement of each ant within

each construction step. This update is performed using the Equation 5.13, where ρ is the evaporation rate and $\Delta_{i,j}^{(k)}$, in this particular case, is determined by the heuristic matrix, that is $\Delta_{i,j}^{(k)} = \eta_{i,j}$.

$$\tau_{i,j}^{(n-1)} = \begin{cases} (1-\rho)\tau_{i,j}^{(n-1)} + \rho\Delta_{i,j}^{(k)}, & if\,(i,j)\,is\,visited \\ & by\,current\,k-th\,ant \\ \tau_{i,j}^{(n-1)}, & otherwise \end{cases} \tag{5.13}$$

The second update occurs after the movement of all K ants within each construction step, and the matrix is updated according to Equation 5.14, where $\varphi \in (0, 1]$ is the pheromone decay coefficient.

$$\tau^{(n)} = (1-\varphi)\tau^{(n-1)} + \varphi\tau^{(0)} \tag{5.14}$$

Another issue that has to be established is the ant's movement permissible range ($\Omega_{(l,m)}$). In this paper, the 8-connectivity proposed in paper [56] was chosen.

Finally, the decision process consists in a binary decision made at each pixel location to determine whether it is an edge or not by applying a threshold T on the final pheromone matrix $\tau^{(N)}$. The threshold T is proposed to be adaptively chosen based on the Otsu's method [87].

5.3.3. Retinal images

The DRIVE (Digital retinal images for vessel extraction) dataset, a publicly available dataset developed by Niemeijer et al. [88] was used to test the proposed approach. It is composed of 40 images, which 7 of them present signs of mild early diabetic retinopathy, with 565x584 pixels and 8 bits per color channel. These images were captured with a Canon CR5 non mydriatic 3 charge-coupled device camera at 45 field of view (FOV), and they are JPEG compressed, which is very common in screening programs. This dataset has been used in the literature [82, 68, 72, 75] and the results are shown in Table 5.1.

Another publicly available dataset named DiaRetDB1 (Diabetic retinopathy database, calibration level 1) [89] was used to evaluate the performance of the proposed approach. The dataset consists of 89 images of which 84 contain at least mild nonproliferative signs (microaneurysms) of the diabetic retinopathy, and 5 are considered as normal (with no signs of the diabetic retinopathy). The images were taken in the Kuopio University Hospital. The signs of diabetic retinopathy in the dataset are relatively small, but they appear near the macula which is considered to threaten the eyesight. Images were obtained with the same 50 FOV digital fundus camera

with varying imaging settings such as flash intensity, shutter speed, aperture and gain controlled by the system. Moreover, the images present a varying amount of noise, but the optical aberrations (dispersion, transverse and lateral chromatic, field curvature, coma, distortion) and the photometric accuracy (color or intensity) are the same. As a result, the system induced photometric variance over the visual appearance of the various retinopathy findings can be considered as small.

A third dataset, named HCAA, was used in this work and it comprises images provided by Hospital Center of Alto Ave, EPE—Unit of Guimarães keeping the privacy protection of the patient information. This dataset consists of 50 images of which only 8 have no signs of diabetic retinopathy. Various levels of this ocular pathology are present in all the other images oscillating among mild, moderate and severe nonproliferative retinopathy and proliferative retinopathy. Moreover, the images were acquired with different digital fundus camera and present different characteristics such as resolution and dimension.

The two last datasets described correspond to good practical situations where the commonly imaging conditions were used, i.e., the conditions encountered in hospital. Therefore, the chosen datasets can be an effective way to evaluate the performance of the proposed approach for being applied in real screening programs.

5.4. Results and Discussion

In the first step, the anisotropic diffusion parameters were empirically determined and are represented in Table 5.2. The ACO algorithm parameters were the same used by Tian et al. [56], already experimentally determined by Nezamabadi-pour et al. [55] and are also indicated in Table 5.2.

All retinal images from the datasets were converted to size of 128×128 to be considered for analyzing by the proposed algorithm. The average computational time for the proposed approach was approximately 75 seconds. This time increased to 1260 seconds, when the input image size was 256×256 and the results are very similar. Using such a small size is advantageous since it works as a multi resolution decomposition and as a result it minimizes the number of OD candidates.

Results of the proposed approach applied to pathological images with the red and bright lesions characteristics of diabetic retinopathy are shown in Figure 5.2 and Figure 5.3. These Figures illustrate the original image (a), the original gray level image (b), the result of the diffusion process (c) and the result of the ACO algorithm with each of the Equation 5.9-5.12 as shown in d–g, respectively. It can be noticed from these Figures that the proposed approach could be an effective way to roughly segment the optic disc, especially using the second or the fourth function in the heuristic information. The other two functions also detect pixels not belonging to the optic disc, particularly pixels near the contour of the FOV, around the main blood vessels and around the bright lesions. Moreover, a qualitative analysis of

Table 5.2.: Parameter values of the proposed algorithm

Algorithm	Parameter	Value
Anisotropic Diffusion	t, number of iterations	15
	c, diffusion coefficient function	g_2
	K, in diffusion coefficient function	2
	λ, rate of diffusion	1/7
	η_s, spatial neighborhood	4-neighborhood
Ant Colony Optimization	K , total number of ants	$\lfloor\sqrt{M_1 \times M_2}\rfloor$
	τ_{init}, initial value of each component of the pheromone matrix	0.0001
	α, weighting factor of the pheromone information	1
	β, weighting factor of the heuristic information	0.1
	λ, adjusting factor of the function in Equation 5.9- 5.12	10
	ρ, evaporation rate	0.1
	L , total number of ant's movement steps within each construction step	300
	φ, pheromone decay coefficient	0.05
	N , total number of construction steps	3

all tested images shows that the second and fourth function are considerably less affected by the variability existing in the images. This was expected as the first and third functions operate in a proportional way over all the gray values of the image while the second and fourth functions enhance more the highest gray levels.

Results of applying the proposed approach to three images with different number of ants are shown in Figure 5.4. From above to below, Figure 5.4 shows the original color image and the result of ACO algorithm with 128 and 500 ants, respectively. The average computational times of the proposed approach with 128 and 500 ants are approximately 75 seconds and 630 seconds, respectively. As can be seen by Figure 5.4 center and below the use of different number of ants results in different segmentations, being the most accurate segmentation the one with the major number of ants. However, the difference between the results does not seem to be so significant to justify the discrepancy in computation time.

To evaluate and quantify the performance of the proposed approach, the OD centers and diameters were manually determined in all the images. The estimated OD center is considered acceptable if it is located within the circular OD area considered, i.e., if the distance between the estimated location and the manually segmented location is smaller than half of the manually determined diameter. For the determination of the estimated OD location, the centroid of the region with the biggest area from

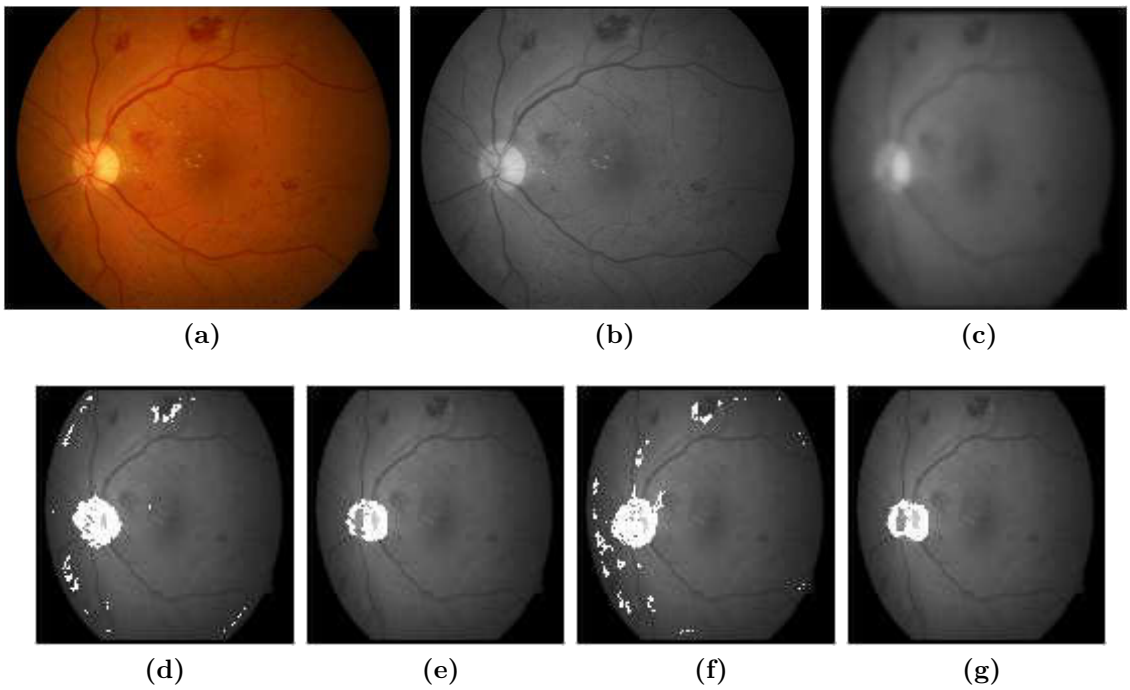

Figure 5.2.: Experimental results (a) original image with principally red lesions, (b) original gray-level image, (c) image resultant of the diffusion process, (d)–(g) results of applying the ACO algorithm with the four equations superimposed on the original image , respectively

the binary images corresponding to the second function was calculated. Figure 5.5 shows the results of this process applied to several images, where the OD location estimated is represented by a cross (×). Figure 5.6 illustrates the results for each of the images from the datasets in terms of the ratio (r) (Equation 5.15). *Dist* is the distance between the estimated OD location and the manually segmented location; *Radius* is the manually determined radius of the OD.

$$r = \frac{Dist}{Radius} \tag{5.15}$$

The optimal value of r is 0, meaning that the estimated OD location is equal to the manually segmented OD location. If the value of r is between 0 and 1, the estimated localization of the OD can be considered acceptable as the estimated OD location is inside the OD. On the other hand, a value of r bigger than 1 means that the estimated OD location is outside of the OD, corresponding to the outliers. In the DiaRetDB1 database, there are six obvious outliers corresponding to a success rate of 93.25 %. In the HCAA dataset, the proposed method achieved a success rate of 94 % as it could not correctly locate the OD in three images. In the DRIVE dataset,

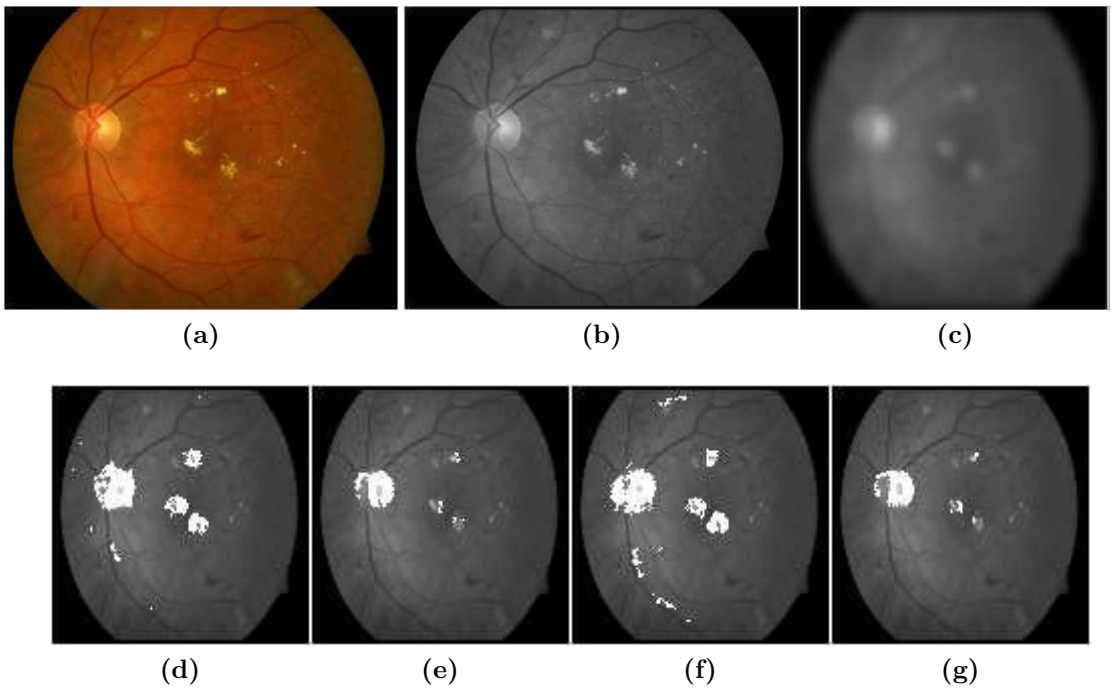

Figure 5.3.: Experimental results (a) original image with principally bright lesions, (b) original gray-level image, (c) image resulting from the diffusion process, (d)–(g) results of applying the ACO algorithm with the four equations superimposed on the original image , respectively

the algorithm was able to locate the OD in all the images achieving a performance of 100 %.

Figure 5.7 illustrates three representative images of the DiaRetDB1 database where the approach failed. The problem of the first image (left) is the presence of a large bright lesion characteristic of a more advanced stage of the diabetic retinopathy. The second image presents poor contrast causing the OD difficult to see. In the last image (right) the proposed approach also roughly segmented the OD, but the ants were more concentrated in the artifact resulting from a bad acquisition of the image. Nevertheless, this approach combined with a method to segment the blood vessels could be an effective way to overcome these problems due to the possibility to detect the OD as the point of convergence of blood vessels.

From Figure 5.5, it can be seen that this approach overcomes the main problems characteristic of the retinal images resulting from the screening programs. That is with ACO algorithm preceded by anisotropic diffusion, it can be possible to locate the OD in images with great variability between them and inside them without any other preprocessing. In addition, conversely to the works described in literature, the algorithm was applied in pathological images and in most of them (94%) it worked well.

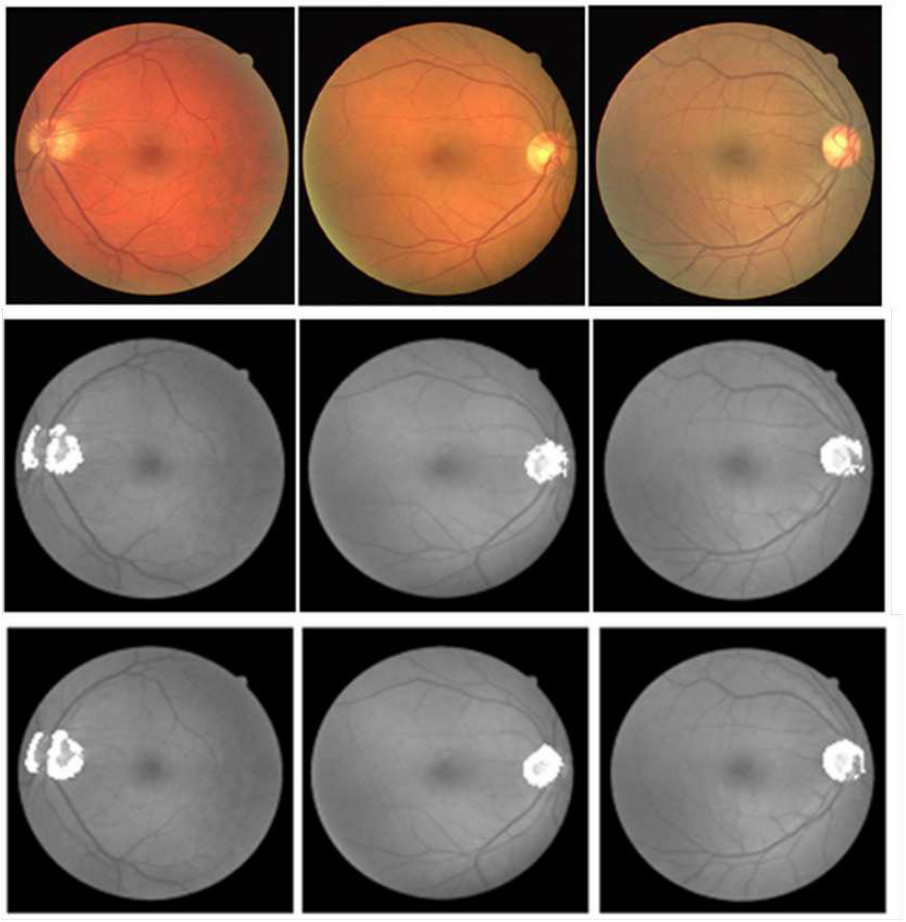

Figure 5.4.: Results of applying the proposed approach to three color images (above) with 128 ants (center) and 500 ants (below)

Furthermore, this approach in general outperforms the work developed by Kavitha and Ramakrishnan [64] in segmenting the optic disc. They used the ACO algorithm in the same way preceded by adaptive histogram equalization technique considering an exponential distribution function. With their approach they could segment the optic disc and also some of the blood vessels. However, as the images of the paper show [64], their algorithm is affected by noise and by the presence of a great variability in the image background. With the approach proposed here, it is easy to detect the optic disc and to differentiate it from the other pixels also detected, which are significantly fewer than in Kavitha and Ramakrishnan's approach due to the use of the anisotropic diffusion.

Although it is useful sometimes to completely segment the OD, such as for the glaucoma diagnosis in which the OD diameter increases, this is not the reasoning of this work. As the aim of this project is to develop a system for the detection of DR in fundus images resulting from screening programs, the location of the OD is sufficient to distinguish it from the bright lesions characteristic of the pathology.

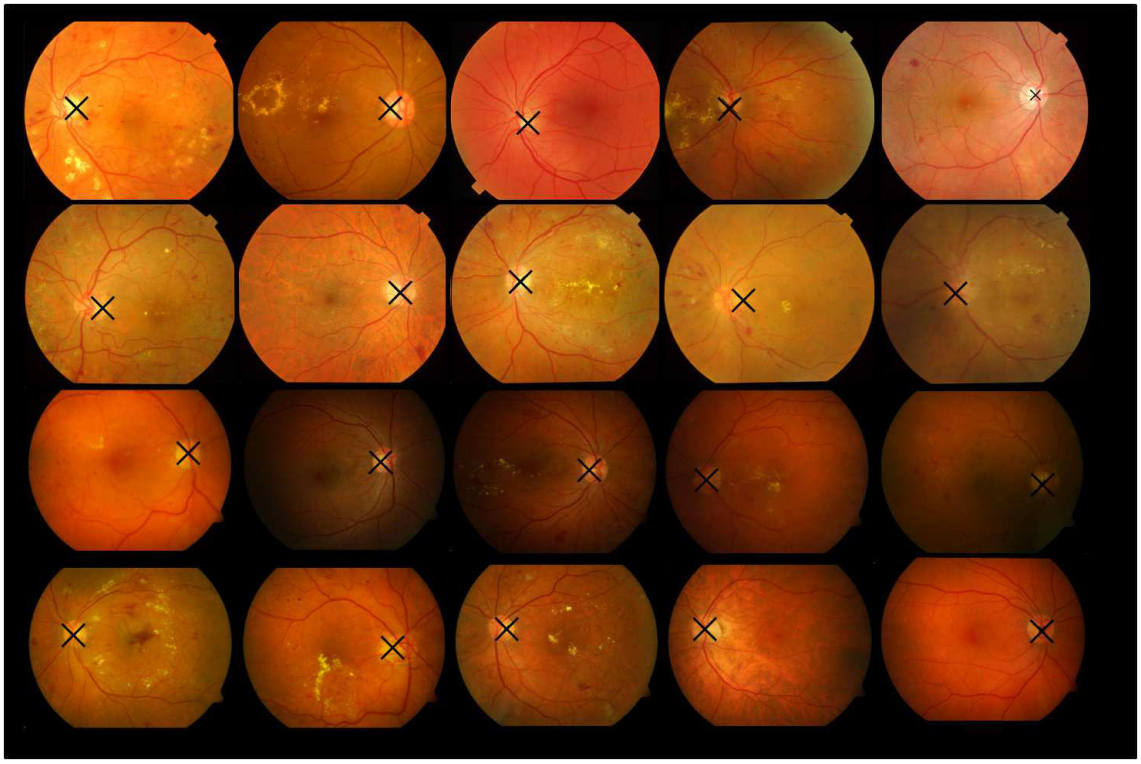

Figure 5.5.: Results of applying the proposed approach to twenty different images, from the DiaRetDB1 and HCAA datasets, with great variability and various levels of DR. The estimated localization of the OD is marked with a cross (×)

With this purpose, the proposed method achieved success rates higher than 90% in the three datasets used. The results achieved with the DRIVE dataset are good as or better than the ones described in the literature [68, 72, 75, 82]. The comparison with the results obtained with the DiaRetDB1 and HCAA datasets have to be done carefully. Actually, these two datasets are compounded of more diverse and realistic universe of images, regarding intra and inter variations and the existence of lesions. As we intend to develop a reliable system with generalized clinical application, it is important to use real images. In that way, the use of these two datasets can be considered as an advantage of the proposed approach over the methods found in the literature.

5.5. Conclusion

In this study, ACO algorithm preceded by anisotropic diffusion was successfully applied in retinal images to segment the optic disc. The superior performance in pathological images and images with great variability intra and inter images could be considered the major advantage of this approach.

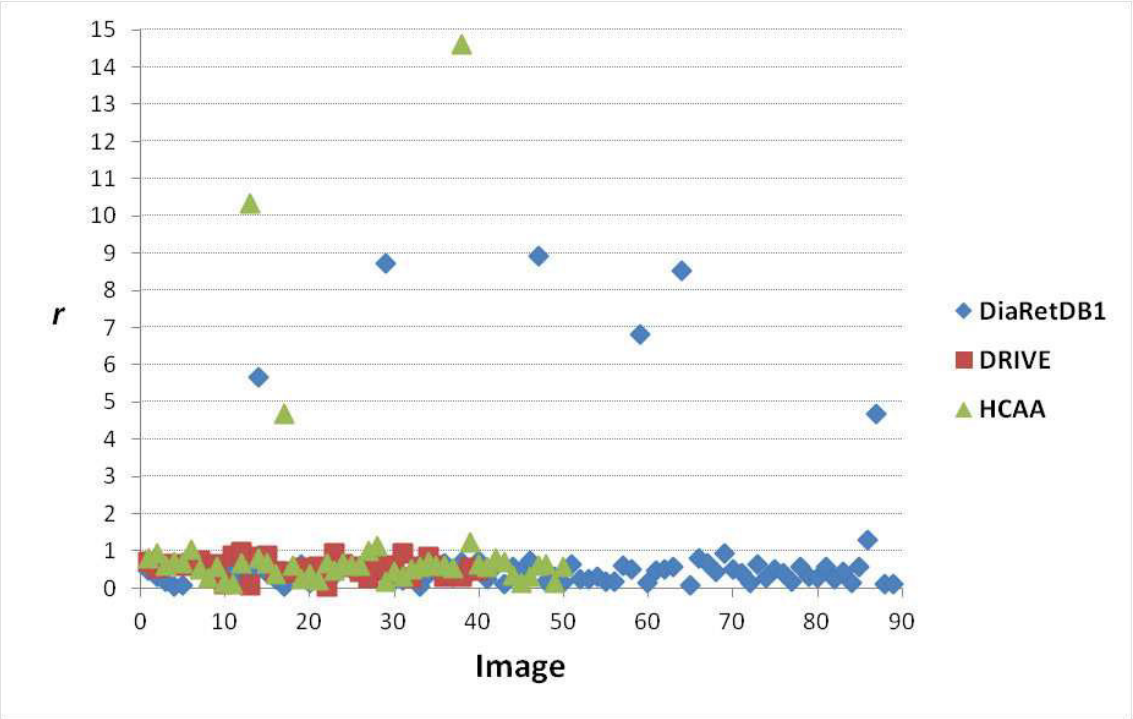

Figure 5.6.: Quantitative results for all the images of the databases used, where each point represents the ratio between the distance from the estimated location and the true location, and the radius of the OD

For this work, the accurate localization of the OD is sufficient since our goal is to develop a system able to detect DR in fundus images. The localization of the OD is important to distinguish it from the bright lesions characteristics of the pathology. The proposed method achieved success rates of 93.25%, 94% and 100% in the DiaRetDB1, HCAA and DRIVE datasets, respectively. The algorithm is affected essentially by the poor contrast of imges complicating the OD detection, by the presence of large bright lesions, and by the large bright artifacts resulting from a bad acquisition of the image. However, these problems could be overcome by considering the OD as the point of convergence of blood vessels and, consequently, by adding the segmentation of the blood vessels.

As the experimental results show, the ACO algorithm could be efficient in extracting other features in the image such as the major blood vessels and macula. The diffusion process applied in the methodology described here is an important way to segment only the OD, and, consequently, to distinguish it from the other features also detected when only the ACO algorithm was used. Then the localization of the OD by a point was a simple task.

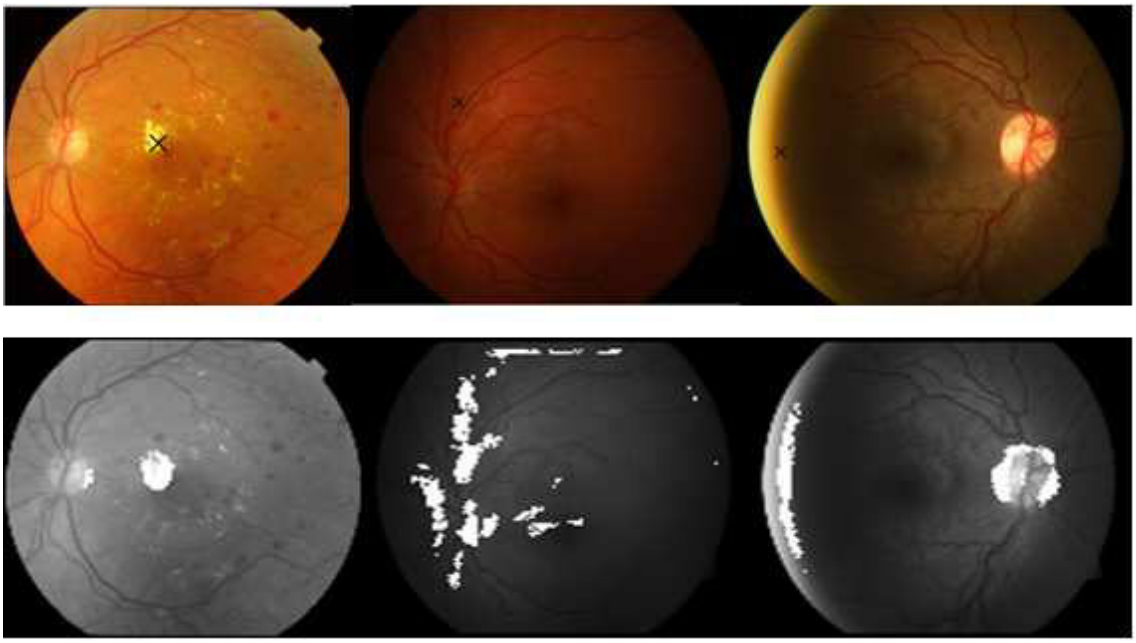

Figure 5.7.: Images where the proposed approach achieves the worst results. Original images with the wrong localization of OD identified by a cross (×) (above) and the results of applying the ACO algorithm (below)

6. Bright lesions detection

This chapter describes a technique to perform the exudate segmentation by means of a new unsupervised approach based on ant colony optimization algorithm. The proposed approach performance was evaluated on an online available dataset and the experimental results shows that the ant colony algorithm performs better than one traditional filter for exudates detection.

6.1. Introduction

Exudates are one of the DR earlier signs. They are an indicator of increased vessel permeability as they are plasma lipid and protein accumulations in the retina. In fundus images they appear as yellow-white dots, shiny and with sharp borders. Moreover, they are frequently observed together with microaneurysms. The main difficulties in accurately detecting exudates in fundus images are brought by noise presence, low contrast, uneven illumination and color variation. Moreover, there is some difficulty in distinguishing among the exudates and drusen, the "bright lesions" associated especially with age-related macular degeneration (AMD) and which can have a similar appearence with exudates.

In this study, a new exudates segmentation approach is proposed based on Ant Colony Optimization. The ACO was already used in fundus images to analysis the OD [64], the macula [65] and segment retinal blood vessel [66, 67]. Chapter 5 describes an ACO based approach to locate the OD. As far as known, this kind of approaches has never been applied to retinal images to detect DR lesions.

6.2. Related work

Several approaches have been proposed in literature to segment bright lesions from the color fundus photographs. Giancardo et al. [90] roughly divided them into four categories: thresholding, morphology, region growing and supervised methods.

Thresholding methods are based on global or local gray level analysis. For instance, Sanchez et al.[91] presented a thresholding method based on a statistical mixture model. This was employed on the enhanced image histogram to determine a dynamic threshold for each image. Then, a postprocessing technique based on edge detection

using Kirsch's method, was applied to distinguish hard exudates from other bright lesions.

Morphology methods consist of applying morphological operators to identify structures with specific shape (such as vessels). These structures are then removed and therefore exudates can be selected [22, 92, 93, 94]. Morphological operators are sometimes combined with other techniques, such as contrast enhancement and clustering methods [94].

Region growing methods segment the image based on the spatial gray level contiguity. For instance, Li and Chutatape [78] used CIE Luv color space images and applied to them a region growing method proceeded by the Canny edge detector. The edge detection decreases the size of the regions and improves significantly the computation time. They also created a fundus coordinate system which allowed the automatic identification of the lesions presence in the macular area.

Supervised methods are the most common in the literature [25, 90, 95, 96, 97, 98]. They consist of building a feature vector for each pixel or pixel cluster, to be classified by a machine learning approach into exudates or non-exudates. The features are based on color, brightness, size, shape, edge strength, texture and contextual information of pixel clusters. The machine learning methods commonly used are Neural Networks (NN) [95, 98], Support Vector Machines (SVM) [90, 97], Linear Discriminant classifiers [25, 96], and Naïve Bayes classifier [90]. Fleming et al. [97] detected candidate exudates using a multi-scale morphological process. For each scale, the result was an enhancement of the bright dots present in the original image. The application of a dynamic threshold reduced the candidates which were false positives. Garcia et al. [95] study made use of the global histograms shape properties. The histogram of the preprocessed images shows one maximum that corresponds to the background. The tail on the right of this maximum corresponds to the bright structures present in the images. In that way, the method consisted in applying a threshold at the gray level of this tail for which the histogram decreased to 10% of the maximum. Moreover, the authors also considered the properties of the local histograms which were obtained by dividing the image into square blocks of side 200 pixels. Niemeijer et al. [96] presented an algorithm which aims to detect exudates and cotton-wool spots and differentiate them from drusen. In a first stage, a k-nearest neighbor classifier was used to detect candidate bright lesions. A linear discriminate analysis was then applied to differentiate among lesion types. Sanchez et al. [25] describes an algorithm based on Fisher's linear discriminate analysis, which made use of statistical recognition and of color information to perform the classification of exudates. The classification rule was automatically adapted to each image.

The results of the above approaches are summarized in Table 6.1. Unfortunately, the majority of these algorithms was tested on independent databases with different characteristics. Therefore, it is not possible to prove their capacity to generalize. Moreover, results were quantified using different evaluation methods, becoming dif-

ficult the comparison between them.

Table 6.1.: Results and methodology categories of literature approaches for the exudates segmentation

Author	Method category	Results	Dataset
Walter et al. 2003 [22]	Morphology	Sensitivity/ Predictive value pair of 92.8%/92.4% (per lesion)	30 images: 15 with exudates
Li et al. 2004[78]	Region growing	Sensitivity/Specificity pair of 100%/71 % (per image)	35 images with exudates
Fleming et al. 2007 [97]	Supervised	Sensitivity/Specificity pair of 95%/84.6% (per image)	13 219 images: 300 with exudates
Niemeijer et al.2007 [96]	Supervised	Area under ROC curve=0.95; Sensitivity/Specificity pair of 95%/88% for the detection of bright lesions of any type (per lesion)	300 images: 100 with bright lesions and 200 without
Sanchez et al. 2008 [25]	Supervised	Sensitivity of 88% and mean number of false positive per image of 4.83±4.64 (per lesion); Sensitivity/Specificity pair of 100%/100% (per image)	83 images: 25 for training and 58 for testing (36 with exudates)
Sopharak et al. 2008 [92]	Morphology	Sensitivity/Specificity pair of 80%/99.5% (per lesion)	60 images: 40 with exudates
García et al. 2009 [95]	Supervised	Sensitivity/ Predictive value pairs of 88.1%/80.7 % with MLP, 88.5%/77.4 with RBF, 87.6%/83.5% with SVM (per lesion) and Sensitivity/Specificity pairs of 100%/92.5% with MLP, 100%/81.5% with RBF, 100%/77.8% with SVM (per image)	117 images: 50 for training and 67 for testing (40 with DR signs)
Sanchez et al. 2009 [91]	Dynamic Thresholding	Sensitivity/Predictive value pair of 90.2%/96.8% (per lesion) and Sensitivity/Specificity pair of 100%/90% (per image)	106 images: 26 for training and 80 for testing (40 images with exudates)

Author	Method category	Results	Dataset
Osareh 2009 [98]	Supervised	Sensitivity/Specificity pair of 96%/94.6% (per image) and Sensitivity/ Predictive value pair of 93.5%/92.1% (pixel level)	300 images: 150 with DR signs
Welfer 2009 [93]	Morphology	Sensitivity/Specificity pair of 70.5%/98.8 % (per image)	DIARETDB1[89]
Amel 2012 [94]	Morphology	Sensitivity/ Predictive value pair of 95.9%/92.3%	50 images from MESSIDOR[99]
Giancardo 2012 [90]	Supervised	Area under ROC curve between 0.88 and 0.94 depending on the dataset/features used	MESSIDOR[99]; HEI-MED[90] and DIARETDB1[89]

6.3. Materials and methods

As exudates have the highest contrast with the background in the green plane of the RGB color model [22], this was chosen to implement the proposed approach. This approach is mainly constituted of two parts. First, a preprocessing phase is developed to find a binary image with exudates candidates based on its high intensity gray level. Since sharpness of exudates edges is an important attribute to distinguish them from other bright structures [25], edge strength for each candidate is then evaluated. This is performed by analyzing the resultant image of applying ACO in image windows of size 128×128. An outline of the proposed approach is illustrated in Figure 6.1.

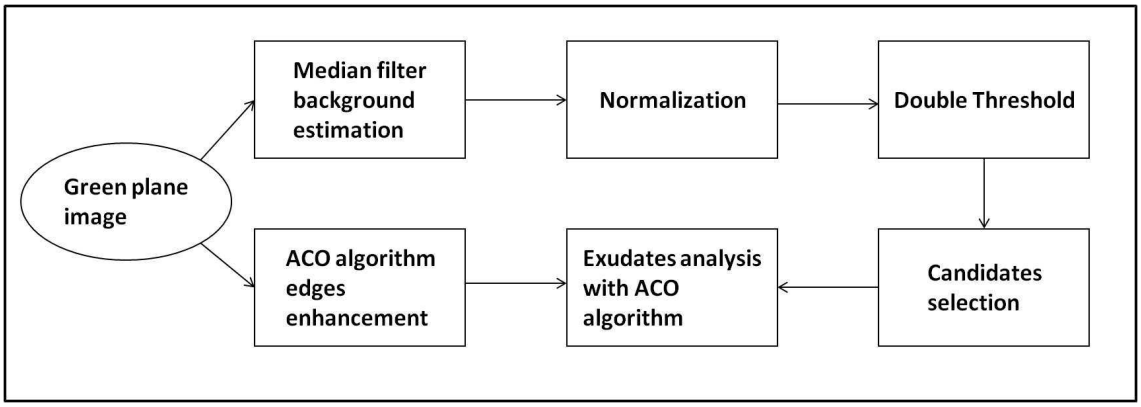

Figure 6.1.: Schematic representation of the proposed approach

For evaluating the edge strength with different preprocessing phases, other authors [25, 91, 100] used a traditional edge detector, the Kirsch filter (subsection A.3.1).

In order to compare the proposed approach with those, a part of the Giancardo's approach [100] were also implemented and evaluated in the same way.

6.3.1. Preprocessing

The intra and inter image variability of fundus images, mainly due to retinal pigmentation and acquisition process, affects the exudates automatic segmentation. Therefore, a preprocessing step for image normalization is very important to improve the algorithm capacity for generalizing.

The intensity variation in the background across the image can be eliminated by estimating the background image and subtracting that from the original green plane image. The background image is estimated by applying a median filter (subsection A.2.2) with a 50x50 pixel kernel. The size of this filter was chosen according to the widest blood vessel of the database. The obtained shaded corrected image shows a characteristic gray level distribution: the highest histogram peak is always centered on zero and there is a clear distinction between dark and bright structures. The left histogram tail with negative values belongs to dark structures such as vessels, macula and dark lesions. The positive histogram tail corresponds to the bright structures including optic disc, bright lesions, and other bright structures. Figure 6.2 shows three different color retinal images and the respective, green plane image, normalized gray level image and histogram of the normalized image (from left to right).

At this point, and since all the normalized images have similar histogram characteristics, it is possible to select all the exudates candidates with a simple hard threshold. However, it was experimentally noticed that the use of two hard thresholds with posterior morphological reconstruction can improve results (Figure 6.3). Applying a low threshold value (T_1) permits the selection of all exudates and respective borders. With a higher threshold value (T_2), the bright intensity peaks, which mostly correspond to exudates, are detected. In fact, in that way it is possible to eliminate several false positives and maintain the correct candidates border that are really exudates. The values for T_1 and T_2, experimentally determined, are 0.008 and 0.02 respectively. In the resultant binary image (I_{cand}) all bright lesions should be identified.

The preprocessing step finalizes with candidates elimination that belong to optic disc. The OD was detected by the method described in chapter 5.

6.3.2. Ant Colony Optimization Algorithm

The artificial ant colony system used in this approach for the exudates detection follows the same algorithm used for the optic disc location and it is summarized in Algorithm 6.1. For determining the heuristic information, the function $V_c(I_{i,j})$

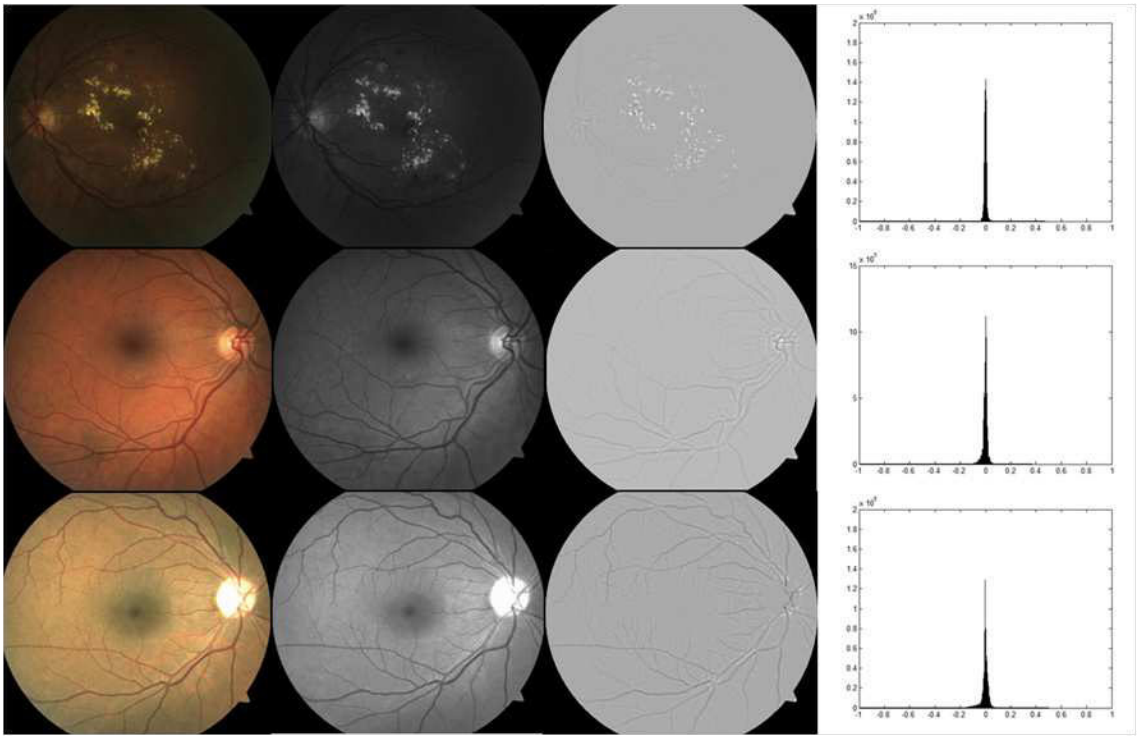

Figure 6.2.: (From left to right): original color image; green plane image; normalized gray level image; normalized image histogram

used was the function mathematically expressed in Equation 5.10. The quadratic function was chosen because it enhances more the highest gray levels, representing an advantage in this case as we are looking for exudates.

Due to the large image size and to reduce computation time, the ACO algorithm was independently applied on non-overlapping image windows of size 128×128.

Algorithm 6.1 The Ant Colony Optimization algorithm implemented

1. Determination of the heuristic information and initialize the resultant image $I_{res} = 0$
2. For each original image window of size 128×128
   i. Initialize randomly the positions of the K ants and the pheromone matrix $\tau^{(0)}$
   ii. For the construction step index n=1:N
      1. For the ant index k=1:K
         i. Consecutively move the k^{th} ant for L steps according to the probabilistic transition matrix $p^{(n)}$(Equation 5.6), and locally update the pheromone matrix according to Equation 5.13
      2. Global update of the pheromone matrix according to Equation 5.14
3. Assign pheromone matrix $\tau^{(N)}$ to the correspondent window on the resultant image

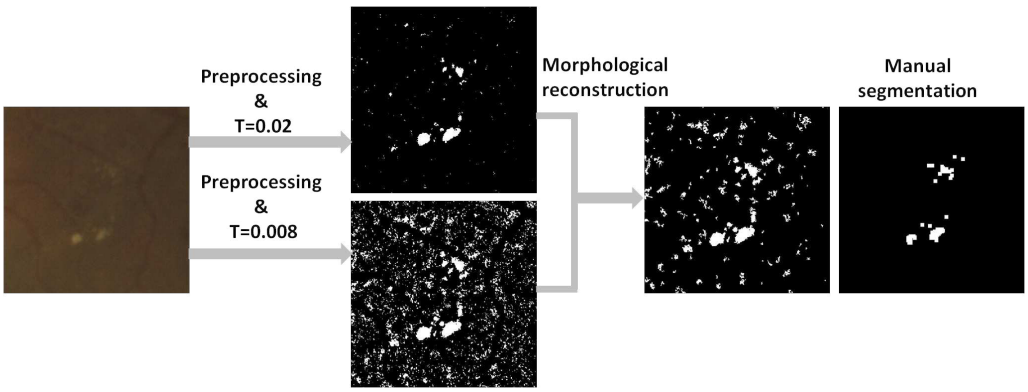

Figure 6.3.: Using two hard thresholds with posterior morphological reconstruction eliminates a number of false positives and maintains the correct candidates' border.

6.3.3. Exudates detection

From I_{cand} the object candidates were obtained using 8-neighbor connected component analysis. As proposed by Sanchez et al. [91] the edge strength of each object candidate was determined as the mean intensity under the object in the edge-enhanced image resulting from the ACO algorithm step. A candidate was then considered an exudate if its edge strength value is bigger than a threshold (th). th is an algorithm parameter which determines the minimum value that an edge must have to be considered as a sharp boundary. To detect more exudates, a lower value has to be chosen, but false positives also increase.

To reduce the number of false positives that usually appears close to blood vessels, the segmented vasculature map obtained with the method of Zana and Klein [101] was used to eliminate the blood vessels edges found by the ACO algorithm. Then, to evaluate the final output the following thresholds were employed $th \in \{0 : 0.005 : 0.02\}$.

6.3.4. Giancardo's approach

Giancardo's approach [100] is, as well as the proposed method, constituted of two main parts. First, the intensity component of the HIS color space was used to estimate the background image. Then, a morphological reconstruction step was used to enhance the normalization as it seems to improve the removal of nerve fiber layer and other structures close to OD. After normalization, a small hard threshold was applied and candidates were selected from the resulting image. For each of the exudate candidates, edge strength was defined by the average intensity under the candidate in the Kirsch resultant image. The Kirsch filter was applied in the original image green plane. Figure 6.4 illustrates the schematic of this method.

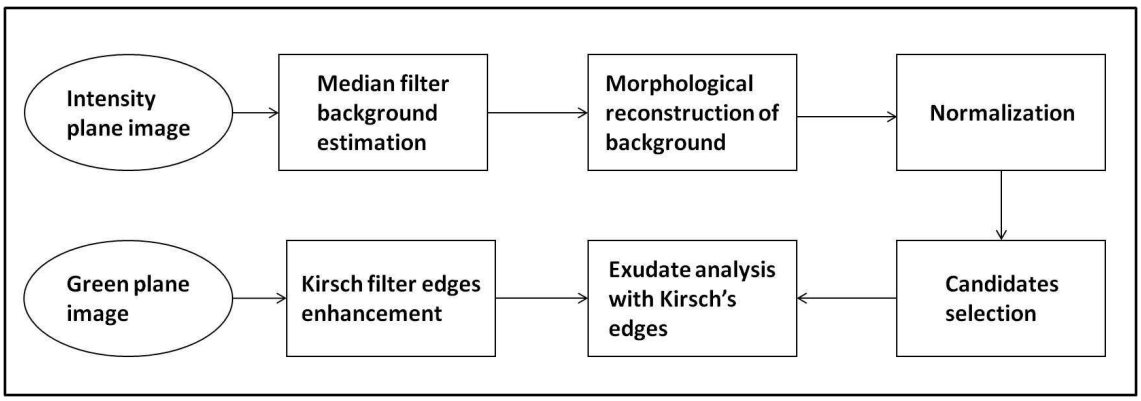

Figure 6.4.: Schematic representation of the Giancardo´s approach with Kirsch filter

To make a fair comparison between Giancardo´s approach and the proposed approach, a step was added to the former. The segmented vasculature map used in our approach was added to eliminate the blood vessels edges enhanced by Kirsch filter.

The Giancardo's study also used stationary wavelets to evaluate the peak intensity of each candidate. However, they reported [100] that the Kirsch approach generally showed better results. Moreover, the proposed approach follows the same idea of the Giancardo's Kirsch approach as the candidates are evaluated in terms of edge strength. In that way, the comparison in this study is just between the proposed approach and the Giancardo´s approach that used Kirsch edges.

6.3.5. Retinal images and system performance evaluation

The HEI-MED (Hamilton Eye Institute Macular Edema Dataset), a publicly available dataset developed by Giancardo et al. [90] was used to test the approaches. This dataset is composed by 169 images representative of various degrees of DR. The images present a great variability among them as they belong to patients with different age and ethnicity. Moreover, the authors developed an image quality metric ranging from poor, good and excellent and referred that the percentages of each category are 8%, 18% and 74%, respectively. In addition, the dataset contains the bright lesions manual segmentation for each image, where the exudates are distinguished from other bright lesions, such as cotton wool spots and drusen.

To evaluate the approaches performance two different criteria were used: the pixel based criterion and image based criterion. For the first, all pixels belonging to a candidate that partially or totally overlaps a manually segmented bright lesion were considered true positive (TP). All candidate pixels outside this criterion were registered as false positives (FP). All exudate pixels manually segmented that were not segmented by this approach were considered false negatives (FN). In the image

based criterion, the capacity of the algorithm to exclude healthy images was evaluated. An image was considered healthy if it does not contain any exudate, and pathological if it contains at least one exudate.

Researchers frequently evaluate their approaches performance in terms of sensitivity (Equation 6.1) versus predictive positive value (Equation 6.2) (see Table 6.1). However, this does not seem to be a good quantitative evaluation as predictive positive value is prevalence dependent. Therefore, if images have a big quantity of exudates, the prevalence would be naturally bigger than in images with few exudates. To avoid this, the proposed approach was also evaluated in terms of Receiver operating characteristic (ROC) curves, which plot the true positive rate (Sensitivity) in function of the false positive rate (1-Specificity). Therefore, to determine the ROC curve, specificity values have to be calculated (Equation 6.3). The problem in calculating the specificity is that if all image pixels are considered, the number of true negative (TN) pixels will be huge comparing with FP values and so, the specificity will always have high values. To overcome this problem, we propose to calculate the TN as a function of the threshold value (Equation 6.4). When th is 0, the FP number has its maximum. Increasing th by 0.005 the FP number decreases and pixels that were false positive became true negative pixels (Figure 6.5). On the other side the TN number has its minimum when th=0 and afterward it increases with the threshold variation. In that way, if the TN number is considered zero when th=0, then its value can be compared to the FP number and the specificity value will be more representative of the approach capacity to exclude pixels that are not exudates. In this study, ROC curves were constructed following this idea.

In addition to the ROC curves, the approaches were also evaluated in terms of the accuracy (Equation 6.5).

$$Sensitivity = \frac{TP}{TP + FN} \tag{6.1}$$

$$PPV = \frac{TP}{TP + FP} \tag{6.2}$$

$$Specificity = \frac{TN}{TN + FP} \tag{6.3}$$

$$TN(th) = FP(th - 0.005) - FP(th) + TN(th - 0.005) \tag{6.4}$$

$$Accuracy = \frac{TP + TN}{FP + TN + TP + FN} \tag{6.5}$$

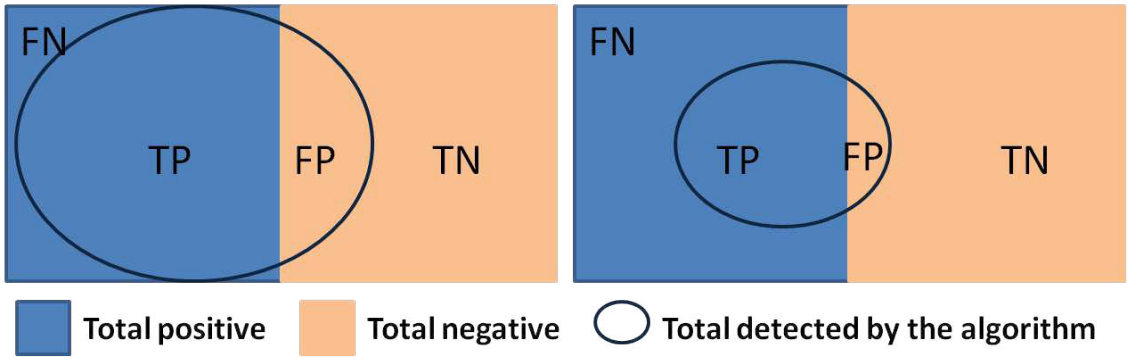

Figure 6.5.: Schematic representing statistical measures: FN, TP, TN and FP. From left to right represents what happens when threshold increases: the TP and FP decreases and becomes FN and TN, respectively.

6.4. Results and discussion

The results of the proposed approach applied to images with exudates from HEI-MED dataset are shown in Figure 6.6. The latter illustrates (from left to right): original color image; binary image resulting from the preprocessing step with the exudates candidates; gray level image resulting from the ACO algorithm; green plane image with the exudates segmented by the proposed approach. From the preprocessing phase results a binary image with all exudates segmented and a lot of false positives. The ACO algorithm resultant image reveals exudates edge enhancement. The combination of both images taking into account the edge strength of each candidate can remove the most part of FP pixels.

The lesion segmentation performance of the proposed algorithm was evaluated by determining the overall sensitivity, specificity, accuracy and predictive positive values for each threshold value. Figure 6.7 illustrates the proposed approach and Kirsch approach ROC curves and the respective Area Under Roc Curve (AUC) values. AUC is an accuracy measure, that is, it measures the approach capacity to distinguish between normal and exudate pixels. Therefore, the proposed approach performs better than the Kirsch approach since the respective AUC values are 0.975 against 0.971. Since the candidates of both approaches were obtained by different processes, Figure 6.7 also contains the ROC curve of a different approach that begins with the proposed candidate detection method and uses the Kirsch filter to enhance edges. The respective AUC demonstrates that the ACO edge enhancement method performs better than the Kirsch filter.

Table 6.2 describes the quantitative results for these three approaches when the overall accuracy reaches its maximum. It can be noticed how the three methods perform comparably, with the proposed approach performing somewhat better in terms of sensitivity.

Despite being important the performance evaluation in terms of pixel-based crite-

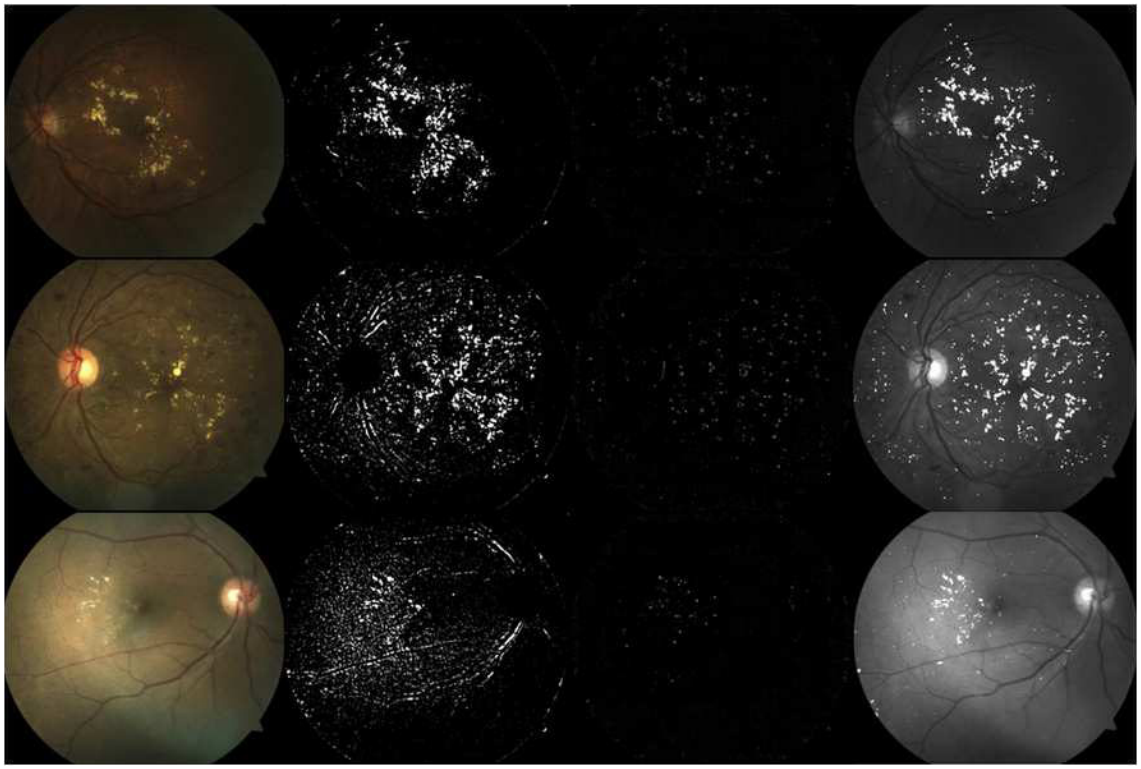

Figure 6.6.: From left to right: original color image; binary image with exudate candidates (I_{cand}); ACO algorithm gray level resultant image; green plane image with the exudates segmentation

rion, image-based criterion is crucial when goal is the development of a system for the diabetic retinopathy diagnosis. Thus, the detection of a single exudate in an image with many of them is as useful and important as the detection of an exudate in an image with only one lesion of this type. Consequently, the algorithm capacity to distinguish patients with or without bright lesions should be evaluated. Figure 6.8 illustrates the proposed and Kirsch approaches ROC curves calculated with all images from the HEI-MED dataset and using image-based criterion. In spite of the AUC value for the Kirsch approach being higher than for the proposed approach, the discrepancy is very small. Furthermore, the shape of the curves is irregular and intersects several times, indicating that for some threshold values, the proposed approach has better performance than the Kirsch approach. For other threshold values, the opposite is observed. The point is that none of the approaches perform as needed for clinical practices and both need improvements. The same applies to the approaches found in literature that are described in section 6.2. A comparison between our approach and those found in literature is not possible, since the retinal image datasets used and the way to measure performance were not the same. Therefore, the comparison was limited to the segmentation step of the Giancardo's approach [90] that was described in a previous work [100], since their database was used in this study and their approach follows similar ideas.

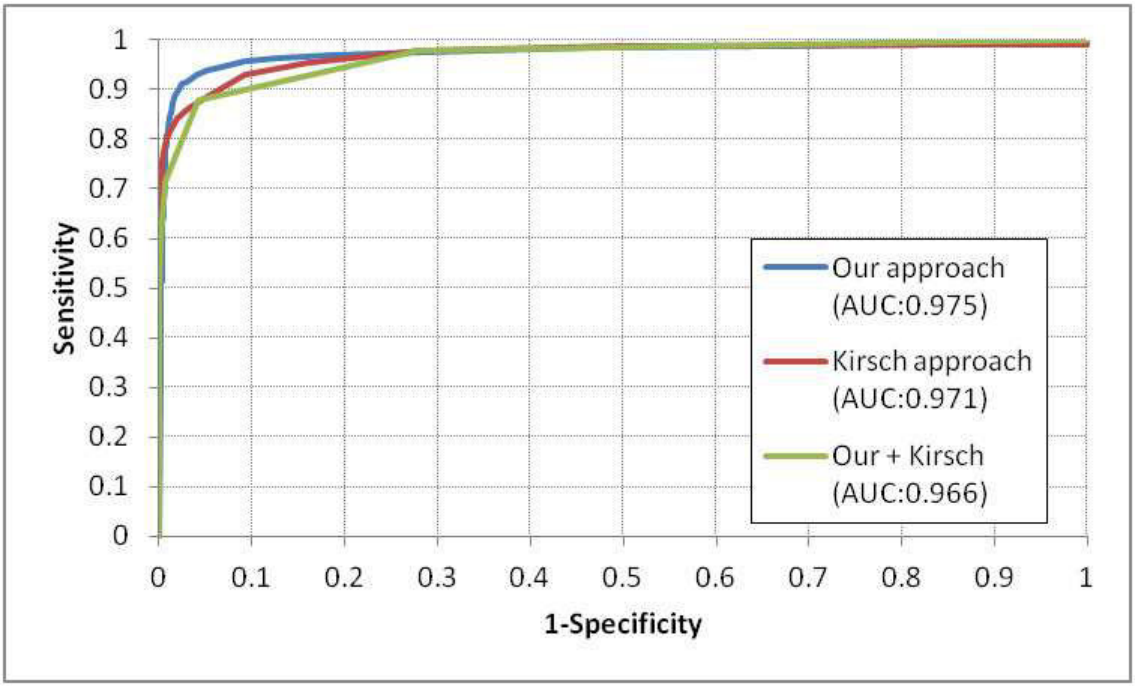

Figure 6.7.: ROC curves using all images and the pixel-based criterion

Table 6.2.: Quantitative results using pixel-based criterion for the three approaches and using all images

Approach	Accuracy	Sensitivity	Specificity	PPV
Our	0.9785	0.8082	0.9916	0.7301
Kirsch	0.9767	0.7575	0.9961	0.8348
Our+Kirsch	0.9786	0.5986	0.9988	0.8944

Although the preprocessing phase is very important to normalize images and to locate exudates at a global level, the diversity of brightness and size become difficult the detection of all the exudates. Since exudates often appear in groups, failing in the detection of some very faint exudates is not relevant. Nevertheless, when only a few faint exudates are present in the retina, this method may fail in the identification process, even if the ACO algorithm has succeeded in their detection.

6.5. Conclusion

In this chapter, a new algorithm based on ACO is described for exudates detection in color fundus images. The contributions of this study are the use of an online available dataset, which permits future comparisons with other approaches, and the development of a new unsupervised method for the exudates detection. Using the pixel based criterion, the experimental results show that the proposed approach

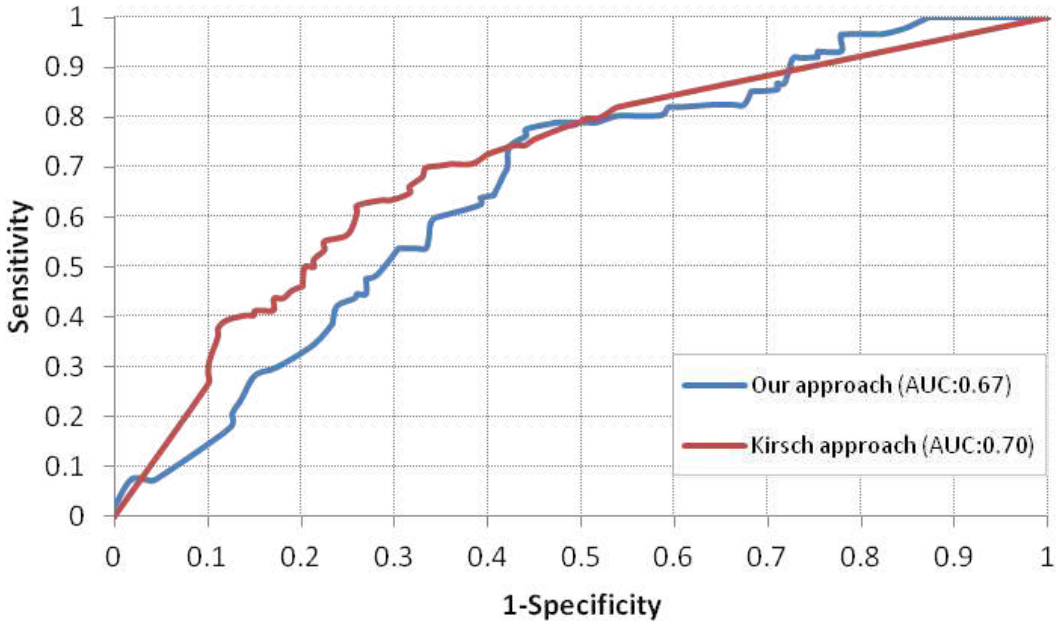

Figure 6.8.: ROC curves using all images and the image-based criterion

yields better AUC than the Giancardo's method with Kirsch filter. With the image-based criterion none of the approaches performs as needed for clinical practices.

The application of an ant colony to locally explore the image gray level variation is the greatest novelty of this study. The ACO algorithm can be seen as an agent-based algorithm, because it contains several agents with memory moving on the image (environment) and that communicate indirectly through the environment [102]. Furthermore, it presents some MAS properties, such as self-organized mechanisms that allow the emergence of complex behaviors, which, in this case, are the edges enhancement. In this way, a new category of approaches based on MAS is being applied to retinal images for the exudates segmentation.

7. Blood vessels segmentation

This chapter presents a new approach based on an agents' organization enabling vessel detection. This multi-agent approach is preceded by a preprocessing phase in which the fundamental filter is a Kirsch derivative improved version. This first phase allows the environment construction where agents are situated and interact. Then, blood vessel edges detection emerges from agent interaction. According to this study, competitive results as compared with those present in the literature were achieved.

7.1. Introduction

The retinal blood vessels segmentation is of major importance for clinical purposes. In fact, by analyzing the vascular structures it is possible to have the early diagnosis of several chronic pathologies, such as arteriosclerosis, hypertension or diabetic retinopathy.

In retinal photographs, blood vessels appear as elongated features, much darker than the background, and their width is smaller than a certain value (up to 0.2mm [103]). They enter into the retina by the optic disc and they can be seen as a connected line segments series. The main difficulties in accurately segment vessels in fundus images are brought by noise presence, low contrast between vasculature and background, vessels width, brightness and shape variability. Furthermore, the presence of pathological features, such as exudates or hemorrhages, causes large abnormal region in the retinal image. To solve this variability problem, it is important to adapt locally image interpretations instead of applying only one algorithm on the entire image. A multi-agent system approach is thus proposed as a solution since agents allow several algorithms cohabitation. In fact, agents can analyze problems which they are locally confronted with, and then select the most suitable algorithm to their local context [43].

Therefore, the association of MAS and image processing has been revealed as an expanded research area. As far as known, multi-agent approaches have never been applied to the retinal images. In this study, two new approaches based on the previous work of Mahdjoub et al. [43] were applied to the digital color fundus images for the retinal blood vessel edge detection and segmentation tasks. These new approaches use some image processing algorithms as concrete perception and action tools for defining autonomous agents that interact among themselves and

with the environment (the image). Then the blood vessel segmentation emerges as a global behavior.

7.2. Related work

Retinal vasculature segmentation has become crucial for several medical diagnostic systems and numerous research efforts have been done in this field. The most common techniques reported in the literature are based on matched filters, machine-learning algorithms, blood vessels geometry and colors properties as main features.

The matched filtering approaches [104, 105, 106, 107, 108] consist on the blood vessels enhancement followed by a multi-threshold probing scheme. In these methods it is assumed that the vessel cross section can be modeled as a Gaussian function. For instance, Gabor filters were used by applying a multi-scale analysis scheme to the image in order to enhance the different widths blood vessels. That is, Gabor filters were applied as line detectors with variable thickness to obtain a bank of filters at different scales for multi-resolution filtering and analysis. Then, a multi-threshold probing scheme was applied to determine an appropriate threshold for each area being probed, based on the local and regional attributes of the blood vessels. Zhang et al. [108] improved this approach by considering not only the response to the matched filter but also the local mean of it. In fact, the response of the matched filter with the first-order derivative of Gaussian function is strong and has a local mean close to zero around vessels peak position. In contrast, for the non-vessels structures both response and its local mean are high.

The machine-learning approaches are frequently compounded by an image analysis step followed by a classification step. The work developed by Staal et al. [109] began with the image ridges extraction from the green plane, used to compose primitives in the form of line elements. With these primitives the image was divided into patches by assigning each image pixel to the closest primitive. Finally local features were extracted from each patch to be used in a kNN classifier. Each pixel of an image was represented by a feature vector in [110] and [111] to classify it as a vessel or a non vessel pixel. These vectors included the two-dimensional Morlet wavelet transform responses taken at multiple scales. In [110] the feature vector also contained the pixel's intensity in the green plane. In [111] the pixel feature space also included the Gaussian gradient responses taken at different scales and some color information. For the classification step it was employed a Bayesian classifier with class-conditional probability density functions. In Ricci and Perfetti [112] study, the inverted green channel image was scanned and two orthogonal line detectors were applied to each pixel. The line detector evaluated the average gray level along fixed length lines passing through the target pixel at different orientations. These detectors results and the pixel's intensity formed a feature vector used in a supervised classification with Support Vector Machines. Salem et al. [113] presents an algorithm called radius based clustering algorithm that used a distance based principle to map the

distributions of the data and did not have to specify the number of clusters. The data resulted from a first segmentation phase in which three features were extracted from each image pixel: the green channel intensity; the local maxima of the gradient magnitude (recognition of the parallel edges of the vessels); the local maxima of the largest eigenvalue (recognition of piecewise linear property of the vessels).

Other techniques present in literature made use of the vasculature geometry such as shape and measurements, and of the vasculature contrast to help in extracting vessels. In [114] each image pixel from the green plane was tested by a vessel shape kernel at different directions to determine the directional local contrast. This one was compared to a certain threshold value, which determined the lowest level of contrast of blood vessels that can be detected by the algorithm. In that way, each image pixel was classified as vessel or background. Huang and Yan [115] proposed an algorithm to detect the blood vessel that quantitatively measured the salient properties of retinal vessels and combined the measurements by Bayesian decision to determine a confidence value for each detected vessel segment. The salient properties of vessels used in this work were the dark appearance and the continuous linear structure of the blood vessel in retinal images. Lam and Yan [116] algorithm firstly locates the pixels which are in thin concave regions by applying the Mumford-Shah model, and secondly extracts the connected vessels by skeletonization from these regions. Recently, they presented an extension of their preliminary study [117]. Following the vessels properties, they located centerlines using the normalized gradient vector field.

Al-Diri et al. [118] proposed an algorithm for segmenting and measuring retinal blood vessels. This began with the identification of an initial set of potential vessel segment centerline pixel by using a generalized morphological order filter. Then a segment growing algorithm was applied to convert the map obtained in the last stage into a set of segments, each consisting of a series of profiles. This last algorithm was based on the Ribbon Twins model that used two pairs of contours to detect each vessel edge while maintaining width consistency. Finally, a junction resolution algorithm was applied to extend the discrete segments and resolve various crossings, junctions and joining.

Many other approaches are found in the literature to obtain a vasculature map: morphological operators combined with other techniques [24, 119, 120]; a vessels signals frequency domain analysis applying a band of Local-Mean-Interpolation filters [121]; multi-window Radon transform [122]. Narasimha-Iyer et al. [69] presented a vessel detection method where starting from initial seed-points, vessels are tracked recursively using directional templates.

Most of the above algorithms were implemented and tested with the STARE (structured analysis of the retina) [104] and DRIVE [88] databases and results are summarized in Table 7.1. These approaches were generally evaluated in terms of area under the ROC curve and accuracy, that is the fraction of pixels correctly classified. Despite some of them present good results comparing with the 2nd observer manual

segmentation [109, 112], they often have difficulty in distinguishing the blood vessels from the other retinal structures. This is due to the use of centralized mechanisms at the macro level that cannot be locally adapted to the image properties. Therefore, none of the methods presented in the literature perform as needed because of retinal image complexity.

Table 7.1.: Results from works reported in literature related to the retinal blood vessels segmentation

	STARE		**DRIVE**	
	AUC	**Accuracy**	**AUC**	**Accuracy**
2nd observer	-	0.9351	-	0.9473
Hoover et al. (2000) [104]	0.759	0.9275	-	-
Staal et al. (2004) [109]	0.9614	0.9516	0.9614	0.9441
Soares et al. (2006) [110]	0.9671	0.9480	0.9614	0.9466
Oloumi et al. (2007) [106]	-	-	0.96	-
Li et al. (2006) [105]	0.85	-	-	-
Ricci and Perfetti (2007) [112]	0.968	0.9646	0,9633	0.959
Mendonça and Campilho (2006) [119]	0.842	-	0.7315	0.9463
Estrabidis and Figueiredo (2006) [122]	0.863	-	-	-
Lam and Yan (2008) [117]	0.9392	0.9474	-	-
Zhang et al (2010) [108]	-	0.9484	-	0.9382

7.3. Materials and methods

The proposed approaches use MAS models to improve retinal blood vessels edges detection resulting from a preprocessing phase. This preprocessing phase consists of a conventional image processing algorithms group (Figure 7.1) and provides adapted information (environment) for the MAS model.

7.3.1. Image preprocessing

For this first step the green plane (I_{green}) was chosen because it represents the plane where vasculature has the highest contrast with the background. Since fundus photographs often contain an intensity variation in the background across the image, any slow gradient in the background of I_{green} was removed, resulting in a "shade corrected" image (I_{sc}). This was made by estimating the background image I_b and subtracting that from I_{green}. The I_b is estimated by applying a median filter with a 25×25 pixel kernel. The size of this filter was chosen according to the DRIVE database widest blood vessel width [2].

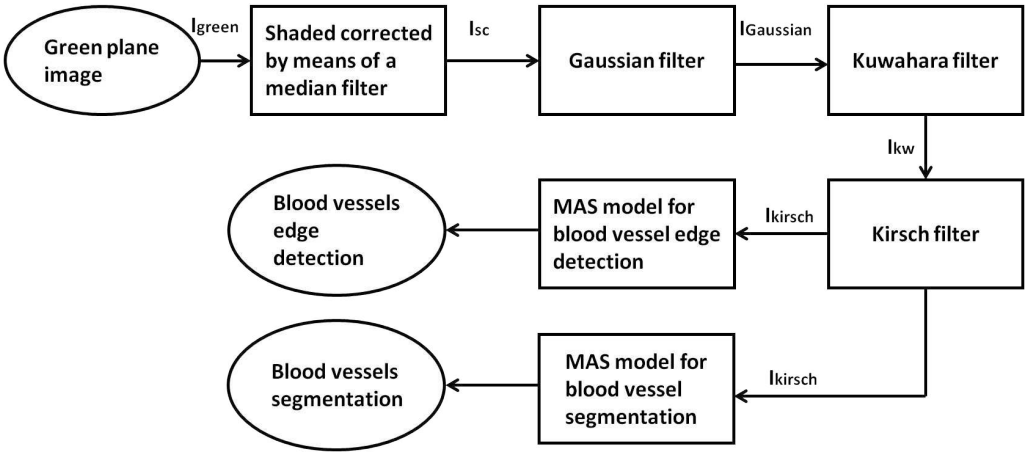

Figure 7.1.: Schematic representation of the preprocessing phase

Affected DR fundus images often present bright lesions. Since this approach goal is to segment blood vessels that are dark structures, the bright structures can be removed from I_{sc}, as soon as the shade corrected image has negative values for all pixels having an intensity lower than the background. In that way, all pixels with a positive value were set to zero in I_{sc}. A Gaussian filter (see subsection A.2.1; width 3 pixels; $\sigma = 2$) was then applied to attenuate the high frequency noise and other undesirable details resulting in image $I_{gaussian}$.

In order to remove fundus image noise while preserving the edges, Kuwahara filter (see subsection A.2.3) was applied to $I_{gaussian}$. Finally, a Kirsch filter modified version (see subsection A.3.2) was employed in the image resulted from the last step (I_{kw}). This improved Kirsch filter [43] enables edges detection with a two pixel thickness whose external edge is represented by a positive or negative value, whereas the internal edge has an opposite value (Figure 7.2 a). This enables the MAS model detection process as the agents determine the edges thanks to these two internal and external edges presence. Moreover, the blood vessels gradient has a specific pattern (Figure 7.2 b) since they can be represented by two parallel linear segments series. Thus, agents search for blood vessels edges by looking for this specific gradient pattern.

7.3.2. Multi-agent system models

MAS is composed by an agents set and their environment. The environment contains the green plane image in which each pixel contains the gray level intensity and a boolean value defining if the pixel has already been explored by an agent. Moreover, when located in the environment the agents perceive the modified Kirsch gradient which defines a right visible edge. Agents are of several kinds with different behaviors according to their current state and perception.

Each of the agents presents its own sensors, behavior and influences (reactions) over

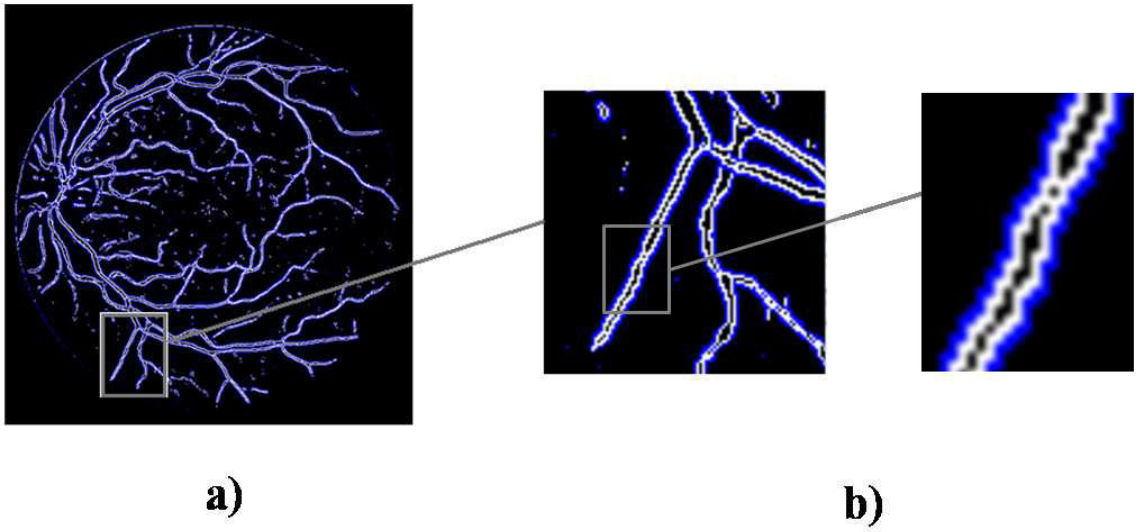

Figure 7.2.: a) Resultant image of the modified Kirsch filter where the blue and white pixels represent negative and gradient values, respectively. b) Expanded version of one section of image a), where is possible to see a characteristic pattern in the blood vessel gradient values.

the environment (see Table 7.2 and Table 7.3 for details). The sensors allow the agent to perceive, for instance, its current position; environment information; its current position correspondent gradient; messages destined to it; connections between the agent and its neighbors. The behaviors are the agent deliberative steps. According to the returned sensors perceptions, agent deliberates by sending influences to the system (agents or environment). A behavior may have several possible influences. The influences are all the actions an agent can carry out. These can be: agent movement; influences on the environment, like black board modifications revealing to other agents positions already treated; messages sending; agents' removal and addition.

7.3.2.1. Agents and behaviors for the blood vessel edge detection

The MAS model developed for the detection of the blood vessel edges is compounded by four kinds of agents: the search agent (SA) explores the environment looking for blood vessels edges; the following agent (FAs) follows a detected edge; the node agent (NA) builds segments; the end agent (EA) confirms if the segment belongs to a blood vessel edge.

The system initializes one SA launched on one of the white points from Figure 7.2, randomly chosen and it has to find edges. Agent evolves in the environment by analyzing the points with positive gradient gathered in one list (L_p). When it finds an edge, it determines the possible directions to follow the contour, creates a NA and moves to another position. The NA creates FAs in the directions given by

the SA and establishes segments with them. The FAs follow the detected edge till its segment no longer corresponds with the explored contour anymore. They then create NAs, give them information about the direction to follow and die. These new NAs create new FAs, and so it carries on. Considering that several agents can follow the same contour, they end up meeting and merging. When there is no direction to follow, the NA creates an EA. These agents clean the small segments not belonging to blood vessels, but to some noise and other background imperfections that still remain after the preprocessing phase, by analyzing the environment information related to the image gray levels. Moreover, EAs are responsible to close edges by creating speculation links with the closest EA.

At the process end, agents must rebuild vessels edge by representing it with a succession of segments .

Table 7.2.: Summary of the agents' sensor, behaviors and influences in the MAS model proposed for the blood vessel edges detection

Agent	Sensor's function	Behavior	Reactions
Search Agent	- Current position - Gradient correspondent to its current position and neighbors - Positive gradient points list (L_p)	Search behavior	- Remove the explored point from the list L_p - Add SA and NA
Node Agent	- Current position - Segment list - Possible directions list	Node behavior	- Establishes the segments to reconstructs the vessels' edges - Add FA and EA
Following Agent	- Current position - Its segment list points (L_{pos}) - NA to which it is connected - Messages destined to it - Gradient correspondent to its current position and neighbors	Edge following behavior	- Mark the environment to say that it has already explored this area - Send messages - Add NA
End Agent	- Current position - NA to which it is connected - EA with which it establishes a link of speculation - Gray level correspondent to its current position and neighbors	Edge end behavior	- Clean the segments not belonging to blood vessels

Search behavior. The search behavior of the agent initially launched by the system is composed of two stages. First, the agent verifies if the pixel where it is located agrees to the conditions: (1) not visited yet by another agent; (2) corresponds

to vessel pattern. To verify if the pixel belongs to a vessel pattern, the agent calculates the line slope formed by its position and the positions of its positive gradient neighbors (Figure 7.3 a). Then, it analysis the gradient values profile in the perpendicular line to it (Figure 7.3 b), and if it corresponds to negative-positive-null-positive-negative values, the pixel belongs to a vessel edge. When verifying the two conditions, it determines the possible directions to follow, launches a NA on its position and moves to another white point, also randomly chosen. Moreover, it launches another SA on the parallel line to the one where it was initially located (Figure 7.3 c). This last SA already knows that it is located on a pixel belonging to a vessel pattern, and thus its behavior is just to determine the possible directions to follow, and to launch a NA on its position before dying. To determine which directions to follow, agents look for the white points in their 8-neighboring having a blue point in the 4-neighboring. This blue point has also to belong to the 8-neighbors of the target pixel. For instance, in Figure 7.3 d), there are just two directions available.

The initially launched SA stops its behavior and disappears when all the points of the list L_p were analyzed.

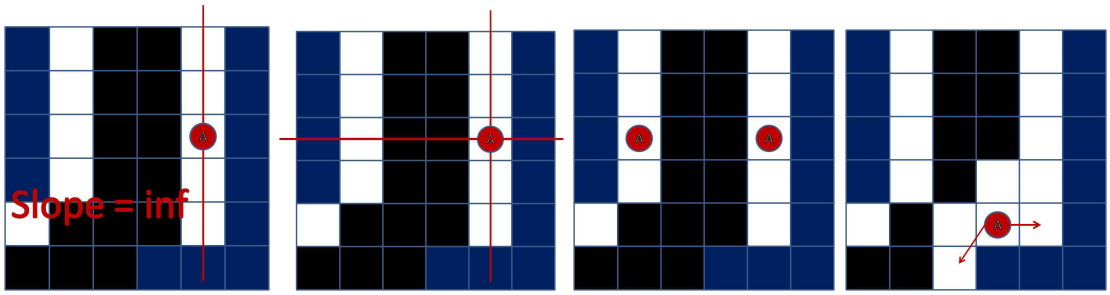

Figure 7.3.: The search agent (red circle) behavior. a) It calculates the slope of the line to determine the perpendicular line (b). Then it verifies the gradient values profile and as the pixel belongs to a vessel pattern it launches another search agent (c); d) Possible directions (red arrows) that the agent has to follow according to the follow agents' restrictions

Node behavior. The node behavior is executed just one time. The NA launches FAs in the directions given by the launcher agent (SA or FA) by means of a possible direction to follow list. If this list is empty it launches an EA. Then the NA establishes segments with those launched agents and keeps these segments in its segment list.

Edge following behavior. When the FA perceives another FA moving on the same line vessel but in the opposite direction, they demand a fusion process with each other by linking respective NAs, since FA is linked with a NA which does not move.

To construct the edge, the FA moves pixel per pixel and it stores the pixel position where it is located in its segment list points (L_{pos}). The aim is to ensure that each position characterizing the edge portion which separates it from its neighbor can be approximated by the segment connecting the two agents (Figure 7.4). That is, the distance between each point and the segment must be lower than a threshold (T_{seg}). To determine this distance, the projection of these points onto the segment is first calculated using Pythagoras theorem by Equation 7.1. Then, Equation 7.2 is checked and if all the distances between $L_{pos[i]}$ and H_i are lower than T_{seg}, the segment is considered valid.

$$\forall L_{pos}[i] \in L_{pos}, \quad \overrightarrow{AH_i} = \mu_i \overrightarrow{AB} \; and \; \mu_i = \frac{1}{2} - \frac{\overrightarrow{CB}^2 - \overrightarrow{AC}^2}{2\overrightarrow{AB}^2} \tag{7.1}$$

$$\forall L_{pos}[i] \in L_{pos}, \quad \overrightarrow{L_{pos}[i]H_i} \leq T_{seg} \tag{7.2}$$

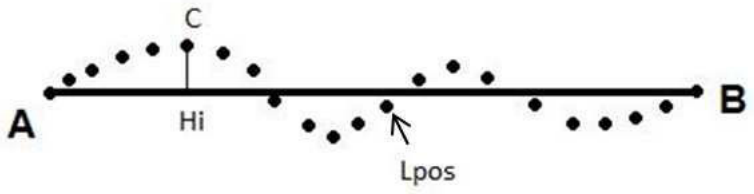

Figure 7.4.: Segment representing a points list

The FAs move by determining the possible directions to follow such as the SAs do. If the FA has just one direction to follow, it checks if the segment formed between the position of its neighbor and its position is a valid segment, and if not, it launches another NA on its position and disappears. If it has more than one direction to follow, it also launches a NA and disappears. After each movement, the FA sends a message to all the FAs to attempt a fusion.

Edge end behavior. If somewhere there is no direction to follow, an EA is launched. The EA behavior is to check if it is located on a blood vessel edge by analyzing the green intensity profile on the perpendicular direction to its segment. It just verifies if the profile is similar to a Gaussian shape such as the blood vessels should be. If the profile does not fit a Gaussian curve, the EA disappears with its segment. If the profile fits a Gaussian curve the EA proceeds its behavior. This process is important to clean the small segments not belonging to the blood vessels, but to some noise and other background imperfections that still remain after the preprocessing phase. After verifying that the segment belongs to a vessel, the EA connects itself

with the closest EA, if the distance between them is lower than a threshold. The link established between the two agents is a link of speculation, since if another EA appears later and nearest to one of the EA, the link of speculation is replaced.

7.3.2.2. Agents and behaviors for the blood vessel segmentation

The MAS model implemented for the blood vessel segmentation is also compounded by four kinds of agents: search agent (SA), following agent (FA), node agent (NA) and region agent (RA). Despite of having similar names and sometimes also similar functions, the agents' behavior of this model is different in many aspects from the agents' behavior of the model previously described.

MAS is initialized with a SA in the "operating" state, launched on one of the white points from Figure 7.2 randomly chosen. This SA has to find edges belonging to blood vessel regions. It evolves in the environment by following positive gradient points. When it finds an edge, it initializes a new contour and launches two NAs belonging to this contour: one in the "active" state and another in the "inactive" one (Figure 7.5 a). Furthermore, the SA changes its state to "suspended". Then the "active" NA has to allow contour extension and closure. Therefore, it determines the possible directions to follow the contour, creates FA and becomes "inactive" (Figure 7.5 b). FA follows the detected edge until there is no direction to follow or until the contour reaches a specific length (Figure 7.5 c). FA launches then an "inactive" NA on its position and an "active" NA on the perpendicular direction where it was moving (Figure 7.5 d). Moreover, FA gives to the "active" NA information about its direction allowing it to launch another FA in the opposite direction (Figure 7.5 e). When this FA reaches the initially launched "inactive" NA (Figure 7.5 f) it launches a RA (Figure 7.5 g) which will be responsible for the contour delimited region. RA sends a message to SA to change its state to "operating" and repeats all the process until all the blood vessels contours are found by MAS. There so, MAS detects one contour each time avoiding regions intersection at this phase. Afterward SA sends a message to all RAs to change their state to "filling". RA fills all the contours taking into account the image gray levels. Finally, RAs attempt fusions with each other.

At the end of the process MAS has to reconstruct the vessels by representing them with a succession of regions initially represented by contours.

Search Behavior SA can be either "operating" or "suspended". In the "operating" state, each agent first verifies if the pixel in which it is located verifies these conditions: (1) not yet visited by another agent; (2) corresponds to vessel pattern. To verify if the pixel belongs to a vessel pattern, the agent behaves in the same way as the SA of the model described in the previous section. When verifying the two conditions it initiates a new contour, launches a NA on its position and a NA on the parallel line to the one where it was initially located (Figure 7.5 a). The

Table 7.3.: Summary of the agents' sensor, behaviors and influences in the MAS model proposed for the blood vessel segmentation

Agent	Sensor's function	Behavior	Reactions
Search Agent	- Current position - State - Gradient correspondent to its current position and neighbors - Positive gradient points list (L_p)	Search behavior	- Remove the explored point from the list L_p - Add Node agents - Send and receive messages
Node Agent	- Current position - State - Contour - Memorized direction - Gradient correspondent to its current position and neighbors	Node Behavior	- Mark the environment to say that it has already explored this area - Add following agent and region agent
Following Agent	- Current position - Contour - Gradient correspondent to its current position and neighbors - Explored points list	Following behavior	- Mark the environment to say that it has already explored this area - Add node agent and region agent
Region Agent	- Contour - State - Gray level correspondent to its current points and neighbors	Region behavior	- Send and receive messages - Delimit the environment (image) in regions to reconstructs the blood vessel structure

two NAs keep the created contour information. Then, the SA changes its state to "suspended" where it will remain until receiving a message to change again for the "operating" state. At the beginning of the "operating" state if the agent cannot verify one of the two conditions it moves to another white point, also randomly chosen. The initially launched SA stops its behavior and disappears when all the list points L_p were analyzed. Before dying, it sends a message to all the RA in order to change its state from "suspended" to "looking".

Node Behavior NA can be "active" or "inactive". In the "active" state it determines the possible directions to follow the contour. To determine these directions, the agents behave like the SA of the model described in section 7.3.2.1 when it is doing the same thing. If there is at least one direction to follow and the memorized direction is null, NA launches FAs in all directions. If the memorized direction is not null, the direction performing the biggest angle with the memorized direction is chosen to launch FA. If there is no direction to follow NA checks if its contour has

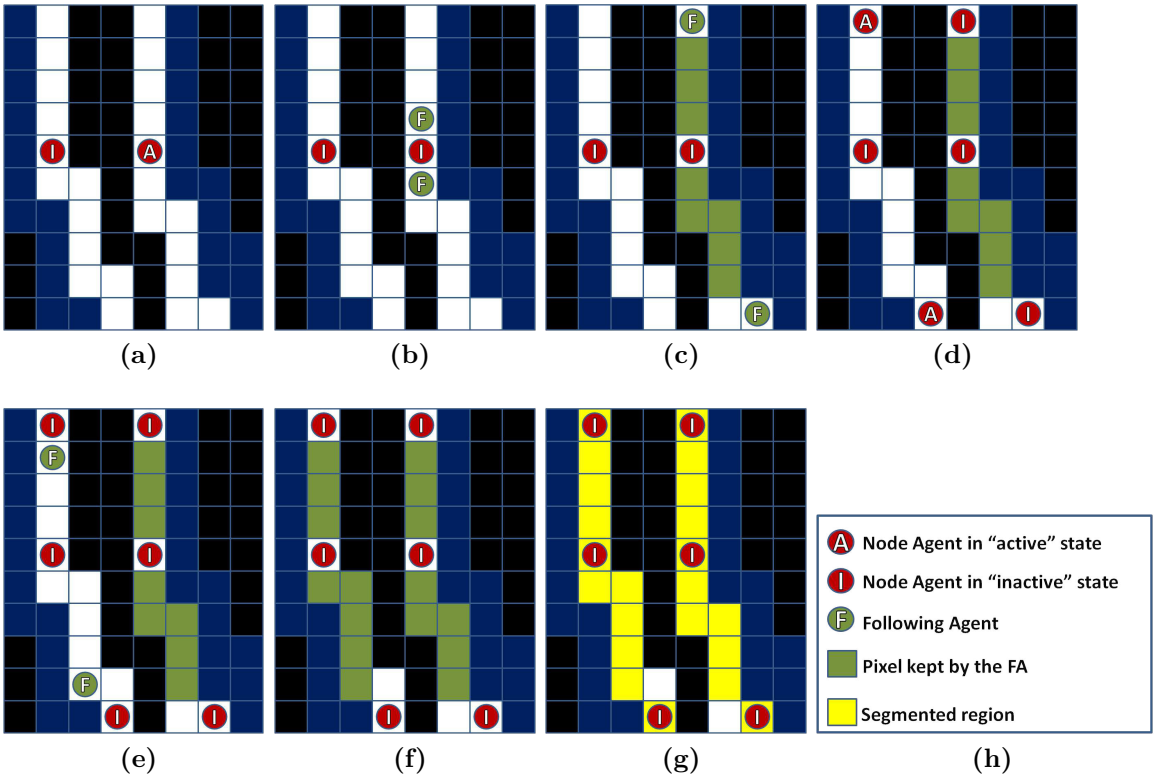

Figure 7.5.: Contour formation graphical representation to which a RA is assigned

already a region agent and if not, launches a RA. At the end of the "active" state NA becomes "inactive".

Following Behavior FA initializes its behavior analyzing the possible directions to follow such as NA does. If there is just one direction to follow, FA adds its position to its explored points list, to the contour points list and moves to the new position. If there is more than one direction to follow, or if the length of its explored points list is bigger than a specific threshold, the agent can act in two ways depending if it was moving away or to the first NA contour. If it was moving away, it has to close the contour and therefore, the agent launches a NA on its position and another in the perpendicular direction to the one which was moving. If it was moving in the NA direction, it adds its position to the contour points list, verifies if the contour has already a RA, and if not, it launches one. After that it dies.

Region Behavior RA can be either in "waiting", "filling" or "fusion" state. When launched by a FA or by a NA it remains in the "waiting" phase until receives a message from SA to change its state to "filling". In this state RA fills the contour by analyzing the gray level points located between each pair of the contour points. For each pair of points, the line equation that contains the two points is calculated

(Figure 7.6 a)-c). Then, the points located between them are determined and for each of them an evaluation related to its gray level intensity is made. That is, the point is added to the region if its gray level value is lower than the gray level values average of the points that are already in the region (Figure 7.6 d). After that, RA builds a region border pixel positions list and changes its state to "fusion". At this state RA attempts a fusion with the neighbor RAs by sending messages to them. RA considers another RA as neighbor if the distance between at least one of its border points and one border point of the other RA is smaller or equal to a specific threshold (D). During fusion process the points located between each border points pair of both agents, with a distance smaller than D, are evaluated in terms of gray level value. In that way, the points located between the two regions are considered to make part of the new region, if their gray level value is smaller than the gray levels average of region pixels of the demanding fusion RA. After keeping all the information about the neighbor RA by updating its own region information, RA kills the neighbor agent and changes its current state to "waiting".

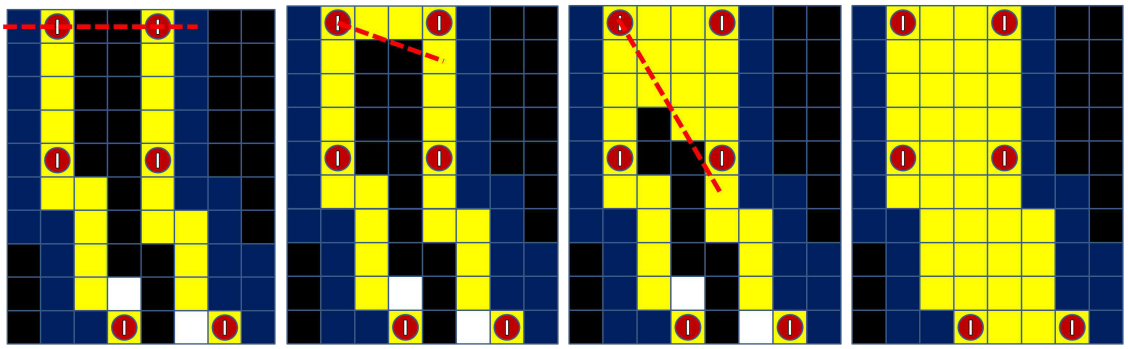

Figure 7.6.: RA "filling" state graphical representation. It analysis the pixels located between each pair of two points belonging to its contour by determining the line linking these two points a) – c); d) at the end, all the points that are inside the contour with a gray level value similar to the contour average gray level value, are added to the region.

7.3.3. Retinal images and the multi-agent platform

The DRIVE database, already referred in section 5.3.3, was used to test the proposed approach. This dataset is equally divided into two images set, called test set and training set. For each of the 40 images, database contains a manual segmentation vasculature map to be used as ground truth. For the test set, a second manual segmentation vasculature map is also included in the dataset.

The proposed MAS models were implemented with MadKit [123], a generic multi-agent platform written in Java and built upon the AGR (Agent/Group/Role) orga-

nizational model (Figure 7.7). That is, MadKit agents play roles in groups and thus create artificial societies.

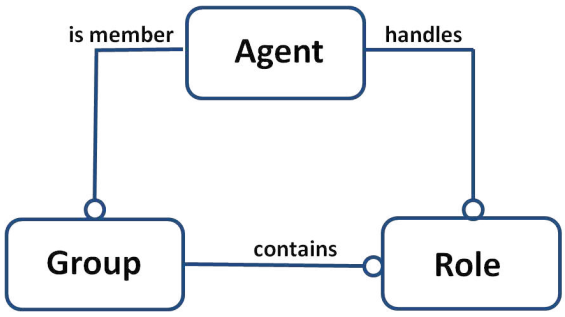

Figure 7.7.: AGR model schematic (adapted from [31])

7.4. Results and discussion

The performance of the MAS for blood vessel edge reconstruction or for segmenting the vessels depends directly on the image processing algorithms used in the preprocessing phase. It also depends on how the system interprets information resulting from this first phase of the approach. To measure the overall approach performance, it is important to compare the resulting image with the information detected by the Kirsch filter. Moreover, the differences between the resulting edge map image and the ground truth vessel map also present in the DRIVE database should be evaluated. In that way, common measurements namely, sensitivity, specificity, predictive value and overall accuracy were used for testing the proposed algorithms. Figure 7.8 and Figure 7.9 show the quantitative results obtained with the MAS model in the DRIVE dataset for the blood vessels segmentation. Figure 7.8 illustrates sensitivity, specificity and predictive values for all the dataset images. Figure 7.9 represents the sensitive values for all the test images using two different ground truth vessel maps, in which some discrepancies can be observed.

The proposed approach results applied to two retinal images are shown in Figure 7.10 and Figure 7.11. These are the images where the MAS model implemented for the vessel segmentation had the best and the worst performance, respectively. The corresponding quantitative results are described in Table 7.4. Figures illustrate the original color image (above left), the Kirsch filter resultant image (above right), the hand labeled segmentation provided with the database (below left), the edge detection (below center) and the vessel segmentation (below right) performed by respective MAS models.

Figure 7.12 illustrates a superimposed image of the hand labeled image with the hand labeled image after morphological opening and with MAS result. This mathematical operator aims to clean the thinnest manually segmented vessels. In this figure, the white pixels represent the pixels common to the three images; the yellow

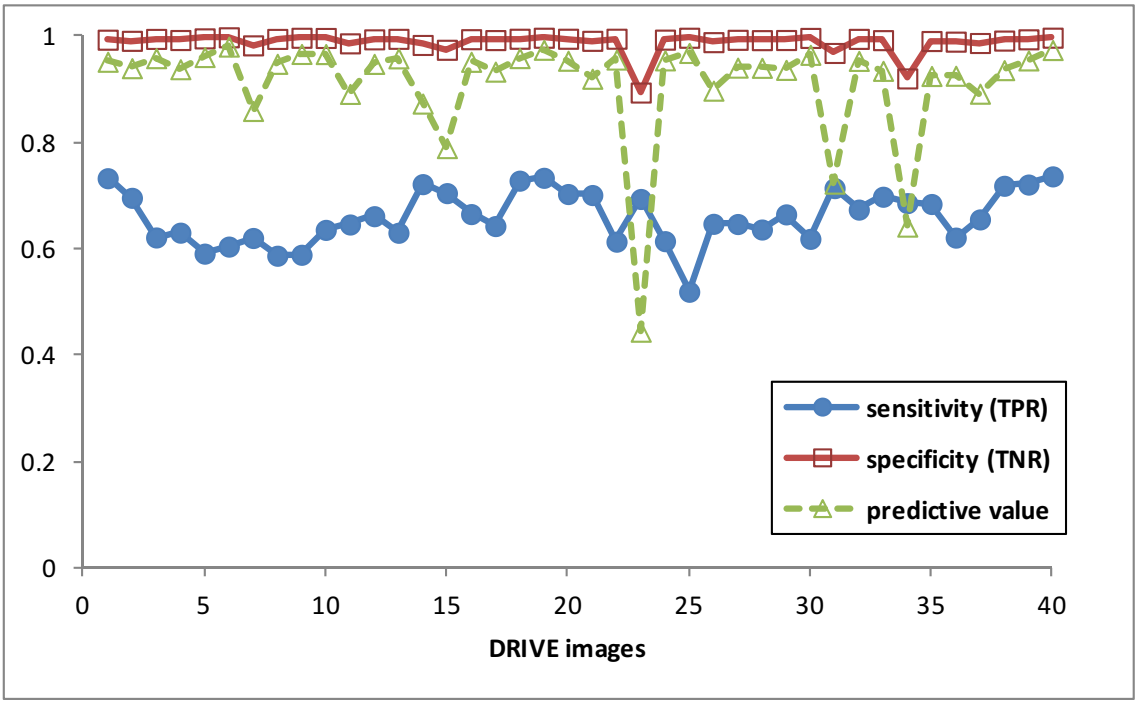

Figure 7.8.: Sensitivity, specificity and predictive values obtained from the 40 images of the DRIVE database with the proposed approach

Table 7.4.: Worst and best quantitative results for the MAS model applied in the DRIVE dataset

	Sensitivity	**Specificity**	**PPV**
Worst result	0.519	0.997	0.968
Best result	0.736	0.997	0.974

and green pixels represent the pixels that belong to blood vessels manually segmented pixels but are not detected by MAS, that is, the false negative pixels; and the false positive pixels are represented in blue. As it can be seen, the most part of false positive pixels are located at the manually segmented vessels border and therefore, they should not be considered as false positive. Actually, manual blood vessels segmentation of retinal images is a very arduous and difficult task, leading two people to segment the same image in different ways. This can be observed in Figure 7.9 where two different hand labeled images for the same color fundus image resulted in different sensitivity values with the same approach.

By analyzing the Kirsch filter images and the corresponding MAS models results from Figure 7.10 and Figure 7.11 it can be observed that the MAS rebuild the most part of the vessels, especially the thicker ones. Some of the thinnest vessels were also segmented but not all, affecting the sensitivity values. In fact, after removing the thinnest vessels from the hand labeled image (green pixels of Figure 7.12) the

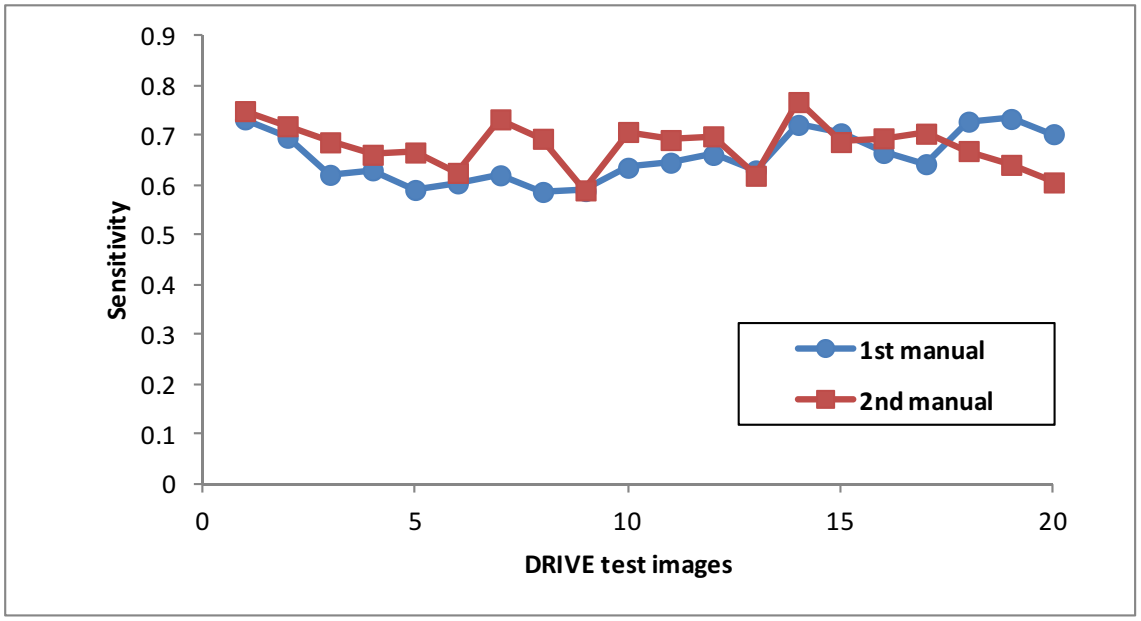

Figure 7.9.: Sensitivity values obtained from the 20 images of the DRIVE database test set, using both hand labeled databases

sensitivity values of the proposed approach increased to values higher than 80%. So, improvements have to be made in the MAS model to deal with smaller vessels.

Moreover, there are some thickest vessels portions not detected by the MAS model mostly near the FOV border and the optic disc contour. This last problem may be related to the preprocessing phase, mainly to Kuwahara filter since this often produces clearly noticeable artifacts. These artifacts may be due to one of the four sub regions selection process that becomes unstable if noise is present or when sub regions have the same variance, since this results in randomly chosen a sub region [124].

Therefore, MAS model is efficient in segmenting the blood vessels from where the edges were already detected in the preprocessing phase, and in excluding the detected pixels that did not belong to vessels (Figure 7.13 arrow a). Furthermore, MAS is able to close edges that were interrupted edges in the Kirsch resultant image (Figure 7.13 arrow b).

Table 7.5 shows different approaches results in terms of overall accuracy when applied to the DRIVE dataset. It can be observed that the proposed approach outperforms at least two traditional methods found in literature. The main advantage of our method is its capacity of excluding pixels that do not belong to vessels, increasing its accuracy value. The difficulty in dealing with the smaller vessels is a common problem with the traditional methods found in literature.

Despite of the improvements that have to be done in the MAS model to deal with smaller vessels, the experiments show that the use of a MAS model at the micro

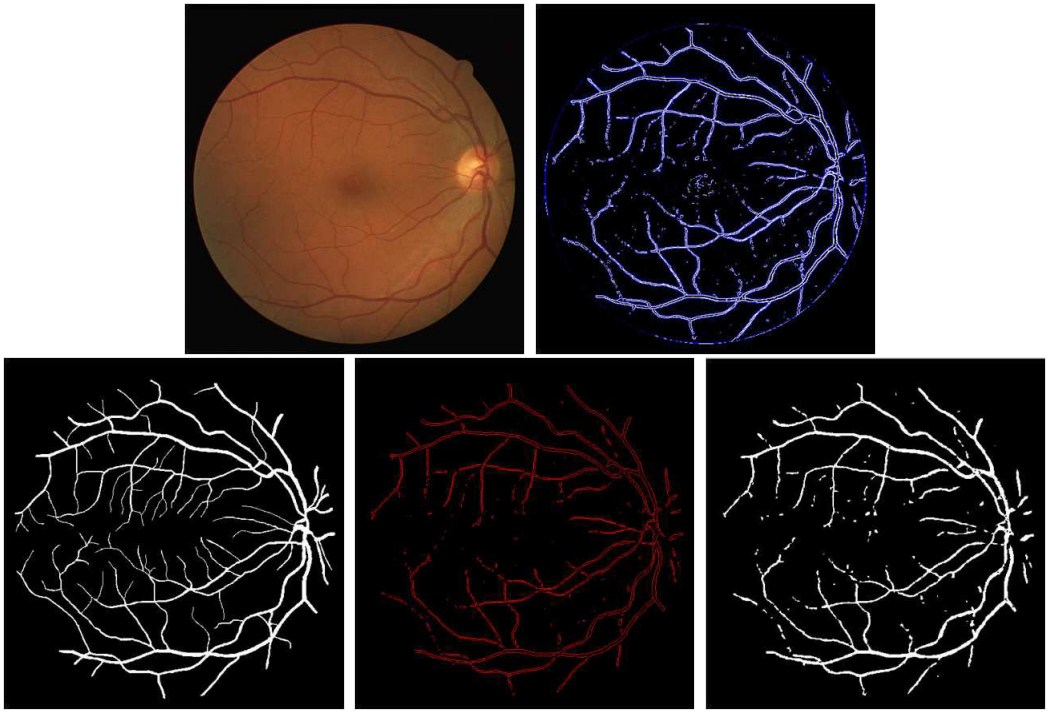

Figure 7.10.: Images resulting where the proposed approach had the best performance in the DRIVE database. From left to right: original color fundus image and Kirsch filter resultant image (above); hand labeled image, blood vessel edge detection using MAS approach and blood vessel segmentation using MAS approach (below).

level could be an effective way to segment structures in complex images as the retinal images. In fact, through environment perception and local interactions, a simple agent organization can have as global behavior the detection of most part of the retinal vasculature.

Table 7.5.: Accuracy of different approaches applied to the DRIVE dataset

	Accuracy
Zhang et al (2010)	0.9382
Staal et al. (2004)	0.9441
Proposed approach	**0.9443**
Mendonça and Campilho (2006)	0.9463
Soares et al. (2006)	0.9466
2nd observer	0.9473
Ricci and Perfetti (2007)	0.9595

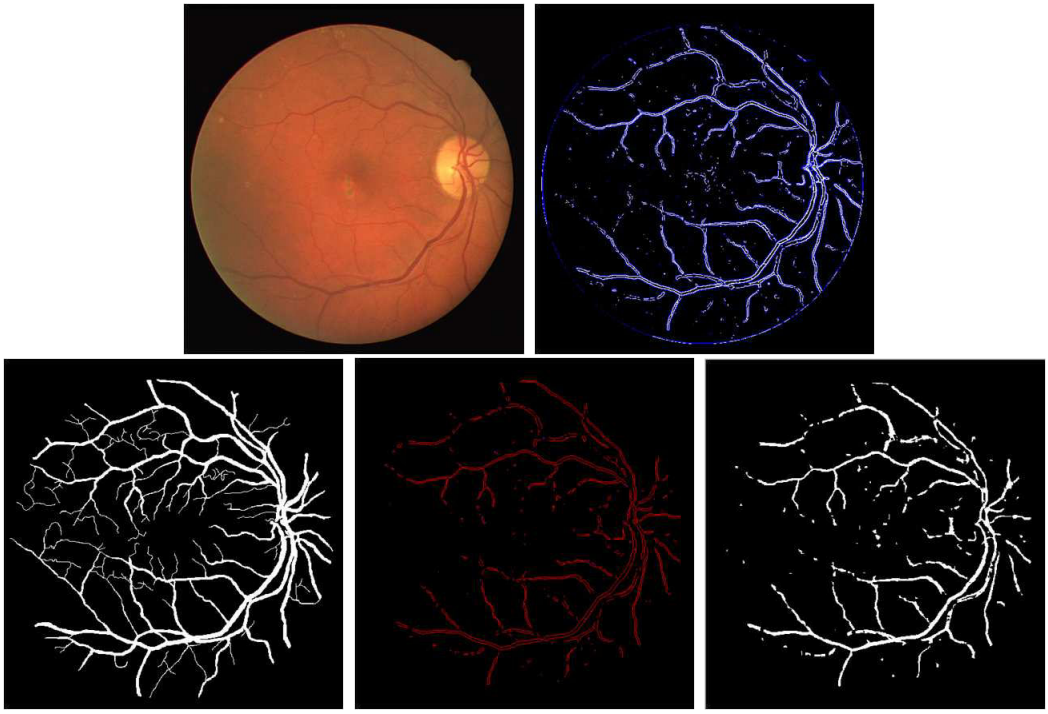

Figure 7.11.: Images resulting where the proposed approach had the worst performance in the DRIVE database. From left to right: original color fundus image and Kirsch filter resulting image (above); hand labeled image, blood vessel edge detection using MAS approach and blood vessel segmentation using MAS approach (below).

7.5. Conclusion

In this study, a MAS approach is proposed where agents enrich a traditional edge detector algorithm allowing local processing adaptation and cooperative behaviors. The system is able to segment the most part of the blood vessels present in the color fundus images. Despite of some problems in detecting the thinnest vessels, the proposed approach results show that the use of the MAS model in the micro level could be an effective way to segment structures in complex images. In fact, for the DRIVE dataset, the proposed approach achieves an accuracy of 0.9443 and performs better than at least two traditional methods found in literature. The thinnest vessels detection problem is common with the methods found in literature. In this case, it can perhaps be overcome by transferring global preprocessing progressively toward local algorithms applied and adapted by agents.

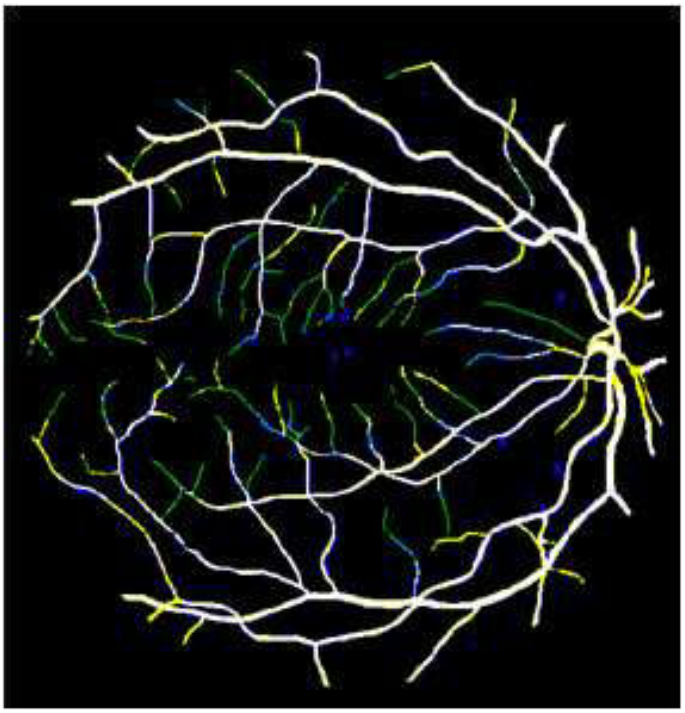

Figure 7.12.: Hand labeled image superimposition with the hand labeled image after the morphological opening and with MAS result

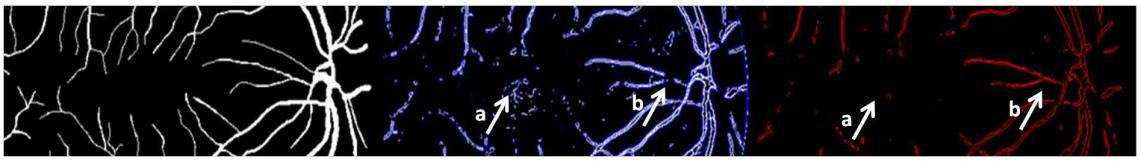

Figure 7.13.: Expanded version of one section of an image, to verify the agent capacity to exclude pixels that do not belong to vessels (arrow a) and to close edges interrupted in the Kirsch image (arrow b). From left to right: ground truth image; Kirsch resulting image; edge detected image resultant from the MAS model.

8. Small dark lesions detection

In this chapter, a multi-agent based approach for the microaneurysms segmentation in color fundus photographs is presented. This multi-agent model is preceded by a preprocessing phase to allow the environment construction where agents are situated and interact. Then, microaneurysms segmentation emerges from agent interaction. In this study, competitive results compared to more traditional algorithms were achieved, especially in detecting microaneurysms close to vessels.

8.1. Introduction

The microaneurysm (MA) presence in the retina is often the diabetic retinopathy first sign and thus its early detection is crucial for blindness prevention. Therefore, it is of great importance to include their automatic detection into a screening program.

This kind of lesion is commonly described as isolated small round objects with 10 μm to 100 μm in diameter. In practice, they may appear as a conglomeration of more than one MA or in association with larger vessels. Microaneurysms are frequently indistinguishable from the dot-hemorrhages in color fundus photographs where both appear red. Nonetheless, these two kinds of lesion represent the same clinical implications and therefore, there is usually no need for an automated MA detector to distinguish between them. The number of microaneurysms is positively correlated with the severity and the DR progression, at least for the early stages of the disease [125].

Since microaneurysms can be easily observed in digital color fundus images and their number have clinical implications, they have been one of the first lesions detected in the automatic image analysis systems. Despite of the number of interesting computational approaches proposed in literature to detect small dark lesions, none of them has shown the required performance for the clinical practices. They generally refer to global approaches and have difficulty in dealing with low contrast between red lesions and background, and in detecting the microaneurysms situated close to the retinal blood vessels. Therefore, a new approach based on a multi-agent system is proposed in this thesis.

Using MAS for medical image analysis has been revealed as a research field in expansion (see section 3.3). Chapter 7 describes an approach for the blood vessels edge detection and segmentation. The new approach proposed in this chapter is also composed by a preprocessing step in which some traditional image processing algorithms

are used to define the environment (image), where autonomous agents are situated and interact among themselves. Then, from the MAS model the microaneurysms segmentation emerges as a global behavior.

8.2. Related work

Several approaches have been proposed in literature concerning the microaneurysms segmentation through fundus image analysis. These approaches are frequently based on morphological [1, 126], template-matched [127, 128] and supervised learning methods [2, 129]. The supervised methods are frequently preceded by one of the two other approaches [1, 126, 128].

Some approaches described in the literature deal with the detection of microaneurysms in fluorescein angiographies. In these kind of images, microaneurysms appear as bright patterns and better contrasted than in the green channel of color images. However, microaneurysms have some characteristics in common in both images: they appear small, isolated and of circular shape, which is fundamental to use morphological approaches. The first algorithm was developed by Laÿ [130] and then improved by other authors [2, 126, 131]. These approaches utilize the top-hat transformation to discriminate between circular, non-connected red lesions and the elongated vasculature. The method consists of morphological opening the green channel images with a linear structuring element at different orientations to obtain the vasculature and, then, remove it from the original image. The length of the structuring element is chosen to be short enough to fit inside curved vessels, and long enough that it cannot fit inside MAs, so that it detects vessels (and other large extended features) but not MAs. However, if the length of the structuring element is increased to allow the larger object detection, the vessel segmentation deteriorates leading to more spurious candidate objects detected on the vessel. This approach has been modified and used subsequently by others authors, like Walter et al. [1] who detected microaneurysms candidates by applying diameter closing and an automatic threshold scheme.

Niemeijer et al. [2] developed a microaneurysm detection approach that has inspired several research groups [126, 131]. The general approach is schematically illustrated in Figure 8.1 and described in following.

First the digital green plane image is shade-corrected to uniform the background illumination of the retinal images. Normally, shade-correction is achieved by estimating the background illumination image by means of a large median or mean filtering. The background image is either subtracted from or divided by the green plane image. The next step consists in detecting the vasculature by morphological opening the shade-corrected image with a linear structuring element at several angles to enhance all vessel segments (top-hat transform). The segmented vessels are then subtracted from the shade-corrected image. The resulting image contains

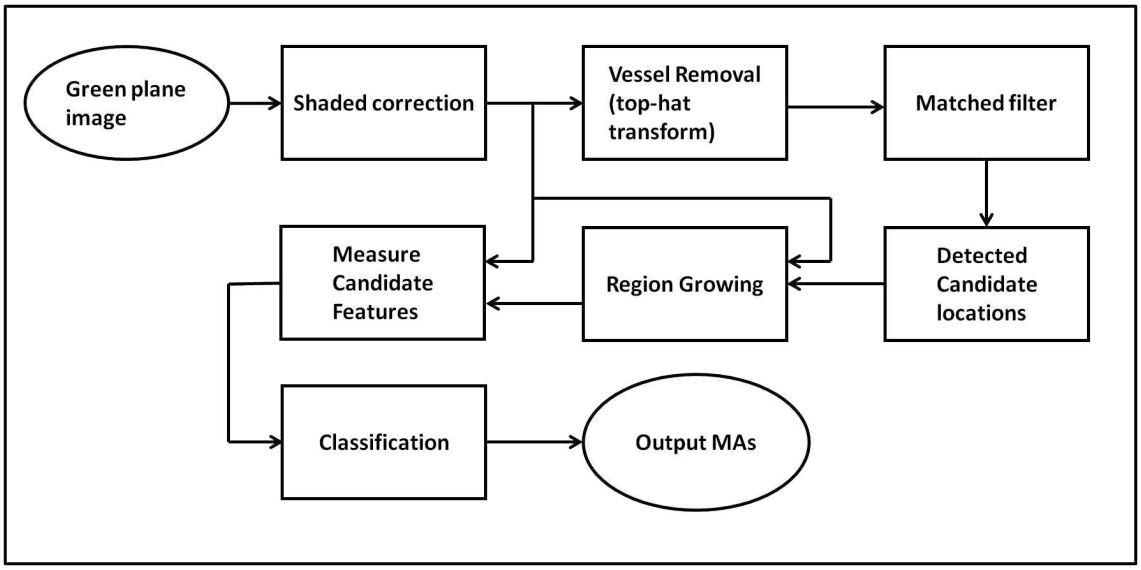

Figure 8.1.: Schematic representation of the "standard" approach for the microaneurysm detection (adapted from [125])

small dark objects, such as MAs, and small fragments left over from the vessels, that are then highlighted by applying a matched-filter with a circularly symmetric 2D Gaussian as kernel. Hereafter, the image is thresholded to detect the candidates MAs, which are used as locations to initiate a region growing process on the shade-corrected image, to delineate the underlying morphology of the candidate. Finally, intensity and shape descriptors are determined in the region-grown object and a classifier is used to ameliorate MA detection. The main drawback of this approach is that this method typically cannot detect MAs close to vessels.

Zhang et al. [132] presented an approach that differs from the "standard" in the way the candidates MAs and vessels are detected. In order to detect candidates, this method applied a non-linear filter with five Gaussian kernels with different standard deviations to the input retinal images. By keeping the maximal correlation coefficient for each pixel a maximal correlation response image was obtained, which was then thresholded with a fixed threshold value to determine the candidates. The vessels were segmented by an adaptive thresholding technique and then they were used to reduce the number of candidates. Finally, the region growing process was applied to determine their precise size and a set of features was extracted for each of them. Recently, the same group [128] improved their method by including a supervised classifier at the last stage which was the dictionary learning with sparse representation.

Sánchez et al. [129] approach began with a normalization process identical to the "standard" approach. Then, an unsupervised mixture model based clustering method was used to extract candidates on the normalized image intensities. A fitted model was obtained by fitting a Gaussian mixture model to the image inten-

sities. The MAs candidates were segmented by applying a threshold to the fitted model. After automatically masking out the vasculature, a set of color, shape and texture features was extracted from the remaining candidates to be used in a logistic regression, in order to determine likelihoods of being microaneurysm.

Mizutani et al. [133] initialized its approach by applying brightness correction, gamma correction and contrast enhancement to normalize the intensity and contrast between images. The MAs candidate extraction was performed using a modified double ring. The original double ring filter detects regions in the image in which the average pixel value is lower than the average pixel value in the region surrounding it. On the other hand, to reduce spurious detections on small capillaries, the modified filter designed by the authors detects regions where the average pixel value in the surrounding region is lower by a certain fraction of the number of pixels under the filter. Hereafter, the original double ring filter with a different parameter setting was used to detect the vasculature and so to remove false positive candidates that remained on it. The region growing process was then performed and a set of features based on color, intensity, shape and contrast was extracted to be used as input of an artificial neural network.

After normalizing the images like the "standard" approach, Giancardo et al. [134] selected as MAs candidates the pixels with an intensity value higher than a specific threshold. Then, on original image windows for which at least a MA candidate exists, the Radon transform was calculated at various scanning angles. From this step results a set of features that was classified through PCA and SVM.

Quellec et al. [127] proposed a method to detect microaneurysms based on template matching in the wavelet domain. In this domain, without other image processing, it was possible to overcome the problems caused by lighting variations or high-frequency noise by choosing the working sub-bands. The authors looked for the wavelet basis that was best able to discriminate lesions from lesion-free areas. The microaneurysms were modeled with 2D rotation-symmetric generalized Gaussian functions, and the wavelet basis was designed empirically, by numerical optimization procedure, using the lifting scheme framework.

Lazar and Hajdu [135] presented an approach where cross-section profiles with multiple orientations were used to construct a multi-directional height map. In this map, each pixel contained a set of height values that represented the difference of the pixel from its surroundings in a particular direction. A score map resulted from applying a modified multilevel attribute opening step on the height map. The dark small circular objects had the highest scores in the score map and therefore, the MAs could be extracted by thresholding.

Antal and Hajdu [136] proposed an ensemble-based framework to select the best combination between preprocessing methods and MAs candidate extractors already described in the literature.

Concerning the microaneurysm detection in color fundus images, Niemeijer et al. [137] created the Retinopathy Online Challenge (ROC) website. The aim is to bring

together the research community efforts towards the creation of algorithms for the detection of MAs, by evaluating their performance on a common dataset and with the same evaluation modality. This permits a fair comparison between algorithms of different groups. So far, 11 groups have submitted their results on the website. All the methodologies published in the literature developed by these groups are described above and results are shown in Table 8.1.

Table 8.1.: Results and methodology categories of ROC approaches

Publication	**Team name**	**Method category**	**Final score**
Cree [131]	Waikato	Morphology and template matching for segmentation and a supervised classification	0.206
Mizutani et al. [133]	Fujita	Supervised	0.310
Sánchez et al. [129]	GIB Valladolid	Supervised	0.322
Zhang et al. [132]	OKMedical	Template matching	0.357
Zhang et al. [128]	OKMedical_II	Template matching and supervised	0.369
Giancardo et al. [134]	ISMV	Template matching and supervised	0.375
Quellec et al. [127]	LaTIM	Template matching	0.381
Niemeijer et al. [2]	Niemeijer et al.	Morphology and template matching for segmentation and a supervised classification	0.395
Lazar et al. [135]	Lazar et al.	Morphology and template matching	0.423
Antal and Hajdu [136]	DRSCREEN	Supervised	0.434

8.3. Materials and methods

The proposed approach aims at segmenting the microaneurysms present in fundus images by means of a MAS model. The information (environment) for the MAS model results from a preprocessing phase consisting of a group of conventional image processing algorithms. An overall of the proposed approach is illustrated in Figure 8.2.

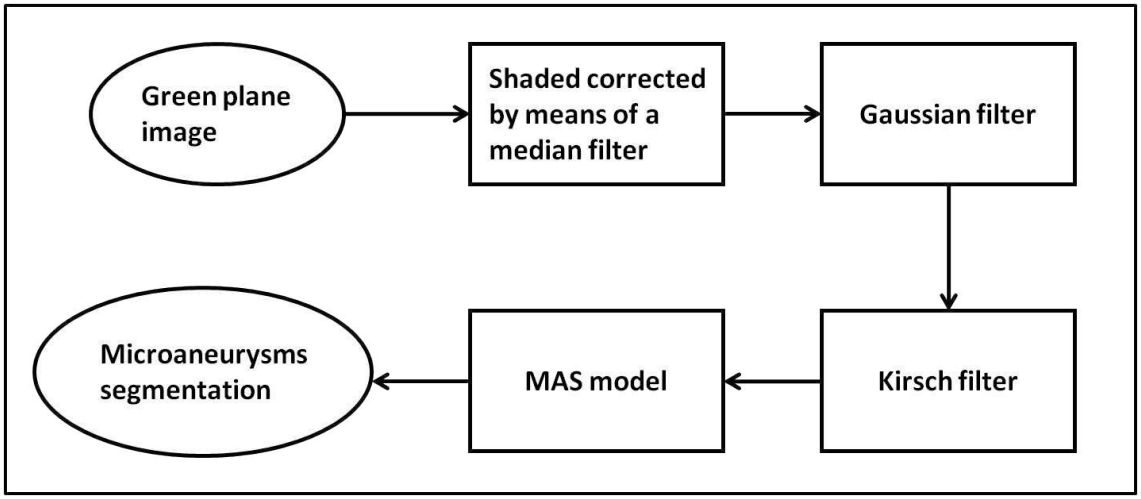

Figure 8.2.: Schematic representation of the proposed approach

8.3.1. Image preprocessing

In this first step, the preprocessing phase from Niemeijer et al. [2] was used. The so obtained image had no background intensity variation across the image and the bright structures were eliminated. Since MA exhibits a Gaussian shape, a Gaussian filter (width=3; σ=1) was then applied to enhance the small dark structures. Finally, the modified Kirsch filter [28] was employed and edges with two pixel thickness were obtained (Figure 8.31 center). This enables the MAS model detection process since microaneurysms presents specific gradient patterns of which some examples can be observed in Figure 8.3 c).

8.3.2. Multi-agent System Model

The MAS model developed for microaneuryms detection is similar with the MAS implemented for blood vessel segmentation. In fact, the agents possess the same reactive architecture and they are situated in an environment that contains the green plane image in which each pixel contains the intensity gray level, and a Boolean value defining if the pixel has already been explored by an agent. Furthermore, when located in the environment, the agents perceive the modified Kirsch gradient. Agents are of two kinds with different behaviors according to their current state and perception: explore agents (EA) and region agents (RA). MAS is initialized with an EA launched on one of the white points from Figure 8.3, randomly chosen. At the end of the process MAS has to segment all the small and isolated dark structures.

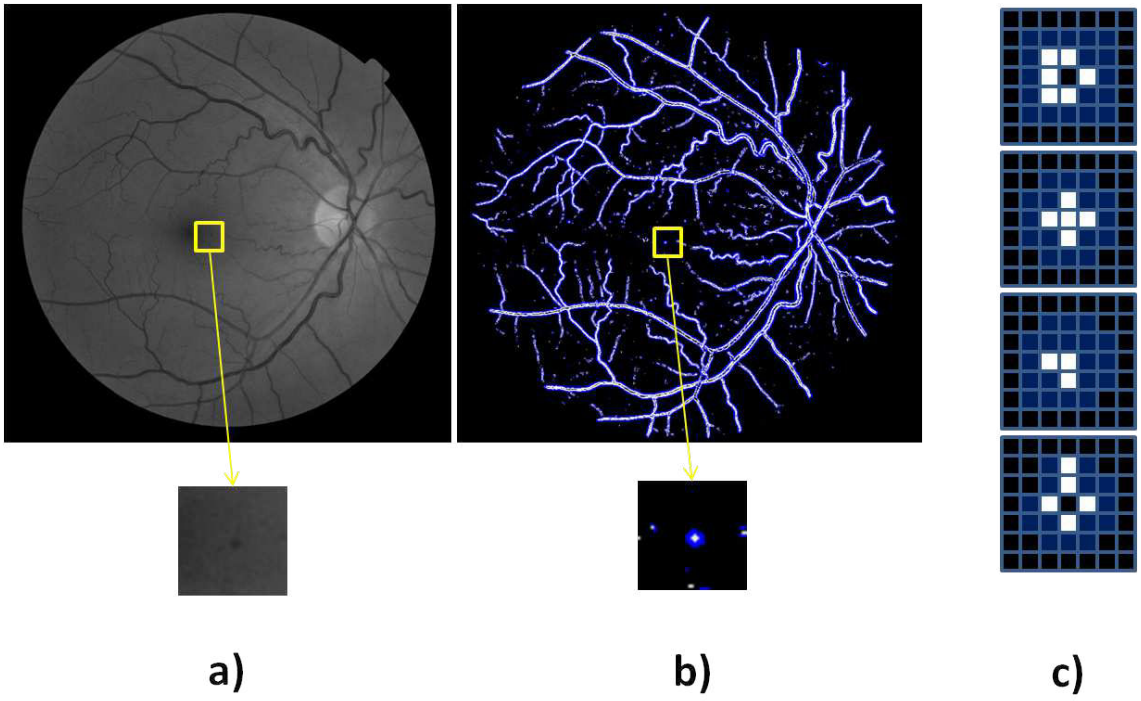

Figure 8.3.: a) Green plane image; b) Modified Kirsch filter resultant image where the blue and white pixels represent negative and positive values, respectively; c) Characteristic gradient pattern of microaneurysms

8.3.2.1. Agents

The agents are reactive and, thus, each of them presents its own sensors, behavior and influences (reactions) over the environment (see Table 8.2).

The system initializes one EA in the "active" state. This EA has to find specific gradient patterns corresponding to microaneurysms. It evolves in the environment by analyzing positive gradient points and its neighbors. When it finds a valid pattern, it launches a RA and becomes "inactive". The RA is launched at the "explore" state, in which it follows an edge until there is no direction to follow. Then the RA changes its state to "waiting" and sends a message to the EA to change its state to "active". This process is repeated until all the positive gradient value points are explored by MAS. Afterward EA sends a message to all RAs to change their state to "joining", in which they attempt for fusion processes with the neighbor RAs. Then, each RA verifies its region contour size and if it is smaller than a threshold (T_c), it fills the region taking into account the image gray level values. Otherwise, the RA disappears with its region. Hereafter, each RA performs a region growing process to allow that the remaining candidates represent the true microaneurysm size. Finally, RA analyzes its region shape and intensity to validate it as a true lesion.

An overview of the proposed MAS model algorithm is illustrated in Figure 8.4.

Table 8.2.: Summary of agents sensor, behavior and influences in the proposed MAS model

Agent	Sensors	Behavior	Reactions
Explore Agent	- Current position - Gradient correspondent to its current position and neighbors - Positive gradient points list (L_p)	Explore behavior	- Remove the explored point from the list L_p - Add RA - Send and receive messages
Region Agent	- Current position - Its points list - Gradient correspondent to its current position and neighbors - Gray level intensity correspondent to its current position and neighbors	Region behavior	- Add RA - Send and receive messages

8.3.2.2. Explore behavior

The explore behavior is composed by two states: "active" or "inactive". In the "active" state, each agent first verifies if the pixel in which it is located verifies these conditions: (1) not yet visited by another agent; (2) corresponds to microaneurysm pattern. To verify if the pixel belongs to a microaneurysm pattern, the agent analyzes the gradient profiles in the neighborhood at four directions (Figure 8.5 a). If it finds the sequences negative-positive-null-positive-negative or negative-positive-negative gradient values in at least two perpendicular directions (Figure 8.5 b) and c), it considers the pixel as a dark structure. When verifying the two conditions it launches a RA on its position and becomes "inactive", where it will remain until receiving a message to change again for the "active" state. At the beginning of the "active" state if the agent cannot verify one of the two conditions, it moves to another white point also randomly chosen. The EA stops its behavior and disappears when all the white points were analyzed. Before dying, it sends a message to all the RA in order to change its state from "waiting" to "joining".

8.3.2.3. Region behavior

RAs initialize their behavior analyzing the possible directions to follow. To determine these directions, agents look for the white points in their 8-neighboring having a blue point in the 4-neighboring. This blue point has also to belong to the 8-neighbors of the target pixel. For instance, in Figure 8.5 d), there are just two directions available. If there is just one direction to follow, RA adds its position to its point list and moves to the new position. If there is more than one direction to follow it chooses one direction to move and launches RAs at the other directions.

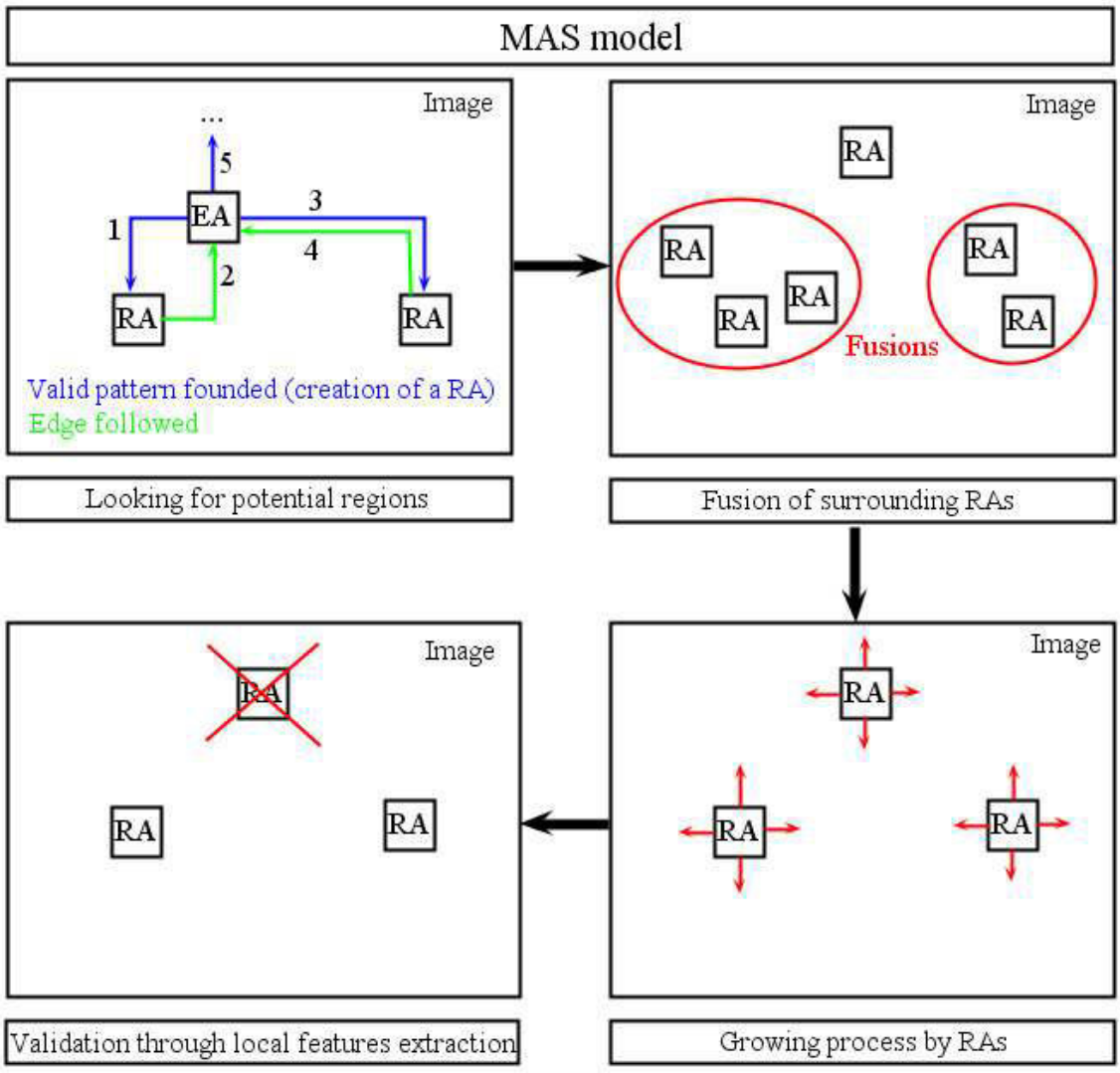

Figure 8.4.: Schematic representation of the proposed MAS model

Finally, if there is no direction to follow, RA activates the EA and changes its state to "waiting" in which it will remain until receives the message from EA.

Thereafter, the region behavior is constituted by four steps. First agents attempt for a fusion with neighbor RAs by sending messages to them. RA considers another RA as neighbor if the distance between at least one of its points and one point of the other RA is smaller or equal to a specific threshold (D). After keeping all the information about the neighbor RA by updating its own region information, RA kills the neighbor agent and changes its current state to "filling". At this state, RA verifies if its region contour size is smaller than T_c and if it is not, it disappears with its region. On the other hand, if the contour is smaller than T_c, it fills the region by analyzing the gray level points located between each pair of the contour points. For each pair of points, the line equation that contains the two points is

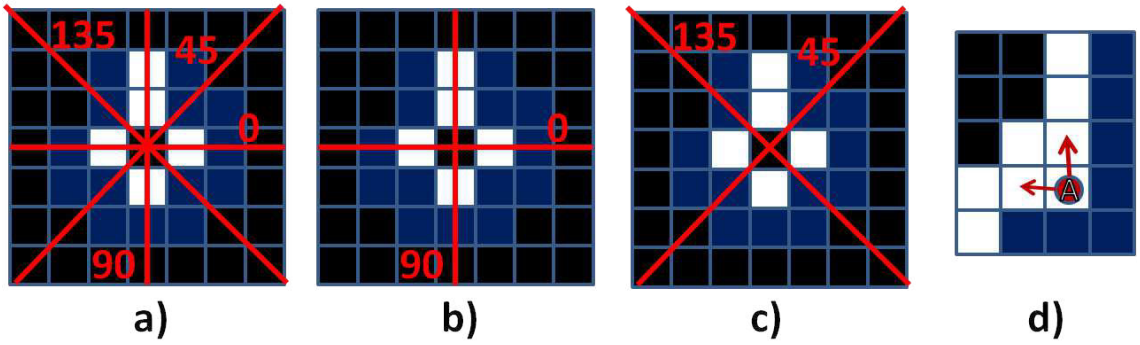

Figure 8.5.: Graphical representation of the Explored Agent behavior a)-c); d)possible directions to follow according to Region Agent restrictions

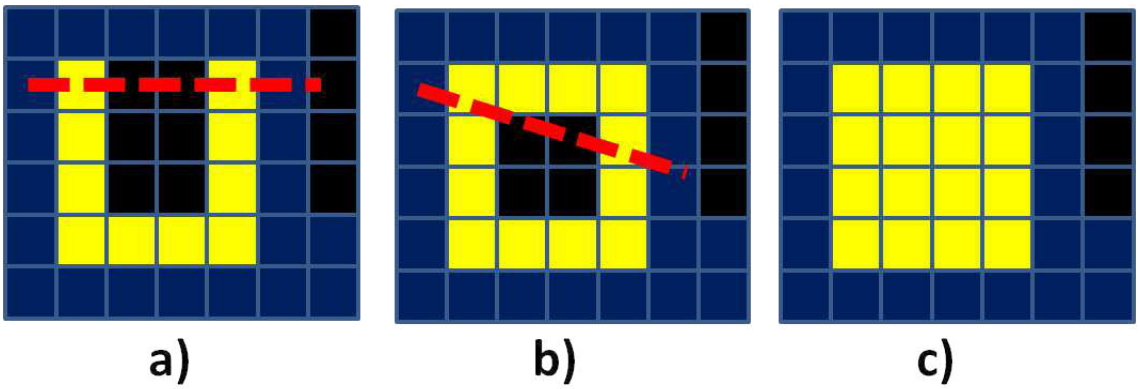

Figure 8.6.: RA "filling" state graphical representation

calculated (Figure 8.6 a)-b). Then, the points located between them are determined and for each of them an evaluation related to its gray level intensity is made. That is, the point is added to the region if its gray level value is lower than the gray level values average of the points that are already in the region (Figure 8.6 c). Hereafter, RA performs a region growing algorithm based on [2]. This algorithm calculates the threshold by $t = I_{darkest} - \alpha(I_{darkest} - I_{bg})$, where $I_{darkest}$ is the candidate lowest intensity in the green plane image, I_{bg} is the corresponding intensity in the background image and α is set to 0.5 [2]. The growing process stops when there are no more pixels in the 8-neighborhood having intensity lower than the threshold or when the region size is bigger than a threshold ($\mathrm{A_{max}}$).

Finally, RA validates its region as a true lesion by means of shape and intensity based features analysis. For region shape analysis, the RA determines elongation, since some detected regions belong to thin blood vessel fragments and should have higher elongation values. Since MAs are round local minimums they can be represented as an inverted 2D Gaussian shape. Therefore, for the region intensity analysis a set of cross-sectional intensity profiles is obtained from the inverted green channel (Figure 8.7). In determining these profiles a window around the region is consid-

ered. Then, the region is dilated for being used as a mask on the inverted green plane, where scanning lines 15º rotated are applied. From these 12 intensity profiles, the Gaussian fitting parameters (the amplitude of the peak of the profile - a; the position of the peak - b; the width of the Gaussian profile - c) (Figure 8.7 below) are determined and analyzed (Table 8.3) for all regions of several images. Analyzing Table 8.3, it is possible to verify that parameter c allows a better discrimination between small red lesions and other dark structures. Therefore, the difference between the maximum and the minimum parameter c values from the 12 profiles is kept as an intensity-based feature (c_range).

The features values used to evaluate the MAS model final output were $elongation \in \{1 : 0.2 : 4\}$ and $c_{range} \in \{0 : 1 : 20\}$.

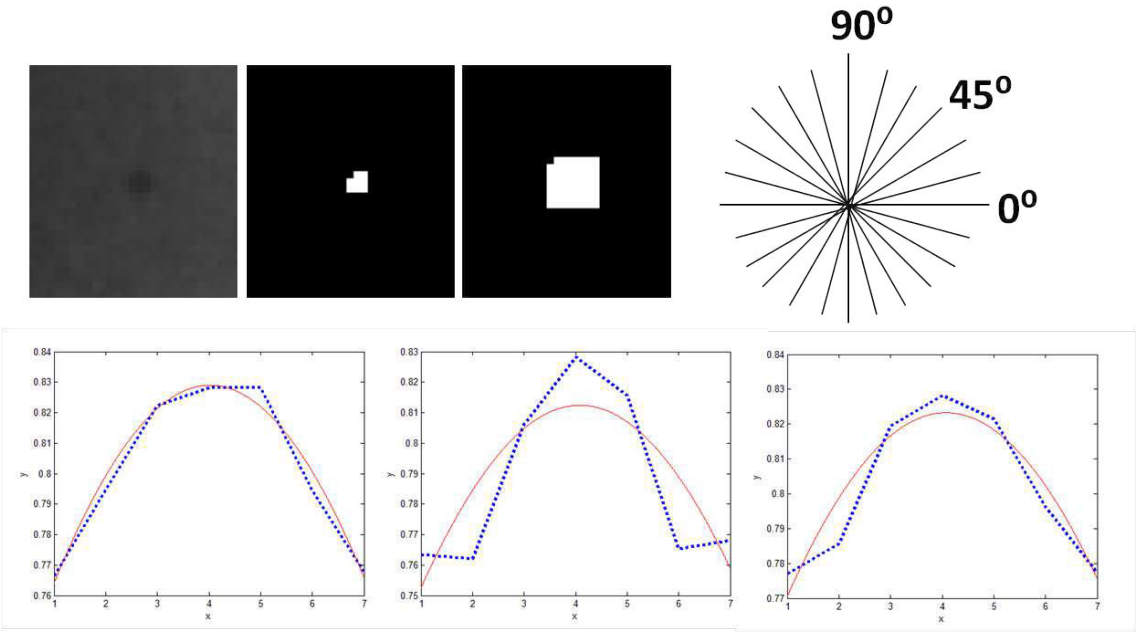

Figure 8.7.: From left to right: window of the green plane image centered at a MA; window of the binary candidates image with a MA candidate; the candidate of the previous image after a dilation; scan lines to be performed on the inverted green plane with the aid of the mask from previous image; MA intensity profiles (dotted blue line) and respective Gaussian fitting function (red line) for orientations 0, 90 and 135.

8.3.3. Retinal images and system performance evaluation

A set of images online available by Quellec et al. [127], called LaTIM (Laboratoire de Traitement de l'Information Médicale) dataset in this thesis, was used for the performance evaluation. This dataset consist of 36 images with 2240 × 1488 pixels and stored in tiff file format. Moreover, the dataset also contains a text file for each

Table 8.3.: Gaussian fitting parameters (a, b and c)

	Small red lesion			**Other**		
	a	**b**	**c**	**a**	**b**	**c**
Minimum	0.676	2.730	7.50	0.538	2.740	5.560
Maximum	0.829	5.209	16.553	0.817	9.102	185.262
Mean	0.742	3.856	11.147	0.700	4.482	17.854
Standard deviation	0.038	0.479	1.856	0.053	0.904	9.567

image, with small red lesions manually annotated by a single diabetic retinopathy expert.

Another publicly available database used in this study was provided in the ROC competition [137]. This database is composed of 100 images, equally divided into a training and a test set. The images were acquired by three different cameras and of different resolutions and sizes, ranging from 768×576 to 1389×1383. All images are stored in JPEG format and compression was set in the camera. All microaneurysms and other irrelevant lesions from the 100 images were annotated by four retinal experts. The irrelevant lesions are objects that despite of not being microaneurysms, they may be identified as such by an automated program. For instance, hemorrhages and pigment spots are similar in appearance to MAs and, thus, they should not be considered as false positives. For the training set, the lesions locations annotated by the four experts were combined by a logical OR. For the test set, the reference standard was obtained in a different way. The annotations of one randomly chosen expert were kept to be used as a human observer performance. The annotated lesions by the other three experts were combined for the final reference standard. "Microaneurysm" in the final reference standard is the object for which at least two experts assigned this label. The other lesions identified by only one specialist were assigned as "irrelevant".

For both datasets, the performance of the proposed approach was evaluated in terms of the free-response receiver operating characteristic (FROC) curve, where per lesion sensitivity values are plotted against the average number of false positives per image. Sensitivity represents the proportion of MA correctly detected by the algorithm, while FP is the number of non-MA identified as MA. For the ROC dataset and to facilitate the comparison with the other methods already submitted on the challenge website, the FROC curve was summarized in several quantitative points. In that way, sensitivity values for the false positive per image rates values of (1/8), (1/4), (1/2), 1, 2, 4, and 8 were achieved and averaged to get a final score. Moreover, only the results obtained with test set and provided by the ROC organizers are demonstrated in next section.

8.4. Results and Discussion

For becoming easier the algorithm parameterization, the size of all images from both datasets were normalized without losing the relevant information to this study. The LaTIM images were resized to 1120×744 pixels and the ROC images to 836×835 pixels. The algorithm parameters were chosen according to the image size and the typical dimension of MAs in fundus images. In that way, T_c=40, D=2 and A_{max}=40 were the values used when applying the proposed approach to both datasets.

The MAS model performance depends on the preprocessing step and how the agents interpret the information provided from this first phase. In that way, it is important to compare the gradient image resulting from the preprocessing step with the binary image resulting from the MAS model. Figure 8.8 illustrates an original color image with manually segmented microaneurysms and the respective, image resultant from the preprocessing phase and binary image provided by the MAS model before the local feature analysis. From this figure, it can be noticed that the MAS model is able to detect small dark structures and excludes most of the edge pixels belonging to blood vessels and some artifacts. In fact, all the four microaneurysms were correctly segmented and the remaining false positives elongated structures would be easily removed with the local feature analysis step.

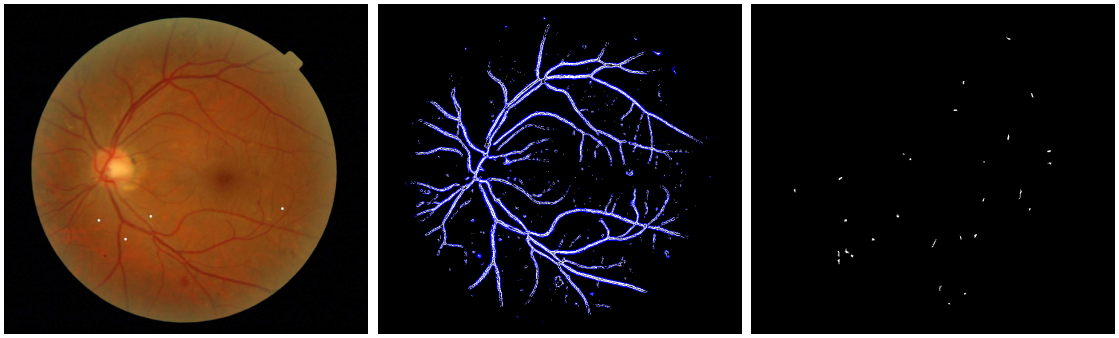

(a) **(b)** **(c)**

Figure 8.8.: a) Manually annotated MA superimposed with the original image; b) image resulting from the preprocessing phase; c) segmentation performed by the MAS model before local feature extraction and analysis

Figure 8.9 illustrates the results for an image before and after the MAS model feature analysis step made by the Region Agent. The final image presents a sensitivity of 1 and 4 FP, which represents a very good performance considering only two features of the objects detected by the MAS. Therefore, it seems that the inclusion of an agent-based learning classifier at last stage should improve the algorithm performance.

The segmentation performance obtained with the MAS model was compared with another approach schematically illustrated in Figure 8.10 (bold). This one consists of the preprocessing and segmentation phases of the "standard" approach referred in

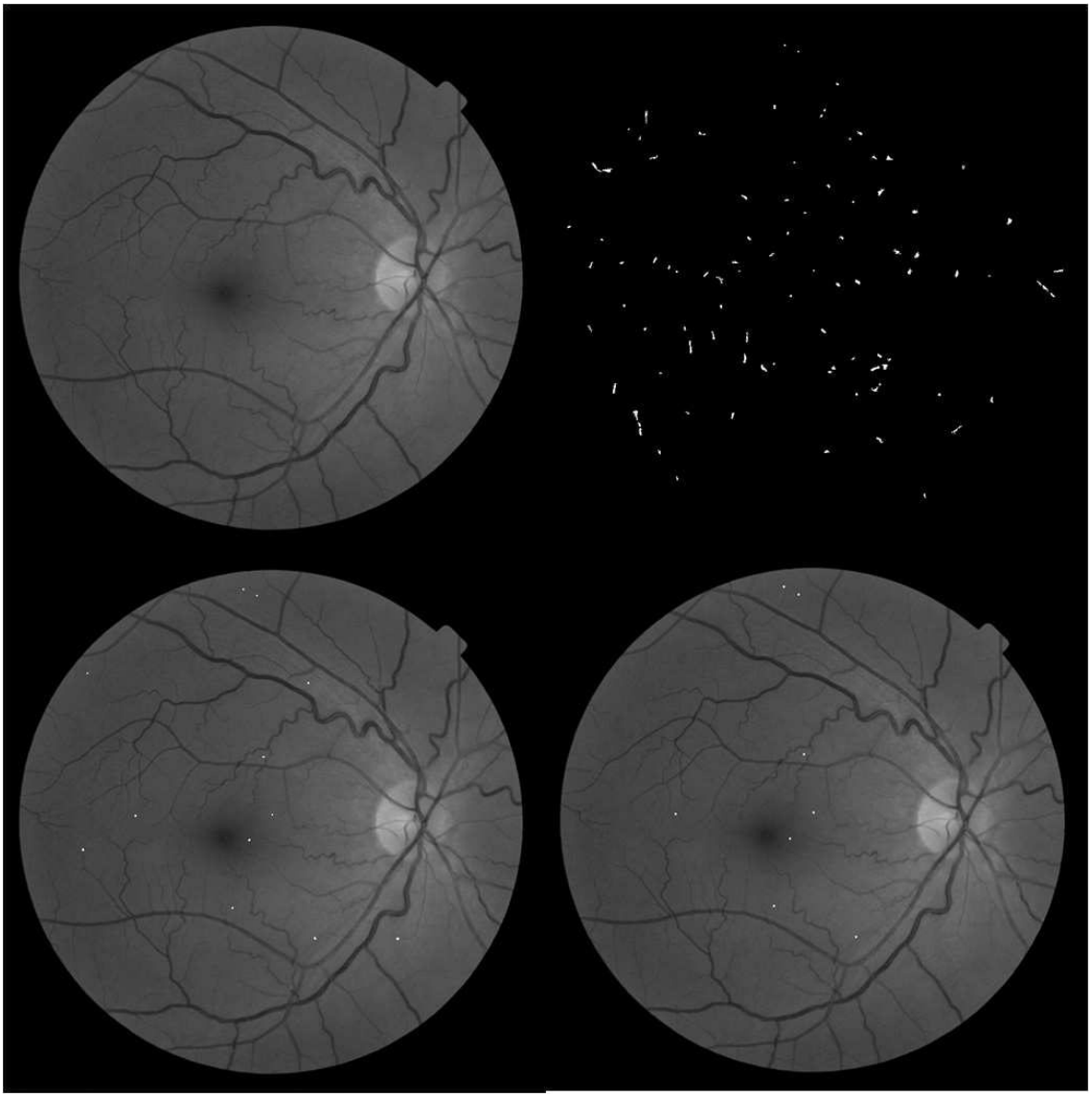

Figure 8.9.: Images resulting from the proposed approach. From upper to below and from left to right: green plane image; binary image with candidates detected by the MAS model before feature analysis; binary image resulting from local feature analysis superimposed with green plane image; binary image with manually annotated MA superimposed with green plane image

section 8.2. That is, only the candidates detection method was considered because the proposed approach is unsupervised and, in that way, a fair comparison is made. The comparative results are illustrated in Figure 8.11, where the curve for the "standard" approach was obtained by varying the threshold value ($t \in \{3 : 1 : 12\}$). From these quantitative results, it can be observed that our approach clearly outperforms the "standard" approach. A qualitative analysis of images resulting from the two approaches reveals that our approach has as advantage the preservation of microaneurysms close to vessels (Figure 8.12). This is very important for clinical practices since this kind of lesions appear close to vessels very often.

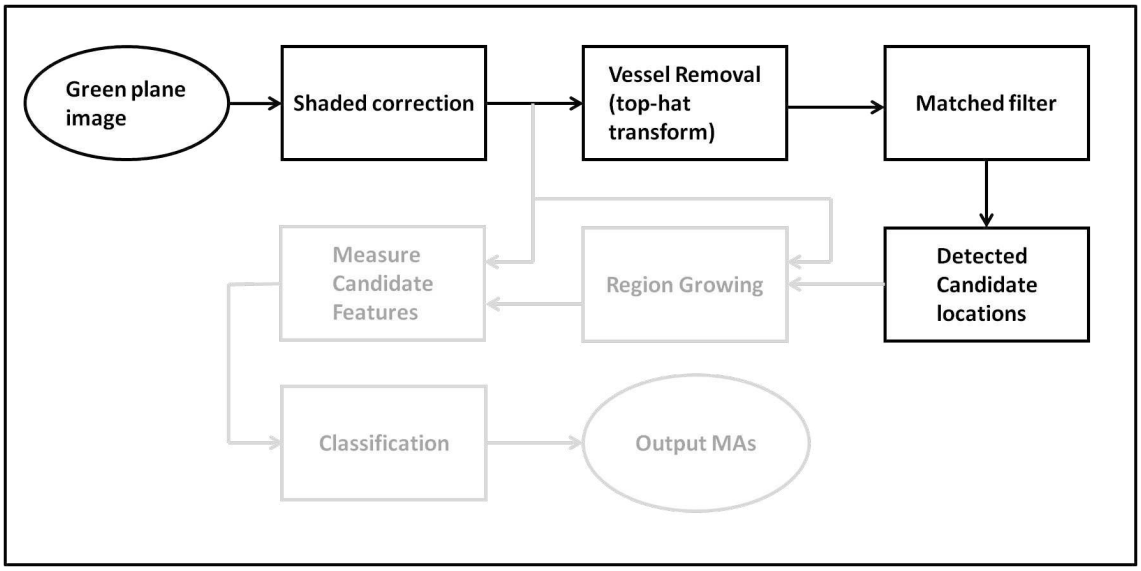

Figure 8.10.: Schematic representation of a classical approach used for microaneurysms segmentation

Figure 8.13 and Table 8.4 demonstrate the FROC curves and the ranked quantitative results, respectively, of the ROC methods already described in section 8.2. The final score of the proposed approach is 0.240 corresponding to the tenth place of the competition. However, a detailed analysis of the proposed approach FROC curve and of Table 8.4 shows encouraging results since for an average number of FP of 8, sensitivity achieves a value higher than 0.5. This is a good performance compared with other methods described in literature. In fact, if the 8 FP row of Table 8.4 is analyzed to compare the approaches, the proposed method corresponds to the sixth better sensitivity value and it rises to the third place if only non supervised approaches are considered. The non supervised approaches that showed better results belong to LaTIM and Lazar et al. groups.

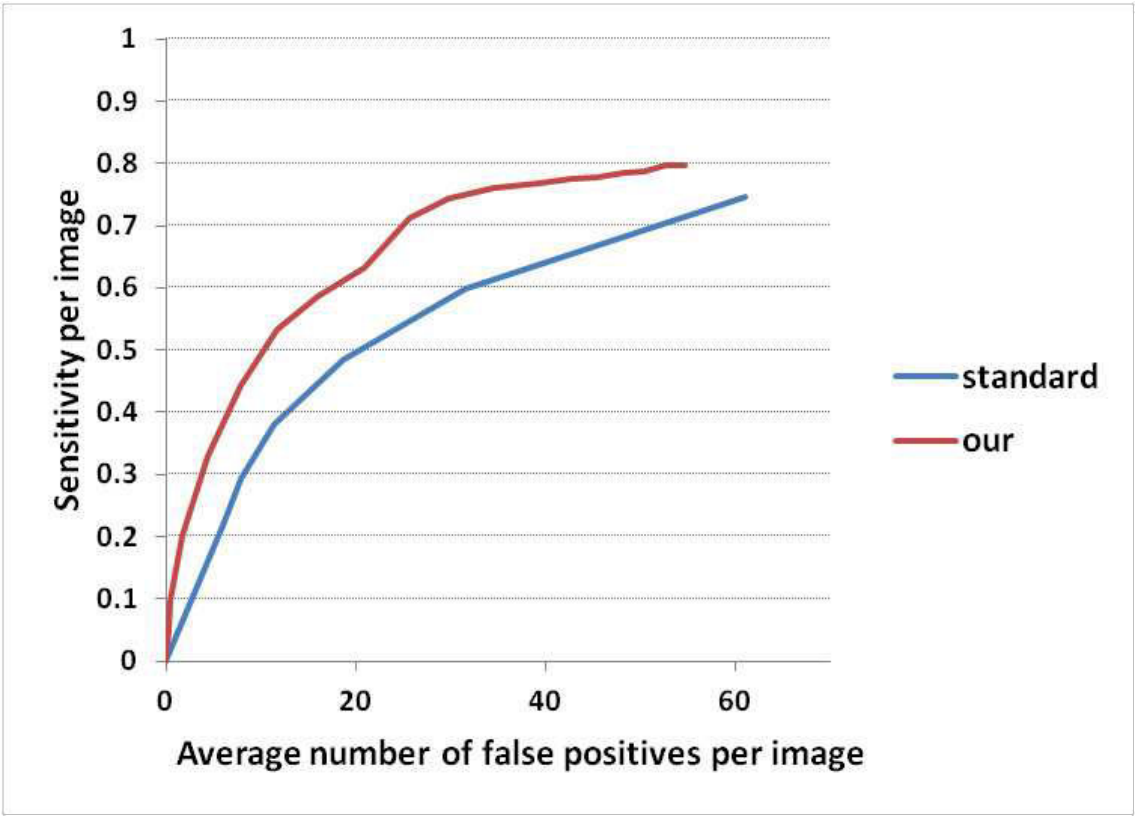

Figure 8.11.: FROC curves obtained with the proposed and "standard" approaches applied to the LaTIM dataset

8.5. Conclusion

In this chapter a small red lesions segmentation algorithm based on a MAS approach is proposed. Through agent local interaction and cooperation it was possible to improve conventional algorithms results, especially in detecting microaneurysms close to vessels. The inclusion of a validation step through local feature analysis allowed the reduction of the average number of FP and encourages the inclusion of some agent learning capacity for the algorithm improvement. Results show that the proposed approach outperforms the "standard" candidates detection approach found in literature. Moreover, considering the ROC challenge a third place can be reached if only non-supervised approaches and 8 FP are taking into account.

The proposed approach overall results show that the use of a MAS model in the micro level could be an effective way to segment red lesions in fundus images, and overcome some common problems found in literature, such as the detection of microaneurysm close to vessels.

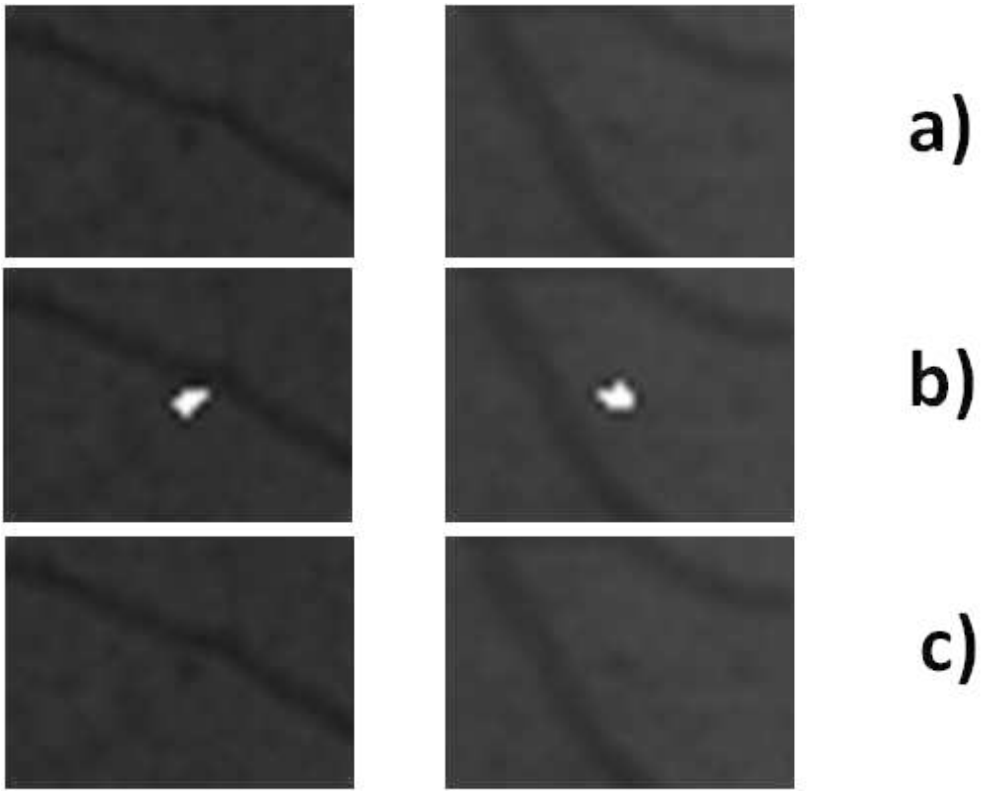

Figure 8.12.: Comparative results related with the detection of microaneurysms close to blood vessels. a) green plane image; b) MAS model result; c) "standard" approach result.

Table 8.4.: Sensitivities of different approaches at various false positive points for the ROC test dataset

Author	**1/8**	**1/4**	**1/2**	**1**	**2**	**4**	**8**	**Final score**
Waikato	0.055	0.111	0.184	0.213	0.251	0.3	0.329	0.206
Our approach	**0.053**	**0.083**	**0.135**	**0.187**	**0.276**	**0.407**	**0.540**	**0.240**
Fujita	0.181	0.224	0.259	0.289	0.347	0.402	0.466	0.310
GIB Valladolid	0.19	0.216	0.254	0.3	0.364	0.411	0.519	0.322
OKMedical	0.198	0.265	0.315	0.356	0.394	0.466	0.501	0.357
OKMedical_II	0.175	0.242	0.297	0.370	0.437	0.493	0.569	0.369
ISMV	0.217	0.270	0.366	0.407	0.440	0.459	0.468	0.375
LaTIM	0.166	0.23	0.318	0.385	0.434	0.534	0.598	0.381
Niemeijer et al.	0.243	0.297	0.336	0.397	0.454	0.498	0.542	0.395
Lazar et al.	0.251	0.312	0.350	0.417	0.472	0.542	0.615	0.423
DRSCREEN	0.173	0.275	0.380	0.444	0.526	0.599	0.643	0.434

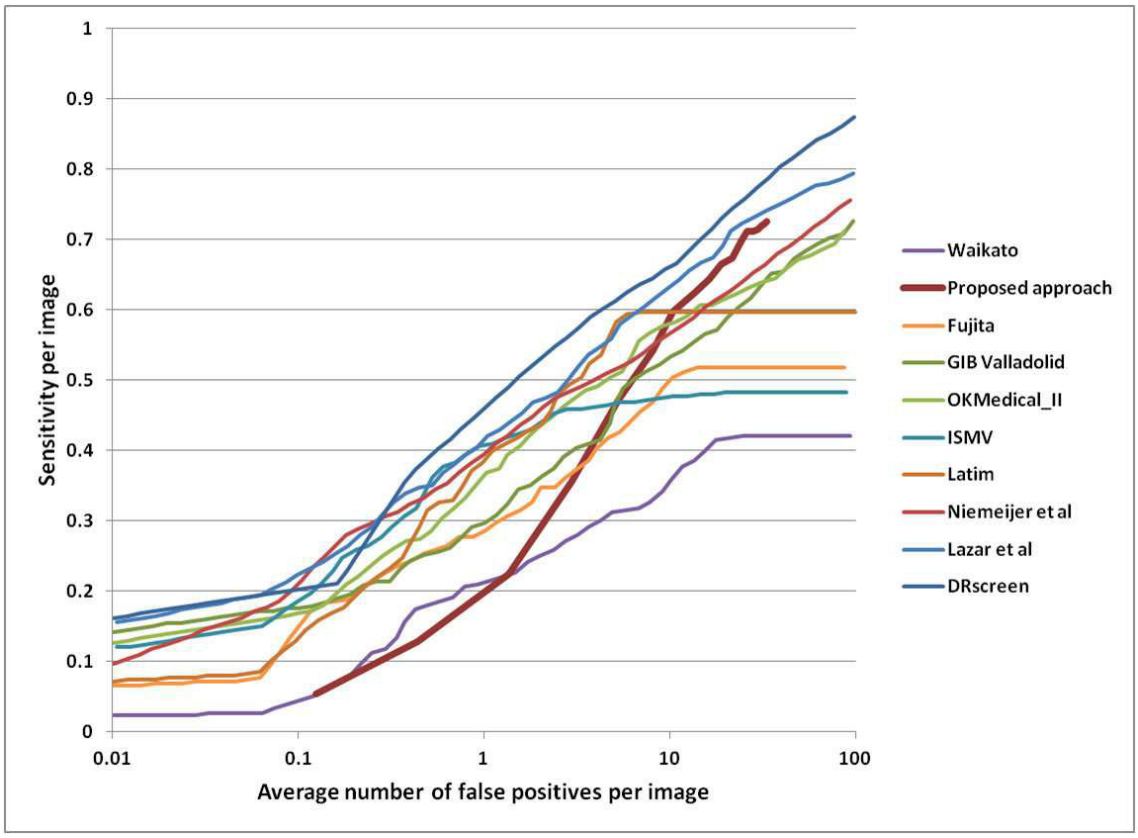

Figure 8.13.: FROC curves of the ROC methods

9. Conclusion

The digital nature of color fundus images and the need of computational tools to be used in screening programs for the early diabetic retinopathy diagnosis have attracted the attention of several research groups. In fact, several approaches reported in literature for aiding in the automatic DR diagnosis are referred throughout this thesis. These methodologies are frequently based on image processing, pattern recognition and machine learning algorithms. Despite of the wide literature for the DR diagnosis through fundus image analysis, none of the algorithms proposed demonstrate the performance needed for clinical practices. The problems of the classic image processing algorithms are that they are limited to macro level results and cannot take into account the local characteristics of a complex image such as the digital color fundus photograph, mainly when this is pathological. Using global approaches as the traditional algorithms, leads to rigid systems not able to adapt and generalize to unknown situations. This is the reason why, in the last years, researchers have been working in multi-agent systems applied to digital image processing (section 3.3). In fact, each agent can locally process image information and deliberate according to its perceptions from the environment and agents surrounding it.

This thesis focuses on the development of new tools based on multi-agent systems, to assist the diabetic retinopathy diagnosis. Two kinds of systems were investigated and applied to digital color fundus photographs: ant colony system and multi-agent system composed of reactive agents with interaction mechanisms between the agents. It is possible to refer ACO algorithm as an agent-based algorithm since it is constituted by a number of agents with memory moving on the image (environment) and that communicates indirectly through the environment [102]. Moreover, through self-organizing dynamics driven by local interactions and communications between ant-like agents, a complex global behavior emerges, which, in this case, consist in the edges enhancement.

In that way, this thesis demonstrates agent-based approaches for the segmentation of the fundus images major features. That is, chapter 5 describes an ACO based approach that effectively detects the OD in fundus images even in pathological or with great variability images. Also an ACO based approach is referred in chapter 6 for the bright lesions segmentation. MAS models were created for the blood vessels segmentation (chapter 7) and for small dark lesions segmentation (chapter 8). The results of the proposed approaches are compared with other results found in the literature and, though they are not always the best, they are very promising. For

instance, the OD detection results achieved with the DRIVE dataset are good as or better than the others described in the literature; the blood vessel segmentation method presents an accuracy of 0.9443 outperforming at least two traditional methods found in literature; the dark lesions segmentation approach achieves a third place in the ROC competition [137] if 8 FP and only non supervised approaches are considered; the bright lesions segmentation approach performs better than another recent approach found in the literature [100], but a comparison with other approaches is not possible due to the use of particular datasets.

Therefore, the main scientific contribution of this thesis is to prove that multi-agent systems based approaches can be efficient in segmenting structures in complex images. The results show that these kind of approaches improved the traditional algorithms results. Actually, MAS models implemented in this work are not an image processing technique on their own, but they are used as tools to improve the traditional results at the micro level. Such an approach overcomes the classic image processing algorithms that are limited to macro level results and not considers the local characteristics of the images. Hence, it could be a fundamental tool responsible for a very efficient system development to be used in screening programs concerning diabetic retinopathy diagnosis.

9.1. Future work

A relevant point that has to be ameliorated for the improvement and comparison of DR diagnosis approaches is the creation of a more general publicly available database. This database has to be large and representative of the diabetic population and have to include the ground truth information that should be done by a group of ophthalmologists, with further statistical combination between their segmentation. Moreover, a uniformization of the quantitative results evaluation is fundamental for a fair comparison between different approaches. The Retinopathy Online Challenge (ROC) is a good example of such database, where interested research groups submit the results for being evaluated in the same way. Though, many research groups have already joined the challenge and submit their results (see section 3.3), none of these demonstrate an algorithm that is recommendable for clinical practice. As a result, this kind of challenge could be a way to achieve the solution, but there is work to do yet. In addition, the ROC only concerns the detection of red lesions and there is a need for the creation of other programs, like for the bright lesions detection or for the both lesions detection simultaneously.

As future work for this study, the integration of the several proposed approaches described throughout this thesis into a complete automatic system for the diabetic retinopathy diagnosis should be the first step. Furthermore, not all the possibilities of MAS discussed in chapter 3 were used in the proposed approaches. The use of an improved agent society version to make use of all its advantages, with some knowledge a priori about retina properties, complemented with the use of some

other traditional image processing algorithms, may have the potential to develop a system to detect and differentiate all the anatomic and pathological structures of the fundus images, including fovea and the other dark lesions (neovessels and hemorrhages) that were not considered in this study. For instance, the use of some agent learning capacity as well as cognitive or even hybrid agents might help in creating such a system.

Afterward, an exhaustive clinical evaluation of this system has to be done in order to achieve the medical community acceptance of such automatic system. This will permit to better identify the system drawbacks and to improve or propose solutions. When implemented in a clinical environment, the automatic systems should deal with the acquisition process of the fundus image to facilitate the image analysis next steps. For instance, the inclusion of an algorithm to evaluate if the image has enough quality for being analyzed by the automatic system can improve the final result. Moreover, knowing a priori if the image is fovea centered or optic disc centered and if the image corresponds to the right or left eye, can limit the search area for both structures and, consequently, the OD and fovea detection would be easier.

At this point, it is important to remember that the purpose of the computer system to diagnose the diabetic retinopathy is to fill the lack of ophthalmologists and may not totally replace the human tasks. In fact, the acquisition process continues to need a technician, who does not have to be a specialist but someone who can interact with the system.

A. Filters

A.1. Overview

Filters analyzes the value of every pixel in an image. For each one, the new value is calculated according to the pixel values in a local neighborhood, that is a window w centered on that pixel.

The filters used in this study have two principal functions: reduce noise by smoothing or enhance edges.

Filters can be linear if the output values are linear combinations of the pixels in the original images, or nonlinear, otherwise. The linear filters are fast to compute, but, since noise and edges are high-frequency components of images, they are unable to smooth without simultaneously blurring edges. On the other hand, nonlinear filters can reduce noise while preserving edges, but they can be slow to compute.

A.2. Smoothing

For this work, one linear and two nonlinear smoothing filters were considered according to the needs. They are described in following.

A.2.1. Gaussian filter

Gaussian filter is a linear filter that uses a 2D convolution operator to 'blur' images and remove noise and detail. Gaussian smoothing is also frequently used to enhance image structures at different scales. The kernel used to convolve the image is a Gaussian function. In one dimension the Gaussian function is

$$G(x, y) = \frac{1}{\sqrt{2\pi\sigma^2}} e^{-\frac{x^2}{2\sigma^2}}$$

In two dimensions, it is the product of two such Gaussians, one in each dimension:

$$G(x, y) = \frac{1}{2\pi\sigma^2} e^{-\frac{x^2+y^2}{2\sigma^2}}$$

where x is the distance from the origin in the horizontal axis, y is the distance from the origin in the vertical axis, and σ is the standard deviation of the Gaussian distribution. The distribution is shown in Figure A.1.

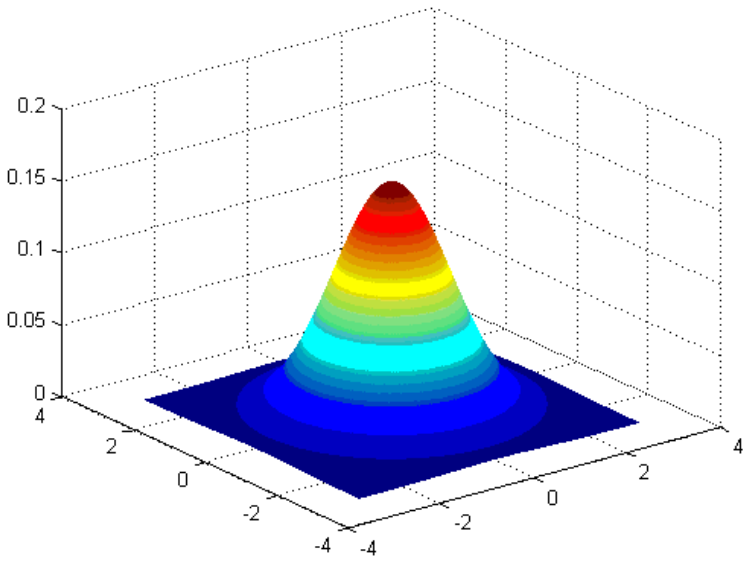

Figure A.1.: 2-D Gaussian distribution with $\sigma = 1$

A discrete approximation of this distribution is used to build a convolution matrix which is applied to the original image. The new value of each pixel corresponds to a weighted average of that pixel's neighborhood. The original pixel value contains the heaviest weight (having the highest Gaussian value) and neighboring pixels contain smaller weights as their distance to the original pixel increases. An example of such kernel is illustrated in Figure A.2.

$$\frac{1}{273}\begin{bmatrix} 1 & 4 & 7 & 4 & 1 \\ 4 & 16 & 26 & 16 & 4 \\ 7 & 26 & \mathbf{41} & 26 & 7 \\ 4 & 16 & 26 & 16 & 4 \\ 1 & 4 & 7 & 4 & 1 \end{bmatrix}$$

Figure A.2.: Matrix of discrete approximation to Gaussian function with σ=1

A.2.2. Median filter

Median filter is a nonlinear digital filtering method, frequently used to remove noise with Laplacian distribution. This filter considers each pixel of the image in turn and replaces it by the median of all pixels in the neighborhood:

$y(i,j) = median\,\{x[i,j],\ (i,j) \in w\}$

A.2.3. Kuwahara filter

The Kuwahara filter is a nonlinear filter that is able to apply smoothing on the images while preserving the edges. The general idea behind this filter is to divide the kernel filter into four rectangular sub regions with one pixel overlap (Figure A.3). The filter response is then defined by the sub region mean with minimum variance. That is, suppose that *I(x,y)* is a grayscale image and that a square window of size 2a+1 centered around a point *(x,y)* in the image is considered. This square is divided into four smaller square regions $Q_{i=1,\ldots,4}$ defined as:

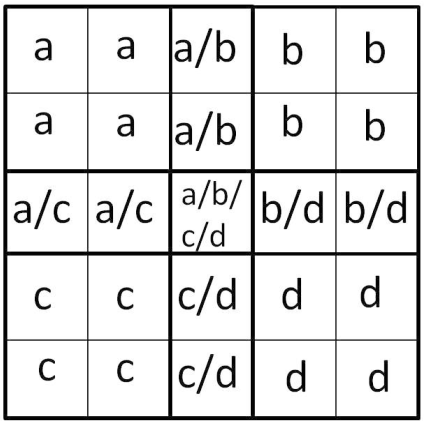

Figure A.3.: The Kuwahara filter considers 4 square subregions a,b,c,d with the pixels located on the central row and column belonging to more than one subregion.

$$Q_i(x,y) = \begin{cases} [x, x+a] \times [y, y+a] & if\ i = 1 \\ [x-a, x] \times [y, y+a] & if\ i = 2 \\ [x-a, x] \times [y-a, y] & if\ i = 3 \\ [x, x+a] \times [y-a, y] & if\ i = 4 \end{cases}$$

where $\times$ is the Cartesian product. The mean m_i and standard deviation σ_i of the four regions centered around the pixel *(x,y)* are determined and used to calculate the value of the central pixel. Thus, the Kuwahara filter output $\Phi(x,y)$ for any point *(x,y)* is then determined by

$$\Phi(x,y) = \begin{cases} m_1 & if\ \sigma_1 = min(\sigma_i) \\ m_2 & if\ \sigma_2 = min(\sigma_i) \\ m_3 & if\ \sigma_3 = min(\sigma_i) \\ m_4 & if\ \sigma_4 = min(\sigma_i) \end{cases}$$

That is, the central pixel takes the mean value of the most homogeneous subregion. By taking into account the homogeneity of the regions, the Kuwahara filter ensures the edges preservation.

A.3. Edge detection

An edge corresponds to a high grayscale variation. Therefore, edge filters should have a stronger output at a location if the pixels in neighborhood reveals a systematic pattern of changes in value. The edge enhancement filters also emphasizes noise in images. That is why they should be applied with a preceding filter to smooth images.

In this work scope only the nonlinear Kirsch filter is considered.

A.3.1. Kirsch filter

The multi-directional Kirsch filter belongs to the template matching filters in which the filter output is the maximum response from a set of linear operators which are sensitive to edges at different orientations:

$$g(i,j) = max_{z=1,\ldots,8} \sum_{k=-1}^{1} \sum_{l=-1}^{1} w_{kl}^{(z)} f(i+k, j+l)$$

The Kirsch filter contains eight operators (weights matrix) corresponding each to a specific direction. They are determined by rotating of 45º the first operator w_0.

$$w_0 = \frac{1}{15} \begin{pmatrix} 5 & 5 & 5 \\ -3 & 0 & -3 \\ -3 & -3 & -3 \end{pmatrix}$$

A.3.2. Improved Kirsch filter

Despite of being a good derivative operator and performing better than other traditional edge detectors for the diagonals detection, the Kirsch filter does not permit the gradient's direction determination. Therefore, to solve this problem, Mahdjoub [28] proposed to change the based-operator to:

$$w_0 = \begin{pmatrix} 1/3 & 1/3 & 1/3 \\ -1/6 & -1/6 & -1/6 \\ -1/6 & -1/6 & -1/6 \end{pmatrix}$$

This improved version of the Kirsch filter enables to have a detected contour with two pixels of thickness. The external contour contains a positive or negative value whereas the internal contour have an opposed value. This enables to detect the contour with precision, between these two contours.

References

[1] T. Walter, P. Massin, A. Erginay, R. Ordonez, C. Jeulin, and J. Klein, "Automatic detection of microaneurysms in color fundus images." *Medical Image Analysis*, vol. 11, no. 6, pp. 555–566, 2007.

[2] M. Niemeijer, B. Van Ginneken, J. Staal, M. Suttorp-Schulten, and M. Abràmoff, "Automatic detection of red lesions in digital color fundus photographs," *Medical Imaging, IEEE Transactions on*, vol. 24, no. 5, pp. 584–592, 2005.

[3] T. Teng, M. Lefley, and D. Claremont, "Progress towards automated diabetic ocular screening: a review of image analysis and intelligent systems for diabetic retinopathy," *Medical and Biological Engineering and Computing*, vol. 40, no. 1, pp. 2–13, 2002.

[4] R. Winder, P. Morrow, I. McRitchie, J. Bailie, and P. Hart, "Algorithms for digital image processing in diabetic retinopathy." *Computerized medical imaging and graphics*, vol. 33, no. 8, pp. 608–622, 2009.

[5] E. Grisan, "Automatic analysis of retinal images: Retinopathy detection and grading," Ph.D. dissertation, University of Padova, 2005.

[6] H. Li, R. Danis, L. Hubbard, J. Florez-Arango, A. Esquivel, and E. Krupinski, "Comparability of digital photography with the ETDRS film protocol for evaluation of diabetic retinopathy severity," *Investigative Ophthalmology & Visual Science*, vol. 52, no. 7, pp. 4717–4725, 2011.

[7] A. Rudnicka and J. Birch, *Diabetic eye disease: identification and comanagement*. Butterworth-Heinemann Medical, 2000.

[8] S. Ghosh, A. Collier, M. Varikkara, and S. Palmer, *Fundoscopy Made Easy*. Churchill Livingstone, 2011.

[9] S. P. de Diabetologia. (2010) Estudo da prevalência da diabetes em portugal. [Online]. Available: http://www.min-saude.pt/NR/rdonlyres/219DAD78-CD13-43CE-9221-42744B24176C/0/EstudoprevalenciaDiabetesemPortugal.pdf

[10] A. Gupta and C. Styles, "An overview of diabetic eye disease," *The British Journal of Diabetes & Vascular Disease*, vol. 10, no. 5, pp. 224–230, 2010.

[11] M. Davis, E. Norton, and F. Myers, "The Airlie classification of diabetic retinopathy," in *Symposium on the Treatment of Diabetic Retinopathy, Airlie House, Warrenton, Virginia*, 1968, pp. 7–37.

[12] D. R. R. S. Group, "A modification of the Airlie House classification of diabetic retinopathy. DRS report number 7," *Invest Ophthalmol Vis Sci.*, vol. 21, pp. 210–216, 1981.

[13] "Grading diabetic retinopathy from stereoscopic color fundus photographs–an extension of the modified Airlie House classification. ETDRS report number 10. Early Treatment Diabetic Retinopathy Study Research Group," *Ophthalmology*, vol. 98, pp. 786–806, 1991.

[14] C. Wilkinson, F. Ferris, R. Klein, P. Lee, C. Agardh, M. Davis, D. Dills, A. Kampik, R. Pararajasegaram, and J. Verdaguer, "Proposed international clinical diabetic retinopathy and diabetic macular edema disease severity scales," *Ophthalmology*, vol. 110, no. 9, pp. 1677–1682, 2003.

[15] S. Garg and R. Davis, "Diabetic retinopathy screening update," *Clinical Diabetes*, vol. 27, no. 4, pp. 140–145, 2009.

[16] G. E. em Retina. (2009) Retinopatia diabética - guidelines. Sociedade Portuguesa de Oftalmologia. [Online]. Available: www.spilm.com/Noticias/artigos/A5_SPO-RETINOPATIADIABTICA-guidelines2009.pdf

[17] A. D. Association *et al.*, "Standards of medical care in diabetes: position statement 2010," *Diabetes Care*, vol. 28, no. 1, pp. 526–36, 2011.

[18] S. Bursell, J. Cavallerano, A. Cavallerano, A. Clermont, D. Birkmire-Peters, L. Aiello, and L. Aiello, "Stereo nonmydriatic digital-video color retinal imaging compared with Early Treatment Diabetic Retinopathy Study seven standard field 35-mm stereo color photos for determining level of diabetic retinopathy," *Ophthalmology*, vol. 108, no. 3, pp. 572–585, 2001.

[19] S. Vujosevic, E. Benetti, F. Massignan, E. Pilotto, M. Varano, F. Cavarzeran, A. Avogaro, and E. Midena, "Screening for diabetic retinopathy: 1 and 3 nonmydriatic 45-degree digital fundus photographs vs 7 standard early treatment diabetic retinopathy study fields," *American journal of ophthalmology*, vol. 148, no. 1, pp. 111–118, 2009.

[20] S. Aldington, E. Kohner, S. Meuer, R. Klein, and A. Sjølie, "Methodology for retinal photography and assessment of diabetic retinopathy: the EURODIAB IDDM complications study," *Diabetologia*, vol. 38, no. 4, pp. 437–444, 1995.

[21] F. P. R. Center. (2012) Department of Ophthalmology and Visual Sciences, University of Wisconsin. [Online]. Available: http://eyephoto.ophth.wisc.edu/index.htm

[22] T. Walter, J. Klein, P. Massin, and A. Erginay, "A contribution of image processing to the diagnosis of diabetic retinopathy-detection of exudates in color fundus images of the human retina," *Medical Imaging, IEEE Transactions on*, vol. 21, no. 10, pp. 1236–1243, 2003.

[23] M. Cree, E. Gamble, and D. Cornforth, "Colour normalisation to reduce interpatient and intra-patient variability in microaneurysm detection in colour reti-

nal images," in *Proc. WDIC 2005 ARPS Workshop Digital Image Computing*, Feb. 2005, pp. 163–168.

[24] T. Walter and J. Klein, "Automatic analysis of color fundus photographs and its application to the diagnosis of diabetic retinopathy," *Handbook of Biomedical Image Analysis*, pp. 315–368, 2005.

[25] R. Hornero, M. Aboy, J. Poza *et al.*, "A novel automatic image processing algorithm for detection of hard exudates based on retinal image analysis," *Medical engineering & physics*, vol. 30, no. 3, pp. 350–357, 2008.

[26] M. Wooldridge, *An introduction to multiagent systems*. Wiley, 2002.

[27] J. Vidal, "Fundamentals of multi agent systems (2009)."

[28] J. Mahdjoub, "Vers un système de vision auto-adaptatif à base de systèmes multi-agents," Ph.D. dissertation, Université Reims Champagne-Ardenne, 2011.

[29] J. Ferber, *Multi-agent systems: an introduction to distributed artificial intelligence*. Addison-Wesley Reading, MA, 1999, vol. 33.

[30] L. Reis, "Coordination in multi-agent systems: Applications in university management and robotic soccer," Ph.D. dissertation, Electrical and Computers Engineering, FEUP, Porto, 2003.

[31] J. Ferber and O. Gutknecht, "A meta-model for the analysis and design of organizations in multi-agent systems," in *Multi Agent Systems, 1998. Proceedings. International Conference on*. IEEE, 1998, pp. 128–135.

[32] G. Morvan, A. Veremme, and D. Dupont, "IRM4MLS: the influence reaction model for multi-level simulation," in *Multi-Agent-Based Simulation XI*. Springer, 2011, pp. 16–27.

[33] A. S. Rao and M. Georgeff, "Modeling rational agents within a BDI-architecture," in *Readings in Agents*, M. Huhns and M. Singh, Eds. Morgan Kaufmann, 1998, pp. 317–328.

[34] M. E. Bratman, "Intention, plans, and practical reason," *Harvard University Press, Cambridge*, 1987.

[35] D. Weyns and T. Holvoet, "Architecture-centric software development of situated multiagent systems," in *Engineering Societies in the Agents World VII*. Springer, 2007, pp. 62–85.

[36] H. Nwana *et al.*, "Software agents: An overview," *Knowledge Engineering Review*, vol. 11, no. 3, pp. 205–244, 1996.

[37] S. J. Russell, P. Norvig, J. F. Canny, J. M. Malik, and D. D. Edwards, *Artificial intelligence: a modern approach*. Prentice hall Englewood Cliffs, 1995, vol. 74.

[38] P. Hoen, K. Tuyls, L. Panait, S. Luke, and J. La Poutre, "An overview of cooperative and competitive multiagent learning," *Learning and Adaption in Multi-Agent Systems*, pp. 1–46, 2006.

[39] I. Breddin, "Self-organisation and emergence," in *Seminar Organic Computing. KBS Department of communications and operations systems. Technical University of Berlin, Tech. Rep.* Citeseer, 2006.

[40] T. De Wolf and T. Holvoet, "Emergence versus self-organisation: Different concepts but promising when combined," *Engineering self-organising systems*, pp. 77–91, 2005.

[41] G. Di Marzo Serugendo, M. Gleizes, and A. Karageorgos, "Self-organisation and emergence in MAS: An overview," *Informatica*, vol. 30, no. 1, pp. 45–54, 2006.

[42] G. Di Marzo Serugendo, N. Foukia, S. Hassas, A. Karageorgos, S. Mostéfaoui, O. Rana, M. Ulieru, P. Valckenaers, and C. Van Aart, "Self-organisation: Paradigms and applications," *Engineering Self-Organising Systems*, pp. 1–19, 2004.

[43] J. Mahdjoub, Z. Guessoum, F. Michel, and M. Herbin, "A multi-agent approach for the edge detection in image processings," *Proceedings of the 4th European Workshop on Multi-Agent Systems 2006*, 2006.

[44] R. Haroun, F. Boumghar, S. Hassas, and L. Hamami, "A massive multi-agent system for brain MRI segmentation," *Massively Multi-Agent Systems I*, pp. 174–186, 2005.

[45] N. Richard, M. Dojat, and C. Garbay, "Automated segmentation of human brain MR images using a multi-agent approach," *Artificial Intelligence in Medicine*, vol. 30, no. 2, pp. 153–176, 2004.

[46] N. Benamrane and S. Nassane, "Medical image segmentation by a multi-agent system approach," *Multiagent System Technologies*, pp. 49–60, 2007.

[47] J. Liu and Y. Tang, "Adaptive image segmentation with distributed behavior-based agents," *Pattern Analysis and Machine Intelligence, IEEE Transactions on*, vol. 21, no. 6, pp. 544–551, 1999.

[48] E. Duchesnay, J. Montois, and Y. Jacquelet, "Cooperative agents society organized as an irregular pyramid: A mammography segmentation application," *Pattern recognition letters*, vol. 24, no. 14, pp. 2435–2445, 2003.

[49] K. Idir, H. Merouani, and Y. Tlili, "Image segmentation through dual pyramid of agents," *Image Analysis and Processing–ICIAP 2005*, pp. 360–366, 2005.

[50] S. Mazouzi, Z. Guessoum, F. Michel, and M. Batouche, "A multi-agent approach for range image segmentation with bayesian edge regularization," in *Advanced Concepts for Intelligent Vision Systems.* Springer, 2007, pp. 449–460.

[51] E. Bovenkamp, J. Dijkstra, J. Bosch, and J. Reiber, "Multi-agent segmentation of IVUS images," *Pattern Recognition*, vol. 37, no. 4, pp. 647–663, 2004.

[52] K. Melkemi, M. Batouche, and S. Foufou, "A multiagent system approach for image segmentation using genetic algorithms and extremal optimization heuristics," *Pattern Recognition Letters*, vol. 27, no. 11, pp. 1230–1238, 2006.

[53] M. Dorigo, M. Birattari, and T. Stutzle, "Ant colony optimization," *IEEE Computational Intelligence Magazine*, vol. 1, no. 4, pp. 28–39, 2006.

[54] R. Mullen, D. Monekosso, S. Barman, and P. Remagnino, "A review of ant algorithms," *Expert Systems with Applications*, vol. 36, no. 6, pp. 9608–9617, 2009.

[55] H. Nezamabadi-pour, S. Saryazdi, and E. Rashedi, "Edge detection using ant algorithms," *Soft Computing-A Fusion of Foundations, Methodologies and Applications*, vol. 10, no. 7, pp. 623–628, 2006.

[56] J. Tian, W. Yu, and S. Xie, "An ant colony optimization algorithm for image edge detection," in *Evolutionary Computation, 2008. CEC 2008.(IEEE World Congress on Computational Intelligence). IEEE Congress on.* IEEE, 2008, pp. 751–756.

[57] A. Jevtic, J. Quintanilla-Dominguez, M. Cortina-Januchs, and D. Andina, "Edge detection using ant colony search algorithm and multiscale contrast enhancement," in *Systems, Man and Cybernetics, 2009. SMC 2009. IEEE International Conference on.* IEEE, 2009, pp. 2193–2198.

[58] L. Ma, K. Wang, and D. Zhang, "A universal texture segmentation and representation scheme based on ant colony optimization for iris image processing," *Computers & Mathematics with Applications*, vol. 57, no. 11, pp. 1862–1868, 2009.

[59] J. Zhang, K. He, J. Zhou, and M. Gong, "Ant colony optimization and statistical estimation approach to image edge detection," in *Wireless Communications Networking and Mobile Computing (WiCOM), 2010 6th International Conference on.* IEEE, 2010, pp. 1–4.

[60] Y. Han and P. Shi, "An improved ant colony algorithm for fuzzy clustering in image segmentation," *Neurocomputing*, vol. 70, no. 4, pp. 665–671, 2007.

[61] W. Tao, H. Jin, and L. Liu, "Object segmentation using ant colony optimization algorithm and fuzzy entropy," *Pattern Recognition Letters*, vol. 28, no. 7, pp. 788–796, 2007.

[62] D.-S. Lu and C.-C. Chen, "Edge detection improvement by ant colony optimization," *Pattern Recognition Letters*, vol. 29, no. 4, pp. 416–425, 2008.

[63] P. Huang, H. Cao, and S. Luo, "An artificial ant colonies approach to medical image segmentation," *Computer methods and programs in biomedicine*, vol. 92, no. 3, pp. 267–273, 2008.

[64] G. Kavitha and S. Ramakrishnan, "An approach to identify optic disc in human retinal images using ant colony optimization method," *Journal of medical systems*, vol. 34, no. 5, pp. 809–813, 2010.

[65] ——, "Identification and analysis of macula in retinal images using ant colony optimization based hybrid method," in *Nature & Biologically Inspired Computing, 2009. NaBIC 2009. World Congress on.* IEEE, 2009, pp. 1174–1177.

[66] M. G. Cinsdikici and D. Aydın, "Detection of blood vessels in ophthalmoscope images using MF/ant (matched filter/ant colony) algorithm," *Computer methods and programs in biomedicine*, vol. 96, no. 2, pp. 85–95, 2009.

[67] S. Hooshyar and R. Khayati, "Retina vessel detection using fuzzy ant colony algorithm," in *Computer and Robot Vision (CRV), 2010 Canadian Conference on.* IEEE, 2010, pp. 239–244.

[68] H. Ying, M. Zhang, and J. Liu, "Fractal-based automatic localization and segmentation of optic disc in retinal images," in *Engineering in Medicine and Biology Society, 2007. EMBS 2007. 29th Annual International Conference of the IEEE.* IEEE, 2007, pp. 4139–4141.

[69] H. Narasimha-Iyer, A. Can, B. Roysam, V. Stewart, H. Tanenbaum, A. Majerovics, and H. Singh, "Robust detection and classification of longitudinal changes in color retinal fundus images for monitoring diabetic retinopathy," *Biomedical Engineering, IEEE Transactions on*, vol. 53, no. 6, pp. 1084–1098, 2006.

[70] A. Hoover and M. Goldbaum, "Locating the optic nerve in a retinal image using the fuzzy convergence of the blood vessels," *Medical Imaging, IEEE Transactions on*, vol. 22, no. 8, pp. 951–958, 2003.

[71] M. Foracchia, E. Grisan, and A. Ruggeri, "Detection of optic disc in retinal images by means of a geometrical model of vessel structure," *Medical Imaging, IEEE Transactions on*, vol. 23, no. 10, pp. 1189–1195, 2004.

[72] A. Youssif, A. Ghalwash, A. Ghoneim *et al.*, "Optic disc detection from normalized digital fundus images by means of a vessels' direction matched filter," *Medical Imaging, IEEE Transactions on*, vol. 27, no. 1, pp. 11–18, 2007.

[73] A. Fleming, K. Goatman, S. Philip, J. Olson, and P. Sharp, "Automatic detection of retinal anatomy to assist diabetic retinopathy screening," *Physics in Medicine and Biology*, vol. 52, pp. 331–345, 2007.

[74] R. Abdel-Ghafar, T. Morris, T. Ritchings, and I. Wood, "Detection and characterisation of the optic disk in glaucoma and diabetic retinopathy," in *Med. Image Understand. Anal. Conf., London, UK.* Citeseer, 2004.

[75] X. Zhu, R. Rangayyan, and A. Ells, "Detection of the optic nerve head in fundus images of the retina using the hough transform for circles," *Journal of Digital Imaging*, vol. 23, no. 3, pp. 332–341, 2010.

[76] A. Reza, C. Eswaran, and S. Hati, "Automatic tracing of optic disc and exudates from color fundus images using fixed and variable thresholds," *Journal of medical systems*, vol. 33, no. 1, pp. 73–80, 2009.

[77] S. Lee, M. Rajeswari, D. Ramachandram, and B. Shaharuddin, "Screening of diabetic retinopathy-automatic segmentation of optic disc in colour fundus images," in *Distributed Frameworks for Multimedia Applications, 2006. The 2nd International Conference on.* IEEE, 2007, pp. 1–7.

[78] H. Li and O. Chutatape, "Automated feature extraction in color retinal images by a model based approach," *Biomedical Engineering, IEEE Transactions on*, vol. 51, no. 2, pp. 246–254, 2004.

[79] T. Chanwimaluang and G. Fan, "An efficient algorithm for extraction of anatomical structures in retinal images," in *Image Processing, 2003. ICIP 2003. Proceedings. 2003 International Conference on*, vol. 1. IEEE, 2003.

[80] J. Lowell, A. Hunter, D. Steel, A. Basu, R. Ryder, E. Fletcher, and L. Kennedy, "Optic nerve head segmentation," *Medical Imaging, IEEE Transactions on*, vol. 23, no. 2, pp. 256–264, 2004.

[81] J. Xu, E. Sung, O. Chutatape, C. Zheng, and P. Chew, "Automated optic disk segmentation via a modified snake technique," in *Control, Automation, Robotics and Vision, 2006. ICARCV'06. 9th International Conference on.* IEEE, 2007, pp. 1–6.

[82] J. Novo, M. Penedo, and J. Santos, "Localisation of the optic disc by means of GA-optimised topological active nets," *Image and Vision Computing*, vol. 27, no. 10, pp. 1572–1584, 2009.

[83] M. Abramoff and M. Niemeijer, "The automatic detection of the optic disc location in retinal images using optic disc location regression," in *Engineering in Medicine and Biology Society, 2006. EMBS'06. 28th Annual International Conference of the IEEE.* IEEE, 2008, pp. 4432–4435.

[84] J. Weickert, *Anisotropic diffusion in image processing.* Stuttgart: Teubner, 1998.

[85] G. Sapiro, *Geometric partial differential equations and image analysis.* Cambridge Univ Pr, 2001.

[86] P. Perona and J. Malik, "Scale-space and edge detection using anisotropic diffusion," *IEEE Transactions on pattern analysis and machine intelligence*, vol. 12, no. 7, pp. 629–639, 1990.

[87] N. Otsu, "A threshold selection method from gray-scale histogram," *IEEE Trans. Systems, Man, and Cybernetics*, vol. 8, pp. 62–66, 1978.

[88] M. Niemeijer, J. Staal, B. van Ginneken, M. Loog, and M. Abramoff, "Comparative study of retinal vessel segmentation methods on a new publicly available database," in *SPIE Medical Imaging*, vol. 5370. Proc. SPIE, 2004, pp. 648–656.

[89] T. Kauppi, V. Kalesnykiene, J. Kamarainen, L. Lensu, I. Sorri, A. Raninen, R. Voutilainen, H. Uusitalo, H. Kalviainen, and J. Pietila, "Diaretdb1 diabetic

retinopathy database and evaluation protocol," *Proc. Medical Image Understanding and Analysis (MIUA)*, pp. 61–65, 2007.

[90] L. Giancardo, F. Meriaudeau, T. Karnowski, Y. Li, S. Garg, K. Tobin, and E. Chaum, "Exudate-based diabetic macular edema detection in fundus images using publicly available datasets," *Medical Image Analysis*, vol. 16, no. 1, pp. 216–226, 2012.

[91] C. Sánchez, M. García, A. Mayo, M. López, and R. Hornero, "Retinal image analysis based on mixture models to detect hard exudates," *Medical Image Analysis*, vol. 13, no. 4, pp. 650–658, 2009.

[92] A. Sopharak, B. Uyyanonvara, S. Barman, and T. Williamson, "Automatic detection of diabetic retinopathy exudates from non-dilated retinal images using mathematical morphology methods," *Computerized Medical Imaging and Graphics*, vol. 32, no. 8, pp. 720–727, 2008.

[93] D. Welfer, J. Scharcanski, and D. Marinho, "A coarse-to-fine strategy for automatically detecting exudates in color eye fundus images," *Computerized Medical Imaging and Graphics*, vol. 34, no. 3, pp. 228–235, 2010.

[94] F. Amel, M. Mohammed, and B. Abdelhafid, "Improvement of the hard exudates detection method used for computer-aided diagnosis of diabetic retinopathy," *International Journal of Image, Graphics and Signal Processing (IJIGSP)*, vol. 4, no. 4, pp. 19–27, 2012.

[95] M. García, C. Sánchez, M. López, D. Abásolo, and R. Hornero, "Neural network based detection of hard exudates in retinal images," *Computer methods and programs in biomedicine*, vol. 93, no. 1, pp. 9–19, 2009.

[96] M. Niemeijer, B. van Ginneken, S. Russell, M. Suttorp-Schulten, and M. Abràmoff, "Automated detection and differentiation of drusen, exudates, and cotton-wool spots in digital color fundus photographs for diabetic retinopathy diagnosis," *Investigative ophthalmology & visual science*, vol. 48, no. 5, pp. 2260–2267, 2007.

[97] A. Fleming, S. Philip, K. Goatman, G. Williams, J. Olson, and P. Sharp, "Automated detection of exudates for diabetic retinopathy screening," *Physics in medicine and biology*, vol. 52, pp. 7385–7396, 2007.

[98] A. Osareh, B. Shadgar, and R. Markham, "A computational-intelligence-based approach for detection of exudates in diabetic retinopathy images," *Information Technology in Biomedicine, IEEE Transactions on*, vol. 13, no. 4, pp. 535–545, 2009.

[99] M.-P. TECHNO-VISION. (2008) Methods to evaluate segmentation and indexing techniques in the field of retinal ophthalmology. [Online]. Available: http://www.http://messidor.crihan.fr

[100] L. Giancardo, F. Meriaudeau, T. Karnowski, Y. Li, K. Tobin, and E. Chaum, "Automatic retina exudates segmentation without a manually labelled training

set," in *Biomedical Imaging: From Nano to Macro, 2011 IEEE International Symposium on*. IEEE, 2011, pp. 1396–1400.

[101] F. Zana and J. Klein, "Segmentation of vessel-like patterns using mathematical morphology and curvature evaluation," *Image Processing, IEEE Transactions on*, vol. 10, no. 7, pp. 1010–1019, 2001.

[102] G. Di Caro, "Ant colony optimization and its application to adaptive routing in telecommunication networks," *Faculte des sciences appliquees*, p. 374, 2004.

[103] K. A. Vermeer, F. M. Vos, H. Lemij, and A. M. Vossepoel, "A model based method for retinal blood vessel detection," *Computers in Biology and Medicine*, vol. 34, no. 3, pp. 209–219, 2004.

[104] A. Hoover, V. Kouznetsova, and M. Goldbaum, "Locating blood vessels in retinal images by piecewise threshold probing of a matched filter response," *Medical Imaging, IEEE Transactions on*, vol. 19, no. 3, pp. 203–210, 2000.

[105] Q. Li, L. Zhang, D. Zhang, and P. Bhattacharya, "A new approach to automated retinal vessel segmentation using multiscale analysis," *Pattern Recognition*, vol. 4, pp. 77–80, 2006.

[106] F. Oloumi, R. Rangayyan, P. Eshghzadeh-Zanjani, and F. Ayres, "Detection of blood vessels in fundus images of the retina using gabor wavelets," in *Engineering in Medicine and Biology Society, 2007. EMBS 2007. 29th Annual International Conference of the IEEE*. IEEE, 2007, pp. 6451–6454.

[107] M. Al-Rawi, M. Qutaishat, and M. Arrar, "An improved matched filter for blood vessel detection of digital retinal images," *Computers in Biology and Medicine*, vol. 37, no. 2, pp. 262–267, 2007.

[108] B. Zhang, L. Zhang, L. Zhang, and F. Karray, "Retinal vessel extraction by matched filter with first-order derivative of Gaussian," *Computers in Biology and Medicine*, vol. 40, no. 4, pp. 438–445, 2010.

[109] J. Staal, M. Abràmoff, M. Niemeijer, M. Viergever, and B. van Ginneken, "Ridge-based vessel segmentation in color images of the retina," *Medical Imaging, IEEE Transactions on*, vol. 23, no. 4, pp. 501–509, 2004.

[110] J. Soares, J. Leandro, R. Cesar, H. Jelinek, and M. Cree, "Retinal vessel segmentation using the 2-D Gabor wavelet and supervised classification," *Medical Imaging, IEEE Transactions on*, vol. 25, no. 9, pp. 1214–1222, 2006.

[111] D. Cornforth, H. Jelinek, J. Leandro, J. Soares, R. Cesar Jr, M. Cree, P. Mitchell, and T. Bossomaier, "Development of retinal blood vessel segmentation methodology using wavelet transforms for assessment of diabetic retinopathy," *Complexity International*, vol. 11, pp. 50–61, 2005.

[112] E. Ricci and R. Perfetti, "Retinal blood vessel segmentation using line operators and support vector classification," *Medical Imaging, IEEE Transactions on*, vol. 26, no. 10, pp. 1357–1365, 2007.

[113] S. Salem, N. Salem, and A. Nandi, "Segmentation of retinal blood vessels using a novel clustering algorithm (RACAL) with a partial supervision strategy," *Medical and Biological Engineering and Computing*, vol. 45, no. 3, pp. 261–273, 2007.

[114] M. Zhang and J. Liu, "Directional local contrast based blood vessel detection in retinal images," in *Image Processing, 2007. ICIP 2007. IEEE International Conference on*, vol. 4. IEEE, 2007, pp. IV–317.

[115] K. Huang and M. Yan, "A region based algorithm for vessel detection in retinal images," *Medical Image Computing and Computer-Assisted Intervention–MICCAI 2006*, pp. 645–653, 2006.

[116] B. Lam and H. Yan, "Blood vessel extraction based on Mumford Shah model and skeletonization," in *Machine Learning and Cybernetics, 2006 International Conference on*. IEEE, 2006, pp. 4227–4232.

[117] ——, "A novel vessel segmentation algorithm for pathological retina images based on the divergence of vector fields," *Medical Imaging, IEEE Transactions on*, vol. 27, no. 2, pp. 237–246, 2008.

[118] B. Al-Diri, A. Hunter, and D. Steel, "An active contour model for segmenting and measuring retinal vessels," *Medical Imaging, IEEE Transactions on*, vol. 28, no. 9, pp. 1488–1497, 2009.

[119] A. Mendonca and A. Campilho, "Segmentation of retinal blood vessels by combining the detection of centerlines and morphological reconstruction," *Medical Imaging, IEEE Transactions on*, vol. 25, no. 9, pp. 1200–1213, 2006.

[120] J. Nayak, P. Bhat, R. Acharya U, C. Lim, and M. Kagathi, "Automated identification of diabetic retinopathy stages using digital fundus images," *Journal of medical systems*, vol. 32, no. 2, pp. 107–115, 2008.

[121] W. Tan, Y. Wang, and S. Lee, "Retinal blood vessel detection using frequency analysis and local-mean-interpolation filters," in *Proceedings of SPIE*, vol. 4322, 2001, p. 1373.

[122] K. Estabridis and R. Defigueiredo, "Blood vessel detection via a multi-window parameter transform," in *Computer-Based Medical Systems, 2006. CBMS 2006. 19th IEEE International Symposium on*. IEEE, 2006, pp. 424–429.

[123] O. Gutknecht and J. Ferber, "Madkit: a generic multi-agent platform," in *Proceedings of the fourth international conference on Autonomous agents*. ACM, 2000, pp. 78–79.

[124] G. Papari, N. Petkov, and P. Campisi, "Artistic edge and corner enhancing smoothing," *Image Processing, IEEE Transactions on*, vol. 16, no. 10, pp. 2449–2462, 2007.

[125] M. J. Cree, "Automated microaneurysm detection for screening," *Automated Image Detection of Retinal Pathology*, pp. 155–184, 2009.

[126] A. Fleming, S. Philip, K. Goatman, J. Olson, and P. Sharp, "Automated microaneurysm detection using local contrast normalization and local vessel detection," *Medical Imaging, IEEE Transactions on*, vol. 25, no. 9, pp. 1223–1232, 2006.

[127] G. Quellec, M. Lamard, P. Josselin, G. Cazuguel, B. Cochener, and C. Roux, "Optimal wavelet transform for the detection of microaneurysms in retina photographs," *Medical Imaging, IEEE Transactions on*, vol. 27, no. 9, pp. 1230–1241, 2008.

[128] B. Zhang, F. Karray, Q. Li, and L. Zhang, "Sparse representation classifier for microaneurysm detection and retinal blood vessel extraction," *Information Sciences*, vol. 200, no. 1, pp. 78–90, 2012.

[129] C. Sánchez, R. Hornero, A. Mayo, and M. García, "Mixture model-based clustering and logistic regression for automatic detection of microaneurysms in retinal images," in *SPIE Medical Imaging*. International Society for Optics and Photonics, 2009, p. 72601M.

[130] B. Laÿ, "Analyse automatique des images angiofluorographiques au cours de la rétinopathie diabétique (thesis doctoralis)," *Paris: School of Mines*, 1983.

[131] M. Cree, "The waikato microaneurysm detector," *the University of Waikato, Tech. Rep*, 2008.

[132] B. Zhang, X. Wu, J. You, Q. Li, and F. Karray, "Detection of microaneurysms using multi-scale correlation coefficients," *Pattern Recognition*, vol. 43, no. 6, pp. 2237–2248, 2010.

[133] A. Mizutani, C. Muramatsu, Y. Hatanaka, S. Suemori, T. Hara, and H. Fujita, "Automated microaneurysm detection method based on double ring filter in retinal fundus images," in *SPIE Medical Imaging*. International Society for Optics and Photonics, 2009, p. 72601N.

[134] L. Giancardo, F. Meriaudeau, T. Karnowski, Y. Li, K. Tobin, and E. Chaum, "Microaneurysm detection with radon transform-based classification on retina images," in *Engineering in Medicine and Biology Society, EMBC, 2011 Annual International Conference of the IEEE*. IEEE, 2011, pp. 5939–5942.

[135] I. Lazar and A. Hajdu, "Microaneurysm detection in retinal images using a rotating cross-section based model," in *Biomedical Imaging: From Nano to Macro, 2011 IEEE International Symposium on*. IEEE, 2011, pp. 1405–1409.

[136] B. Antal and A. Hajdu, "An ensemble-based system for microaneurysm detection and diabetic retinopathy grading," *Biomedical Engineering, IEEE Transactions on*, vol. 59, no. 6, pp. 1720–1726, 2012.

[137] M. Niemeijer, B. Van Ginneken, M. J. Cree, A. Mizutani, G. Quellec, C. I. Sánchez, B. Zhang, R. Hornero, M. Lamard, C. Muramatsu *et al.*, "Retinopathy online challenge: automatic detection of microaneurysms in digital color

fundus photographs," *Medical Imaging, IEEE Transactions on*, vol. 29, no. 1, pp. 185–195, 2010.